

Observational tests of GR and alternative theories of gravity with Galactic Center observations using current and future large facilities

А.Ф. Захаров (Alexander F. Zakharov) *

E-mail: zakharov@itep.ru

*Institute of Theoretical and Experimental Physics,
B. Cheremushkinskaya, 25, 117218 Moscow*

*Bogoliubov Laboratory of Theoretical Physics
Joint Institute for Nuclear Research, Dubna, Russia*

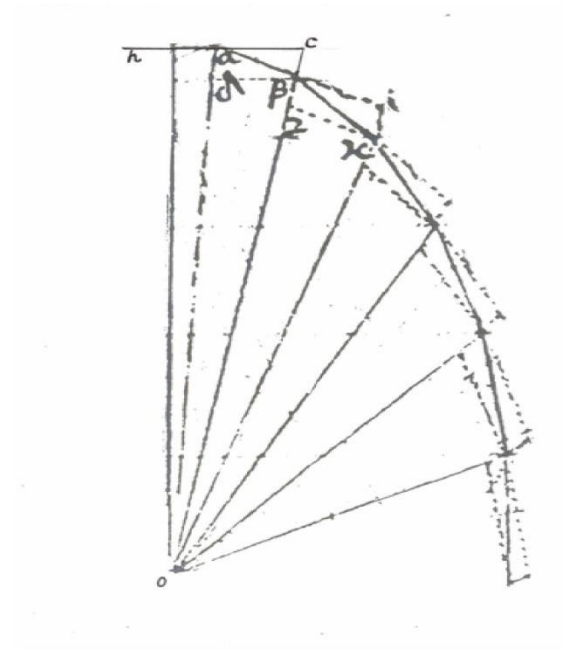
07.06.2019

12 SCSLSA, Vrdnik, Serbia

* in collaboration with P. Jovanovic, D. Borka and V. Borka Jovanovic

- ~~When comedy was king~~
- How GR started to be king
- LIGO-Virgo: BBHs, BNS (kilonova) GW 170817;
- GRAVITY, EHT and M87* images
- We consider shadows and trajectories of bright stars near the GC

R. Hooke proof that $F \sim 1/r^2$
could explain Kepler's laws



In a letter from Newton to Halley, June 20, 1686
Newton complained that “he [Hooke] knew not how to go
about it. Now is not this very fine? Mathematicians
that find out, settle & and do all the business must content
themselves with being nothing but dry calculators & drudges
& and another that does nothing but pretend & grasp at all
things must carry away all the invention as well as
those who were to follow him as of those that went before
him.”

Outline of my talk

- Introduction
- Shadows for Kerr as a tool to evaluate BH characteristics
- Shadows around Reissner-Nordstrom BHs
- Observations of BH at Sgr A and a tidal Reissner-Nordstrom BH
- Bright star trajectories around BH at GC as a tool to evaluate BH parameters and DM cluster
- Constraints on massive graviton theories
- Forecasts for graviton mass improvements
- Constraints on tidal charge
- Conclusions

References

- AFZ, F. De Paolis, G. Ingrosso, and A. A. Nucita, *New Astronomy Reviews*, **56**, 64 (2012).
- D. Borka, P. Jovanovic, V. Borka Jovanovic and AFZ, *Physical Reviews D*, **85**, 124004 (2012).
- D. Borka, P. Jovanovic, V. Borka Jovanovic and AFZ, *JCAP* **11**, 050 (2013).
- AFZ, *Physical Reviews D* **90**, 062007 (2014).
- AFZ, D. Borka, P. Jovanovic, V. Borka Jovanovic, *Advances in Space Research* 54, 1108 (2014).
- AFZ, *J Astrophys. Astron.* **36**, 539 (2015)
- AFZ, P. Jovanovic, D. Borka, V. Borka Jovanovic, gr-qc: 1605.00913v; *JCAP* (2016)
- AFZ, P. Jovanovic, D. Borka, and V. Borka Jovanovic, *JCAP* (2018).
- AFZ, *EPJ C* (2018)

- P. Bergman (GRG1, 1957): “Now to the problems that are more concerned with the special question, where things having physical or model significance are tried out. The most important of these questions which must be settled is, are there gravitational waves? At the present there is no general agreement. The other things to be mentioned are interesting but are of less crucial significance.”



Fig. 2 Professor J. Synge delivering the opening lecture

followed by a short discussion, the session was adjourned and all participants were transferred to Jablonna.

Jablonna is a small town about 20 km from Warsaw. In XVIII century a famous Polish aristocratic family of Poniatowski built there a summer palace and two adjacent buildings with several rooms for their guests and servants. The Palace was surrounded by a park of English style (Fig. 3).

The idea to organize cyclic international conferences on general relativity and gravitation slowly matured over the years after the Second World War. In 1955, to celebrate the fiftieth anniversary of the special theory of relativity, an international conference

K. Thorne about the First Texas Symposium:

K. Thorne about the First Texas Symposium: “ The astronomers and astrophysicists had come to Dallas to discuss quasars; they were not at all interested in Kerr's esoteric mathematical topic. So, as Kerr got up to speak, many slipped out of the lecture hall and into the foyer to argue with each other about their favorite theories of quasars. Others, less polite, remained seated in the hall and argued in whispers. Many of the rest catnapped in a fruitless effort to remedy their sleep deficits from late-night science. Only a handful of relativists listened, with rapt attention.

This was more than Achilles Papapetrou, one of the world's leading relativists, could stand. As Kerr finished Papapetrou demanded the floor, stood up, and with deep feeling explained the importance of Kerr's feat. He, Papapetrou, had been trying for thirty years to find such a solution of Einstein's equation, and had failed, as had many other relativists. The astronomers and astrophysicists nodded politely, and then, as the next speaker began to hold forth on a theory of quasars, they refocused their attention, and the meeting picked up pace.”

- T. Gold (1963) : “[The mystery of the quasars] allows one to suggest that the relativists with their sophisticated work are not only magnificent cultural ornaments but might actually be useful to science! Everyone is pleased: the relativists who feel they are being appreciated and are experts in a field they hardly knew existed, the astrophysicists for having enlarged their domain, their empire, by the annexation of another subject general relativity. It is all very pleasing, so let us all hope that it is right. What a shame it would be if we had to go and dismiss all the relativists again.”

J. A. Wheeler :

In the fall of 1967, Vittorio Canuto, administrative head of NASA's Goddard Institute for Space Studies, invited me to a conference to consider possible interpretations of the exciting new evidence just arriving from England on pulsars. What were these pulsars? Vibrating white dwarfs? Rotating neutron stars? What? In my talk, I argued that we should consider the possibility that at the center of a pulsar is a gravitationally completely collapsed object. I remarked that one couldn't keep saying "gravitationally completely collapsed object" over and over. One needed a shorter descriptive phrase. "How about black hole?" asked someone in the audience. (As it turned out, a pulsar is powered by "merely" a neutron star, not a black hole.) Several years later, Feynman called my language unfit for polite company when I tried to summarize the remarkable simplicity of a black hole by saying, "A black hole has no hair." ... The black hole, it has turned out, shows only three characteristics to the outside world: Its mass, its electric charge, and its angular momentum, or spin.

- "The extent to which the Chinese records of guest stars remain of living interest to current astronomical research may be seen in the field of radio-astronomy, where during the past few years great additions to knowledge have been made. The rapid upsurge of this new and powerful method of study of the birth and death of stars....makes urgently necessary the reduction of the information contained in the ancient and medieval Chinese texts to a form utilizable by modern astronomers in all lands. For this purpose, however, collaboration between competent sinologists and practical astronomers and radio astronomers is indispensable."
Joseph Needham, F.R.S. - distinguished historian
of Chinese Science (1959) in Vol. III. *Mathematics and the Sciences of the Heavens and Earth*
- "The investigation of the remnants of supernovae and their relation to historical records, both written and unwritten, will be one of the most fascinating tasks awaiting the next generation of astronomers..."
Fritz Zwicky (1965)

Crab nebula (remnant of SN AD1054) in different bands



J. A. Wheeler: in “Our Universe: the known and unknown”: “Take up the telescope and turn it on the Crab Nebula. There was no Crab Nebula a thousand years ago. At that time astronomy was at a low level in Europe. Not so in China. There astronomers regularly swept the skies and recorded their observations. In July 1054 they reported a new star. It grew in brightness from day to day. In a few days it out shone every star in the firmament. Then it sank in brilliance, falling off in intensity from week to week. At each date the nova, or supernova as we more appropriately call it, could be compared with neighbor stars for brightness. Out of these comparisons by our Chinese colleagues of long ago one has today constructed a light curve. “

The identification of old Chinese records with Crab Nebula has been done by J. J. L. Duyvendak (1942). In 1054-1056 the Crab Nebula was observed for 21 months (many Chinese records) . See also consequent discussion by N. U. Mayall and J. H. Oort (1942).

The Crab nebula was identified with a radio source in 1963 and as a X-ray source in 1964 and as a pulsar in 1968.

These Chinese observations helped to confirm observationally the Baade – Zwicky hypothesis that neutron stars could be formed in supernova explosions.

Conclusions from Wheeler’s statements: First, sometimes, a time distance between an action and a result could be centuries (or even Millennium) and at this period one could think that the action was useless but it is not. Second a scientific knowledge is a result of activity of skillfull people working in different areas.

Neutron stars (milestones)

- E. Rutherford (1920): Prediction of neutron
- J. Chadwick (1932): Neutron discovery
- L. Landau (1932): см. “Л.Д. Ландау и концепция нейтронных звёзд”, Д.Г. Яковлев и др. (УФН, 2013)
- W. Baade and F. Zwicky (1934): NSs are born in SN explosions
- G. Gamow (1937): Discovery of mass limit for NSs in Newtonian approach
- R. Oppenheimer and G. Volkoff (1939): Discovery of mass limit for NSs in GR
- A. Hewish, J. Bell... (1968): Discovery of pulsars
- F. Pacini, T. Gold (1967-1969): Rotating neutron stars as pulsars

FAIR, Facility for Antiproton and Ion Research (Darmstadt, Germany) and Nuclotron Based Facility (NICA, Dubna, Russia)

- How does the strong force, which binds the particles comprising atomic nuclei work - and where do their masses come from?
- How does matter behave across the wide range of temperatures and pressures found in the past and present Universe?
- How did matter in the early Universe evolve and why does it look the way it does today?
- Where do the atomic elements come from?
- How does the electromagnetic force, which binds atoms and molecules, work under extreme conditions?
- The search for signs of the phase transition between hadronic matter and QGP;
- Search for new phases of baryonic matter Study of basic properties of the strong interaction vacuum and QCD symmetries
- **The Universe in Laboratory**

Rev. John Michell: *Phil. Trans. R. Soc. London*, 74, 35–57 (1784):

VII. *On the Means of discovering the Distance, Magnitude, &c. of the Fixed Stars, in consequence of the Diminution of the Velocity of their Light, in case such a Diminution should be found to take place in any of them, and such other Data should be procured from Observations, as would be farther necessary for that Purpose. By the Rev. John Michell, B. D. F. R. S. In a Letter to Henry Cavendish, Esq. F. R. S. and A. S.*

Read November 27, 1783.

Rev. John Michell: *Phil. Trans. R. Soc. London*, 74, 35–57 (1784):

42 *Mr. MICHELL on the Means of discovering the*

16. Hence, according to article 10, if the semi-diameter of a sphaere of the same density with the sun were to exceed that of the sun in the proportion of 500 to 1, a body falling from an infinite height towards it, would have acquired at its surface a greater velocity than that of light, and consequently, supposing light to be attracted by the same force in proportion to its vis inertiae, with other bodies, all light emitted from such a body would be made to return towards it, by its own proper gravity.

Home

News

Features

Columns & blogs

Archive Archive

Specials

In focus

- X chromosome
- Future computing
- Stem cells
- Bird flu
- Mars
- GM crops

Stories by subject

NEWS CHANNELS

- My news**
- Biotechnology**
- Careers**
- Drug discovery**
- Earth and environment**
- Medical Research**
- Physical Sciences**

Feedback

About this site

About us

For librarians

TOP STORIES

[Air pollution influences crop disease](#)
04 April 2005

[Hunters win hike in polar bear quota](#)
04 April 2005

[Genetic patch treats 'bubble-boy' disease](#)
03 April 2005

[Transgenic cows have](#)

NEWS

Published online: 31 March 2005; | doi:10.1038/news050328-8

Black holes 'do not exist'

[Philip Ball](#)

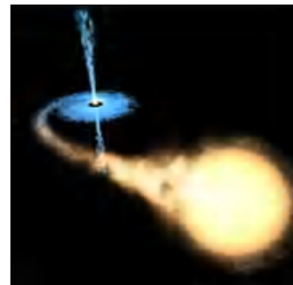
These mysterious objects are dark-energy stars, physicist claims.

Black holes are staples of science fiction and many think astronomers have observed them indirectly. But according to a physicist at the Lawrence Livermore National Laboratory in California, these awesome breaches in space-time do not and indeed cannot exist.

Over the past few years, observations of the motions of galaxies have shown that some 70% the Universe seems to be composed of a strange 'dark energy' that is driving the Universe's accelerating expansion.

George Chapline thinks that the collapse of the massive stars, which was long believed to generate black holes, actually leads to the formation of stars that contain dark energy. "It's a near certainty that black holes don't exist," he claims.

Black holes are one of the most celebrated predictions of Einstein's general theory of relativity, which explains gravity as the warping of space-time caused by massive objects. The theory suggests that



Black holes, such as the one pictured in this artist's impression, may in fact be pockets of 'dark energy'.

© ESA/NASA

Black Holes or Gray Stars? That's the Question: Pseudo-Complex General Relativity

Peter O. Hess, W. Greiner, T. Schöenbach and G. Caspar

Abstract After a short review on attempts to extend General Relativity, pseudo-complex variables are introduced. We restate the main properties of these variables. The variational principle has to be modified in order to obtain a new theory. An additional contribution appears, whose origin is a repulsive, dark energy. The general formalism is presented. As examples, the Schwarzschild and the Kerr solutions are discussed. It is shown that a collapsing mass increasingly accumulates dark energy until the collapse is stopped. Rather than a black hole, a gray star is formed. We discuss a possible experimental verification, investigating the orbital frequency of a particle in a circular orbit.

1 Introduction

General Relativity (GR) is a well accepted theory which has been verified by many experimental measurements. One prediction of this theory is the existence of *black holes*, which are formed once a very large mass suffers a gravitational collapse. Astronomical observations seem to confirm this prediction, finding large mass concentrations in the center of most galaxies. These masses vary from several million solar masses to up to several billion solar masses. However, a black hole implies the appearance of an event horizon, below which an external observer cannot penetrate, thus, excluding a part of space from observation. A black hole also implies a singularity at its center. Both consequences from GR may be, from a philosophical point of view, unacceptable and one would like to find a possibility to avoid them. A black hole is an extreme object and one would not be surprised that GR has to be modified

Peter O. Hess (✉)
Instituto de Ciencias Nucleares, UNAM, C.U., A.P. 70-543, 04510 México D.F., Mexico
e-mail: hess@nucleares.unam.mx

W. Greiner, G. Caspar and T. Schöenbach
FIAS, J. W.-Goethe University, Ruth-Moufang-Str. 1, 60438 Frankfurt am Main, Germany

ON A STATIONARY SYSTEM WITH SPHERICAL SYMMETRY
CONSISTING OF MANY GRAVITATING MASSES

BY ALBERT EINSTEIN

(Received May 10, 1939)

If one considers Schwarzschild's solution of the static gravitational field of spherical symmetry

$$(1) \quad ds^2 = -\left(1 + \frac{\mu}{2r}\right)^4 (dx_1^2 + dx_2^2 + dx_3^2) + \left(\frac{1 - \frac{\mu}{2r}}{1 + \frac{\mu}{2r}}\right)^2 dt^2$$

it is noted that

$$g_{44} = \left(\frac{1 - \frac{\mu}{2r}}{1 + \frac{\mu}{2r}}\right)^2$$

vanishes for $r = \mu/2$. This means that a clock kept at this place would go at the rate zero. Further it is easy to show that both light rays and material particles take an infinitely long time (measured in "coördinate time") in order to reach the point $r = \mu/2$ when originating from a point $r > \mu/2$. In this sense the sphere $r = \mu/2$ constitutes a place where the field is singular. (μ represents the gravitating mass.)

There arises the question whether it is possible to build up a field containing such singularities with the help of actual gravitating masses, or whether such regions with vanishing g_{44} do not exist in cases which have physical reality. Schwarzschild himself investigated the gravitational field which is produced by an incompressible liquid. He found that in this case, too, there appears a region with vanishing g_{44} if only, with given density of the liquid, the radius of the field-producing sphere is chosen large enough.

This argument, however, is not convincing; the concept of an incompressible liquid is not compatible with relativity theory as elastic waves would have to travel with infinite velocity. It would be necessary, therefore, to introduce a compressible liquid whose equation of state excludes the possibility of sound signals with a speed in excess of the velocity of light. But the treatment of any such problem would be quite involved; besides, the choice of such an equation of state would be arbitrary within wide limits, and one could not be sure that thereby no assumptions have been made which contain physical impossibilities.

One is thus led to ask whether matter cannot be introduced in such a way that questionable assumptions are excluded from the very beginning. In fact this can be done by choosing, as the field-producing mass, a great number of

The following table gives μ and $2r_0$ for $M = 1$ as functions of σ_0 (approximately):

σ_0	μ	$2r_0$
0.	1.	∞
.05	.988	19.76
.1	.948	9.48
.15	.97	6.56
.2	1.13	5.65
.23	1.32	5.63
.25	1.82	7.40
.26	2.63	10.1
.268	∞	∞

When the cluster is contracted from an infinite diameter its mass decreases at the most about 5%. This minimal mass will be reached when the diameter $2r_0$ is about 9. The diameter can be further reduced down to about 5.6, but only by adding enormous amounts of energy. It is not possible to compress the cluster any more while preserving the chosen mass distribution. A further addition of energy enlarges the diameter again. In this way the energy content, i.e. the gravitating mass of the cluster, can be increased arbitrarily without destroying the cluster. To each possible diameter there belong two clusters (when the number of particles is given) which differ with respect to the particle velocity.

Of course, these paradoxical results are not represented by anything in physical nature. Only that branch belonging to smaller σ_0 values contains the cases bearing some resemblance to real stars, and this branch only for diameter values between ∞ and $9M$.

The case of the cluster of the shell type, discussed earlier in this paper, behaves quite similarly to this one, despite the different mass distribution. The shell type cluster, however, does not contain a case with infinite μ , given a finite M .

The essential result of this investigation is a clear understanding as to why the "Schwarzschild singularities" do not exist in physical reality. Although the theory given here treats only clusters whose particles move along circular paths it does not seem to be subject to reasonable doubt that more general cases will have analogous results. The "Schwarzschild singularity" does not appear for the reason that matter cannot be concentrated arbitrarily. And this is due to the fact that otherwise the constituting particles would reach the velocity of light.

This investigation arose out of discussions the author conducted with Professor H. P. Robertson and with Drs. V. Bargmann and P. Bergmann on the mathematical and physical significance of the Schwarzschild singularity. The problem quite naturally leads to the question, answered by this paper in the negative, as to whether physical models are capable of exhibiting such a singularity.

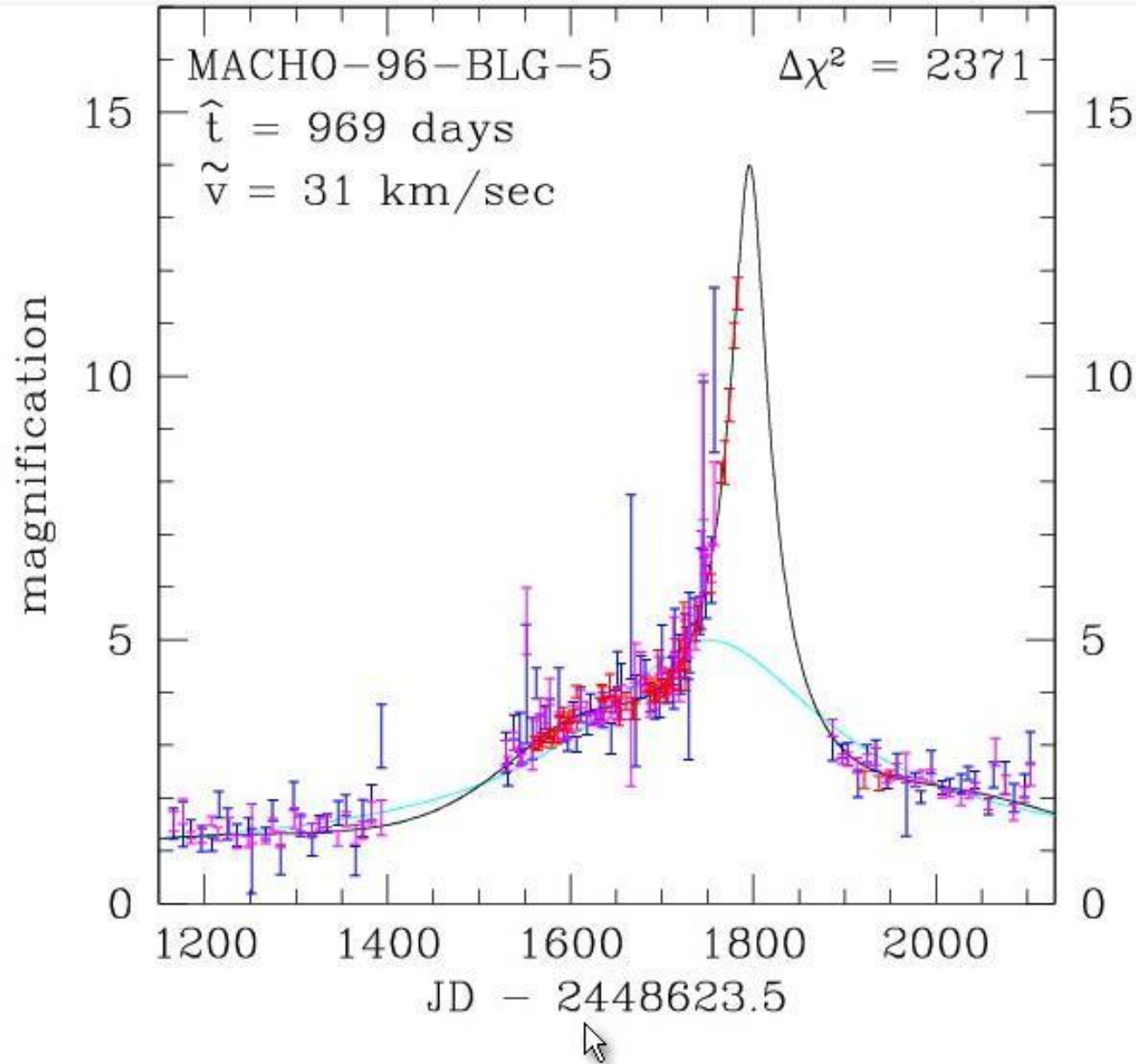


Fig. 7.— MACHO-96-BLG-5 lightcurves normalized to the unlensed flux of the lensed star. The MACHO red and blue data are plotted in magenta and blue, respectively, and the CTIO data are shown in red. The black curve is the parallax fit while the cyan curve is the best fit standard microlensing lightcurve. An additional 4 years of data showing very little photometric variation are not shown.

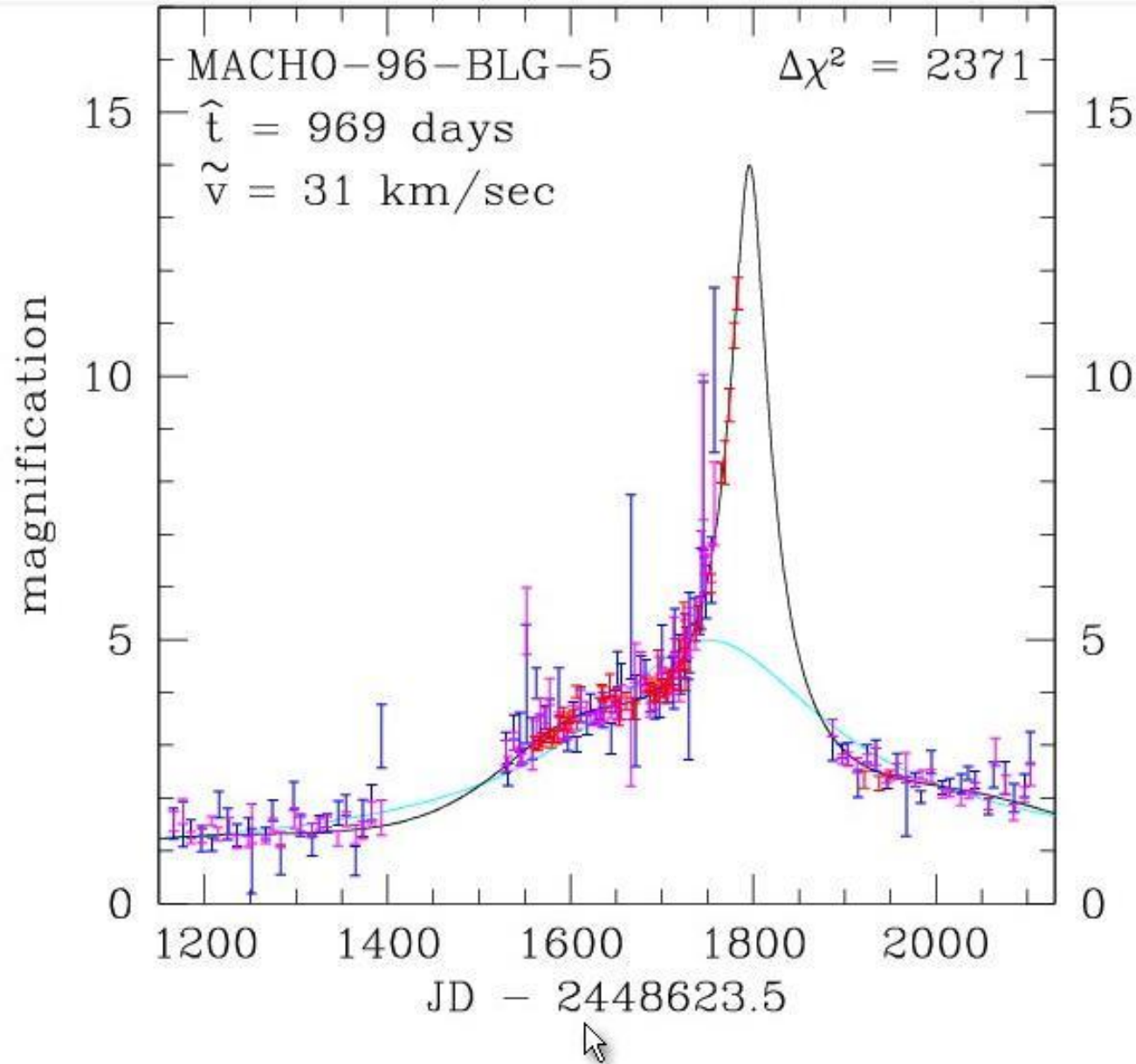


Fig. 7.— MACHO-96-BLG-5 lightcurves normalized to the unlensed flux of the lensed star. The MACHO red and blue data are plotted in magenta and blue, respectively, and the CTIO data are shown in red. The black curve is the parallax fit while the cyan curve is the best fit standard microlensing lightcurve. An additional 4 years of data showing very little photometric variation are not shown.

- Ho1
- Ho2

Black holes in centers of galaxies

(L.Ho,ApJ 564,120 (2002))

Coevolution (Or Not) of Supermassive Black Holes and Host Galaxies

John Kormendy¹ and Luis C. Ho²

¹Department of Astronomy, University of Texas at Austin,
2515 Speedway C1400, Austin, TX 78712-1205; email: kormendy@astro.as.utexas.edu

²The Observatories of the Carnegie Institution for Science,
813 Santa Barbara Street, Pasadena, CA 91101; email: lho@obs.carnegiescience.edu

Abstract

Supermassive black holes (BHs) have been found in 87 galaxies by dynamical modeling of spatially resolved kinematics. The *Hubble Space Telescope* revolutionized BH research by advancing the subject from its proof-of-concept phase into quantitative studies of BH demographics. Most influential was the discovery of a tight correlation between BH mass M_{\bullet} and the velocity dispersion σ of the bulge component of the host galaxy. Together with similar correlations with bulge luminosity and mass, this led to the widespread belief that BHs and bulges coevolve by regulating each other's growth. Conclusions based on one set of correlations from $M_{\bullet} \sim 10^{9.5} M_{\odot}$ in brightest cluster ellipticals to $M_{\bullet} \sim 10^9 M_{\odot}$ in the smallest galaxies dominated BH work for more than a decade.

New results are now replacing this simple story with a richer and more plausible picture in which BHs correlate differently with different galaxy components. A reasonable aim is to use this progress to refine our understanding of BH - galaxy coevolution. BHs with masses of $10^5 - 10^9 M_{\odot}$ are found in many bulgeless galaxies. Therefore, classical (elliptical-galaxy-like) bulges are not necessary for BH formation. On the other hand, while they live in galaxy disks, BHs do not correlate with galaxy disks. Also, any M_{\bullet} correlations with the properties of disk-grown pseudobulges and dark matter halos are weak enough to imply no close coevolution.

The above and other correlations of host galaxy parameters with each other and with M_{\bullet} suggest that there are four regimes of BH feedback. (1) Local, secular, episodic, and stochastic feeding of small BHs in largely bulgeless galaxies involves too little energy to result in coevolution. (2) Global feeding in major, wet galaxy mergers rapidly grows giant BHs in short-duration, quasar-like events whose energy feedback does affect galaxy evolution. The resulting hosts are classical bulges and coreless-rotating-disky ellipticals. (3) After these AGN phases and at the highest galaxy masses, maintenance-mode BH feedback into X-ray-emitting gas has the primarily negative effect of helping to keep baryons locked up in hot gas and thereby keeping galaxy formation from going to completion. This happens in giant, core-nonrotating-boxy ellipticals. Their properties, including their tight correlations between M_{\bullet} and core parameters, support the conclusion that core ellipticals form by dissipationless major mergers. They inherit coevolution effects from smaller progenitor galaxies. Also, (4) independent of any feedback physics, in BH growth modes (2) and (3), the averaging that results from successive mergers plays a major role in decreasing the scatter in M_{\bullet} correlations from the large values observed in bulgeless and pseudobulge galaxies to the small values observed in giant elliptical galaxies.

Table 1 Mass measurements of supermassive black holes in our Galaxy, M 31, and M 32

Galaxy	D (Mpc)	σ_e (km s ⁻¹)	M_\bullet ($M_{\text{low}}, M_{\text{high}}$) (M_\odot)	r_{infl} (arcsec)	σ_* (arcsec)	r_{infl}/σ_*	Reference
(1)	(2)	(3)	(4)	(5)	(6)	(7)	(8)
Galaxy			4.41(3.98–4.84) e6		0.0146	2868.	Meyer et al. 2012
Galaxy			4.2 (3.9 –4.6) e6		0.0139	3013.	Yelda et al. 2011
Galaxy	0.00828	105	4.30(3.94–4.66) e6	41.9	0.0146	2868.	Genzel, Eisenhauer & Gillessen 2010
Galaxy	0.00828	105	4.30(3.94–4.66) e6	41.9	0.0146	2868.	Gillessen et al. 2009a
Galaxy			4.09(3.74–4.43) e6		0.0148	2829.	Gillessen et al. 2009b
Galaxy			4.25(3.44–4.79) e6		0.0139	3013.	Ghez et al. 2008
Galaxy			3.80(3.60–4.00) e6		0.0056	7478.	Ghez et al. 2005
Galaxy			3.7 (3.3 –4.1) e6		0.0075	5583.	Ghez et al. 2003
Galaxy			3.8 (2.3 –5.4) e6		0.0155	2702.	Schödel et al. 2002
Galaxy			2.1 (1.3 –2.8) e6		0.113	371.	Chakrabarty & Saha 2001
Galaxy			3.1 (2.6 –3.6) e6		0.26	161.	Genzel et al. 2000
Galaxy			2.7 (2.5 –2.9) e6		0.39	107.	Ghez et al. 1998
Galaxy			2.70(2.31–3.09) e6		0.39	107.	Genzel et al. 1997
Galaxy			2.55(2.12–2.95) e6		0.39	107.	Eckart & Genzel 1997
Galaxy			2.8 (2.5 –3.1) e6		2.4	17.4	Genzel et al. 1996
Galaxy			2.0 (0.9 –2.9) e6		4.9	8.5	Haller et al. 1996
Galaxy			2.9 (2.0 –3.9) e6		3.4	12.3	Krabbe et al. 1995
Galaxy			2. e6		5	8.4	Evans & de Zeeuw 1994
Galaxy			3. e6		5	8.4	Kent 1992
Galaxy			5.4 (3.9 –6.8) e6		15	2.8	Sellgren et al. 1990
M 31	0.774	169	1.4 (1.1–2.3) e8	5.75	0.053	109.	Bender et al. 2005
M 31			1.0 e8		0.297	19.4	Peiris & Tremaine 2003
M 31			6.1 (3.6–8.7) e7		0.052	111.	Bacon et al. 2001
M 31			3.3 (1.5–4.5) e7		0.297	19.4	Kormendy & Bender 1999
M 31			6.0 (5.8–6.2) e7		0.297	19.4	Magorrian et al. 1998
M 31			9.5 (7 – 10) e7		0.42	13.7	Emsellem & Combes 1997
M 31			7.5 e7		0.56	10.3	Tremaine 1995
M 31			8.0 e7		0.42	13.7	Bacon et al. 1994
M 31			5 (4.5–5.6) e7		0.59	9.7	Richstone, Bower & Dressler 1990
M 31			3.8 (1.1– 11) e7		0.56	10.3	Kormendy 1988a
M 31			5.6 (3.4–7.8) e7		0.59	9.7	Dressler & Richstone 1988
M 32	0.805	77	2.45(1.4–3.5) e6	0.46	0.052	8.76	van den Bosch & de Zeeuw 2010
M 32			2.9 (2.7–3.1) e6		0.052	8.76	Verolme et al. 2002
M 32			3.5 (2.3–4.6) e6		0.052	8.76	Joseph et al. 2001
M 32			2.4 (2.2–2.6) e6		0.23	1.98	Magorrian et al. 1998
M 32			3.9 (3.1–4.7) e6		0.050	9.11	van der Marel et al. 1998a
M 32			3.9 (3.3–4.5) e6		0.050	9.11	van der Marel et al. 1997a, 1997b
M 32			3.2 (2.6–3.7) e6		0.23	1.98	Bender, Kormendy & Dehnen 1996
M 32			2.1 (1.8–2.3) e6		0.34	1.34	Dehnen 1995
M 32			2.1 e6		0.34	1.34	Qian et al. 1995
M 32			2.1 (1.7–2.4) e6		0.34	1.34	van der Marel et al. 1994a
M 32			2.2 (0.8–3.5) e6		0.59	0.77	Richstone, Bower & Dressler 1990
M 32			9.3 e6		0.59	0.77	Dressler & Richstone 1988
M 32			7.5 (3.5–11.5) e6		0.76	0.60	Tonry 1987
M 32			5.8 e6		1.49	0.31	Tonry 1984

Lines based on HST spectroscopy are in red. Column 2 is the assumed distance. Column 3 is the stellar velocity dispersion inside the “effective radius” that encompasses half of the light of the bulge. Column 4 is the measured BH mass with the one-sigma range that includes 68 % of the probability in parentheses. Only the top four M_\bullet values for the Galaxy include distance uncertainties in the error bars. Column 5 is the radius of the sphere of influence of the BH; the line that lists r_{infl} contains the adopted M_\bullet . Column 6 is the effective resolution of the spectroscopy, estimated as in Kormendy (2004). It is a radius that measures the blurring effects of the telescope point-spread function or “PSF,” the slit width or aperture size, and the pixel size. The contribution of the telescope is estimated by the dispersion σ_{tel} of a Gaussian fitted to the core of the average radial brightness profile of the PSF. In particular, the HST PSF has $\sigma_{\text{tel}} \sim 0.036$ from a single-Gaussian fit to the PSF model in van der Marel, de Zeeuw & Rix (1997a).

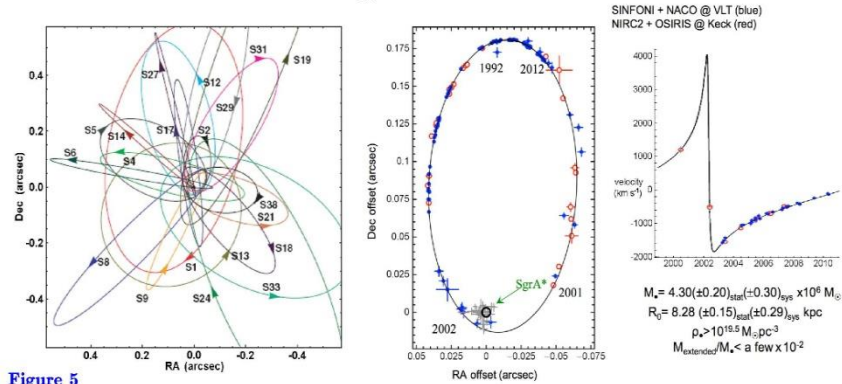


Figure 5

(left) Orbits of individual stars near the Galactic center. (right) Orbit of star S2 around the BH and associated radio source Sgr A* based on observations of its position from 1992 to 2012. Results from the Ghez group using the Keck telescope and from the Genzel group using the European Very Large Telescope (VLT) are combined. This figure is updated from Genzel, Eisenhauer & Gillessen (2010) and is kindly provided by Reinhard Genzel.

These results establish the existence and mass of the central dark object beyond any reasonable doubt. They also eliminate astrophysical plausible alternatives to a BH. These include brown dwarfs and stellar remnants (e. g., Maoz 1995, 1998; Genzel et al. 1997, 2000; Ghez et al. 1998, 2005) and even fermion balls (Ghez et al. 2005; GEG10). Bosen balls (Torres et al. 2000; Schunck & Mielke 2003; Liebling & Palenzuela 2012) are harder to exclude; they are highly relativistic, they do not have hard surfaces, and they are consistent with dynamical mass and size constraints. But a boson ball is like the proverbial elephant in a tree: it is OK where it is, but how did it ever get there? GEG10 argue that boson balls are inconsistent with astrophysical constraints based on AGN radiation. Also, the Sołtan (1982) argument implies that at least most of the central dark mass observed in galaxies grew by accretion in AGN phases, and this quickly makes highly relativistic objects collapse into BHs. Finally (Fabian 2013), X-ray AGN observations imply that we see, in some objects, material interior to the innermost stable circular orbit of a non-rotating BH; this implies that these BHs are rotating rapidly and excludes boson balls as alternatives to all central dark objects. Arguments against the most plausible BH alternatives – failed stars and dead stars – are also made for other galaxies in Maoz (1995, 1998) and in Bender et al. (2005). Exotica such as sterile neutrinos or dark matter WIMPs could still have detectable (small) effects, but we conclude that they no longer threaten the conclusion that we are detecting supermassive black holes.

KR95 was titled “Inward Bound – The Search for Supermassive Black Holes in Galactic Nuclei.” HST has taken us essentially one order of magnitude inward in radius. A few other telescopes take us closer. But mostly, we are still working at 10^4 to 10^5 Schwarzschild radii. In our Galaxy, we have observed individual stars in to ~ 500 Schwarzschild radii. Only the velocity profiles of relativistically broadened Fe K α lines (e. g., Tanaka et al. 1995; Fabian 2013) probe radii that are comparable to the Schwarzschild radius. So we are still inward bound. Joining up our measurements made at thousands of r_g with those probed by Fe K α emission requires that we robustly integrate into our story the rich and complicated details of AGN physics; that is, the narrow- and broad-emission-line regions. That journey still has far to go.

RETRO-MACHOS: π IN THE SKY?

DANIEL E. HOLZ

Institute for Theoretical Physics, University of California, Santa Barbara, CA 93106

AND

JOHN A. WHEELER

Department of Physics, Princeton University, Princeton, NJ 08544

Draft version September 20, 2004

ABSTRACT

Shine a flashlight on a black hole, and one is greeted with the return of a series of concentric rings of light. For a point source of light, and for perfect alignment of the lens, source, and observer, the rings are of infinite brightness (in the limit of geometric optics). In this manner, distant black holes can be revealed through their reflection of light from the Sun. Such retro-MACHO events involve photons leaving the Sun, making a π rotation about the black hole, and then returning to be detected at the Earth. Our calculations show that, although the light return is quite small, it may nonetheless be detectable for stellar-mass black holes at the edge of our solar system. For example, all (unobscured) black holes of mass M or greater will be observable to a limiting magnitude \bar{m} , at a distance given by: $0.02 \text{ pc} \times \sqrt[3]{10^{(\bar{m}-30)/2.5}} (M/10 M_{\odot})^2$. Discovery of a Retro-MACHO offers a way to *directly* image the presence of a black hole, and would be a stunning confirmation of strong-field general relativity.

Subject headings: gravitational lensing—black hole physics—relativity

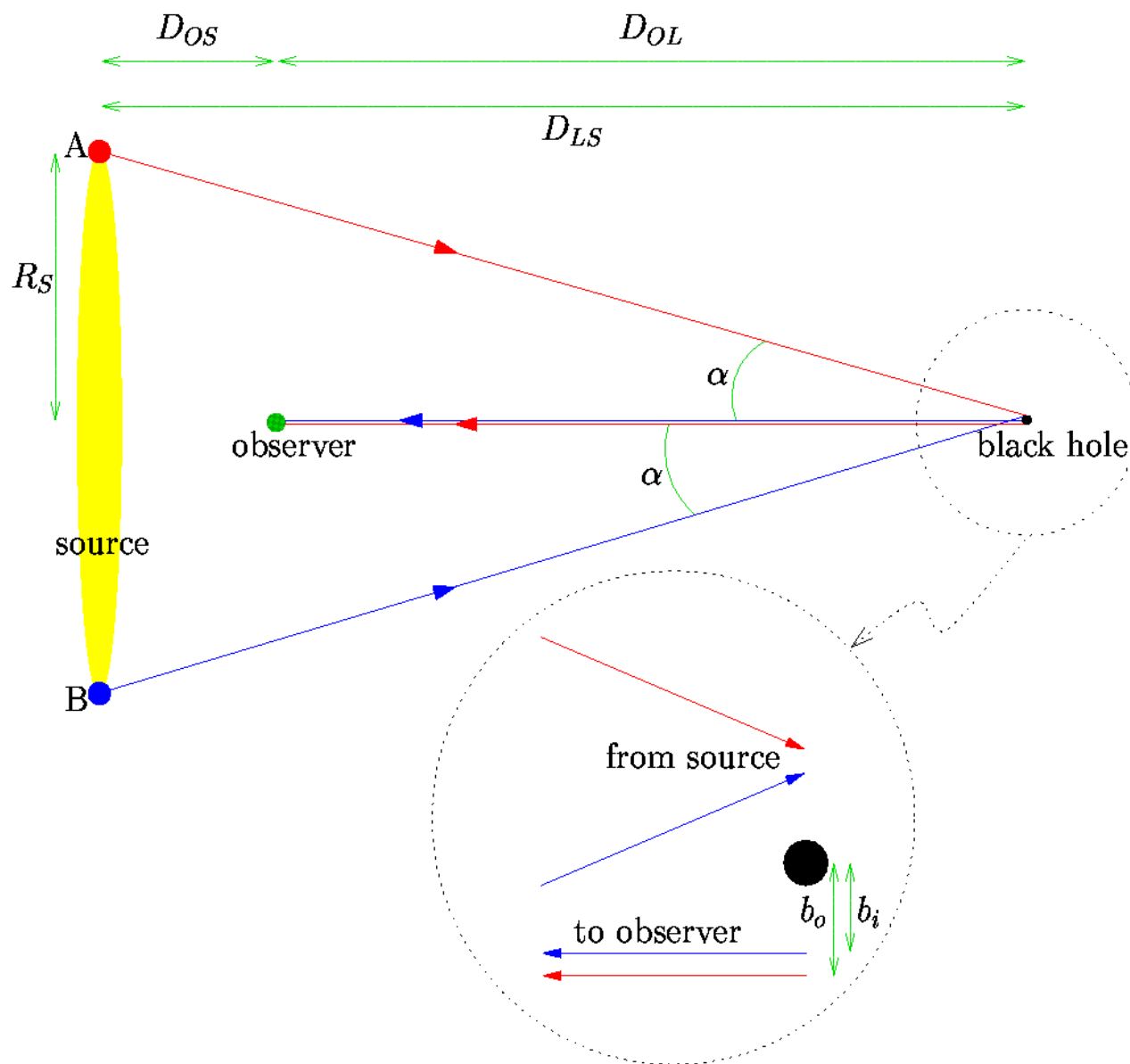


FIG. 1.— Perfect alignment: the (extended) source, observer, and lens are colinear. The resulting image of the source, as lensed by the black hole, is a ring. (The angles in this figure are greatly exaggerated.)

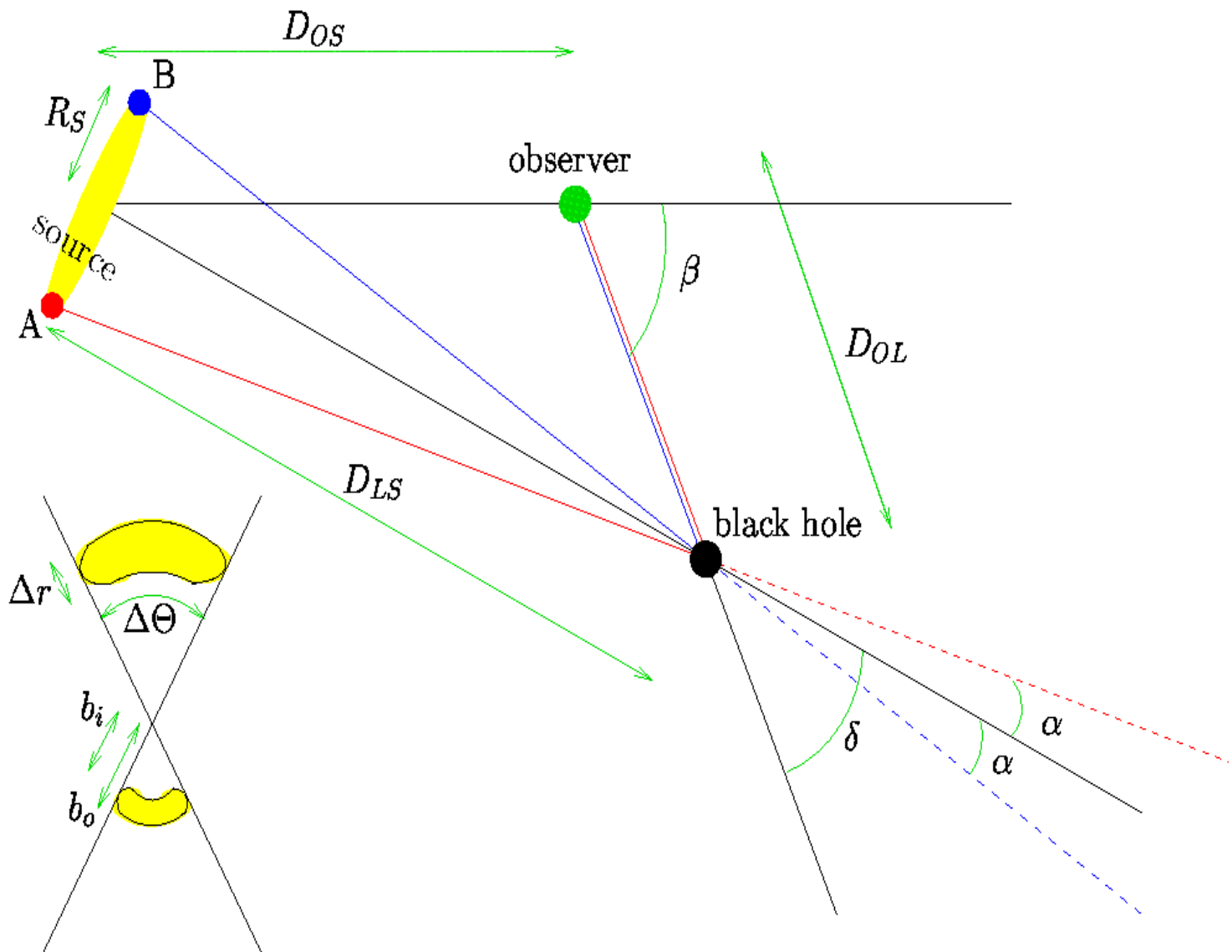


FIG. 2.— Imperfect alignment: the source, observer, and lens are not colinear. Pairs of images are produced, centered on the source–observer–lens plane, on opposite sides of the lens (see inset).

Mirages around Kerr black holes and retro-gravitational lenses

- Let us consider an illumination of black holes. Then retro-photons form caustics around black holes or mirages around black holes or boundaries around shadows.
- (Zakharov, Nucita, DePaolis, Ingrosso,
- *New Astronomy* 10 (2005) (479-489); astro-ph/0411511)



New Astronomy

Top Cited Article 2005-2010

Awarded to:

Zakharov, A.F., Nucita, A.A., Depaolis, F., Inghusso, G.

For the paper entitled:

**“Measuring the black hole parameters in the galactic center with
RADIOASTRON”**

This paper was published in:

New Astronomy, Volume 10, Issue 6, 2005

David Clark
Senior Vice President, Physical Sciences I
Amsterdam, The Netherlands



INTERNATIONAL SERIES OF
MONOGRAPHS ON PHYSICS 69

The
Mathematical Theory
of Black Holes

S. Chandrasekhar

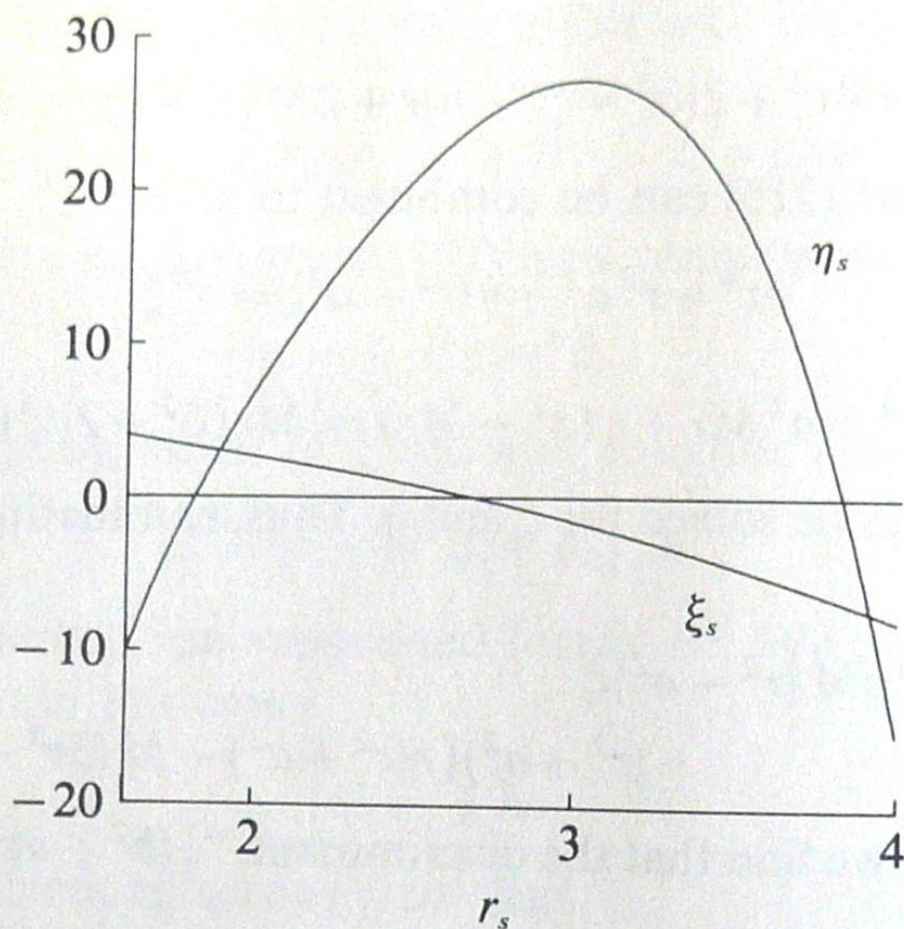


FIG. 34. The locus (ξ_s, η_s) determining the constants of the motion for three-dimensional orbits of constant radius described around a Kerr black-hole with $a = 0.8$. The unit of length along the abscissa is M .

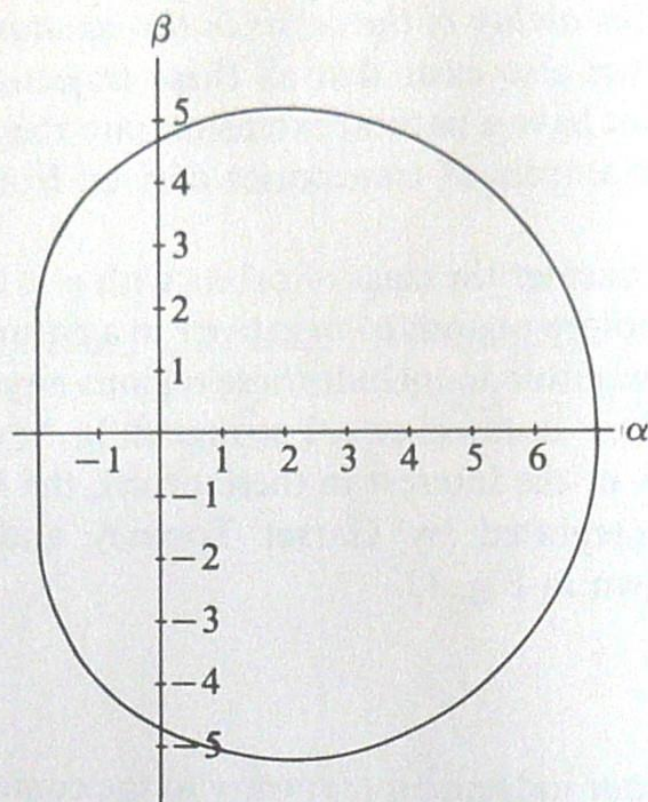


FIG. 38. The apparent shape of an extreme ($a = M$) Kerr black-hole as seen by a distant observer in the equatorial plane, if the black hole is in front of a source of illumination with an angular size larger than that of the black hole. The unit of length along the coordinate axes α and β (defined in equation (241)) is M .

black hole from infinity, the apparent shape will be determined by

$$(\alpha, \beta) = [\xi, \sqrt{\eta(\xi)}]. \quad (242)$$

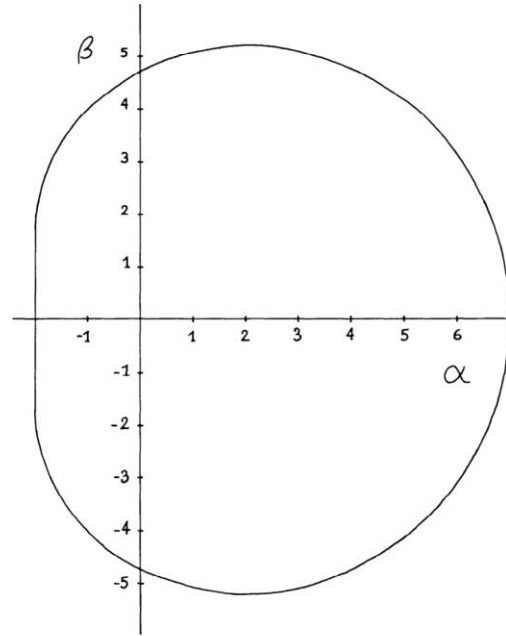


Figure 6. The apparent shape of an extreme ($a = m$) Kerr black hole as seen by a distant observer in the equatorial plane, if the black hole is in front of a source of illumination with an angular size larger than that of the black hole.

is largest there and because of the gravitational focusing effects associated with the bending of the rays toward the equatorial plane. Note that the radiation comes out along the flat portion of the apparent boundary of the extreme black hole as plotted in Figure 6.

D. Geometrical Optics

A detailed calculation of the brightness distribution coming from a source near a Kerr black hole requires more of geometrical optics than the calculation of photon trajectories. I will now review some techniques which are useful in making astrophysical calculations in connection with black holes.

The fundamental principle can be expressed as the conservation of photon density in phase space along each photon trajectory. A phase space element $d^3x d^3p$, the product of a proper spatial volume element and a physical momentum-space volume element in a local observer's frame of reference, is a Lorentz invariant, so the particular choice of local observer is arbitrary. The density $N(x^\alpha, p^{(\beta)})$ is defined

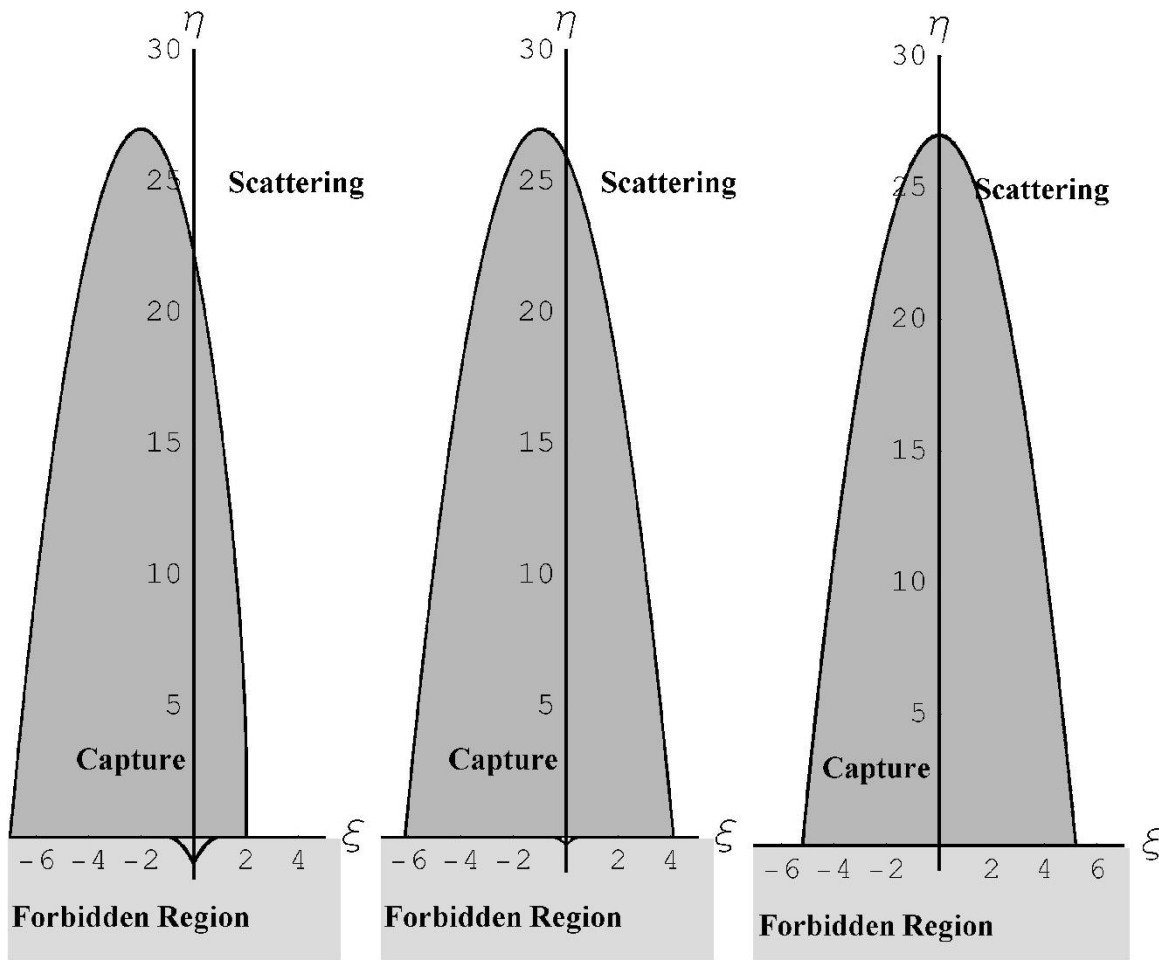


Fig. 1. Different types for photon trajectories and spin parameters ($a = 1, a = 0.5, a = 0$). Critical curves separate capture and scatter regions. Here we show also the forbidden region corresponding to constants of motion $\eta < 0$ and $(\xi, \eta) \in M$ as it was discussed in the text.

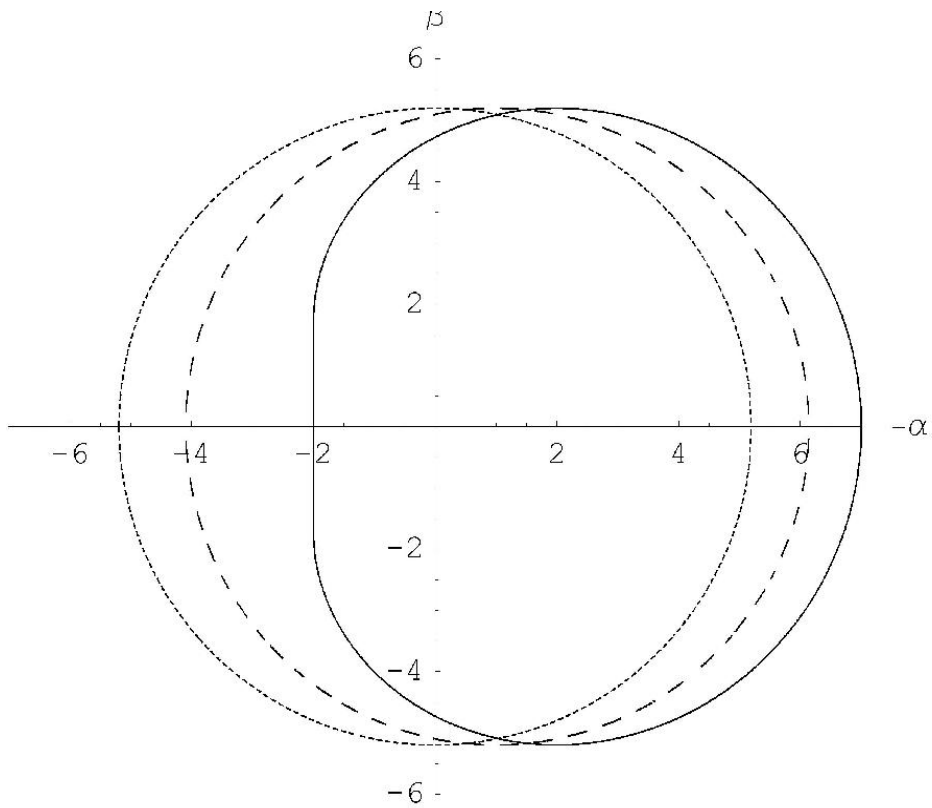


Fig. 2. Mirages around black hole for equatorial position of distant observer and different spin parameters. The solid line, the dashed line and the dotted line correspond to $a = 1$, $a = 0.5$, $a = 0$ correspondingly

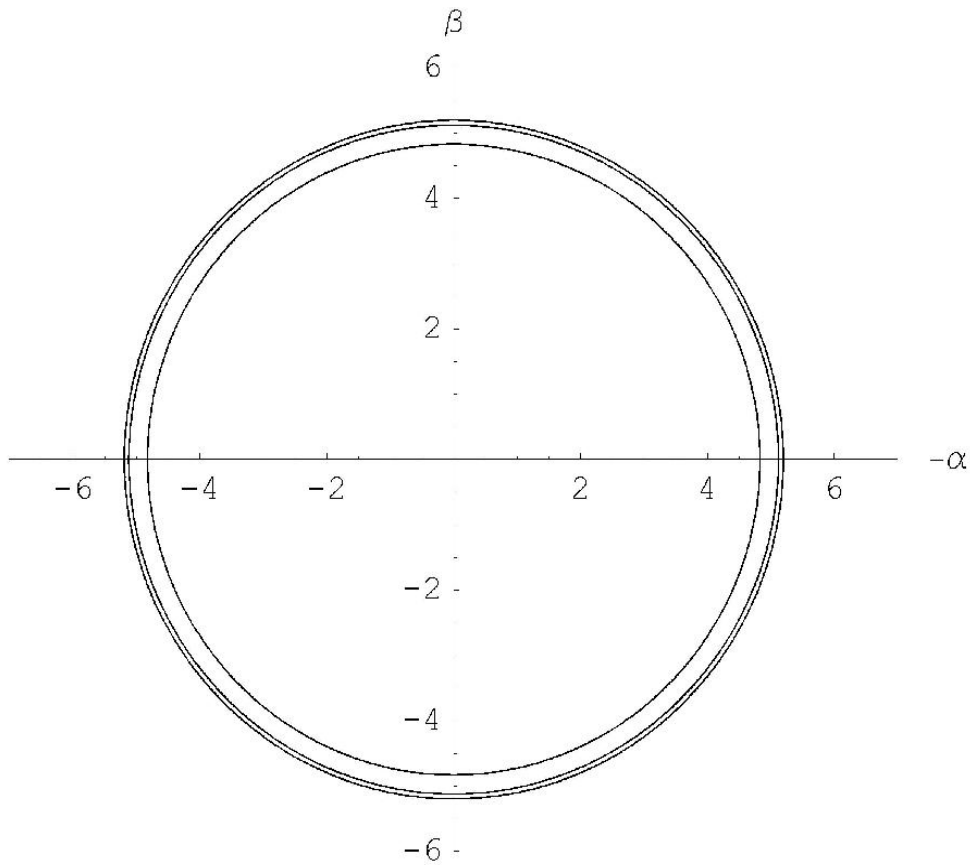


Fig. 3. Mirages around a black hole for the polar axis position of distant observer and different spin parameters ($a = 0, a = 0.5, a = 1$). Smaller radii correspond to greater spin parameters.

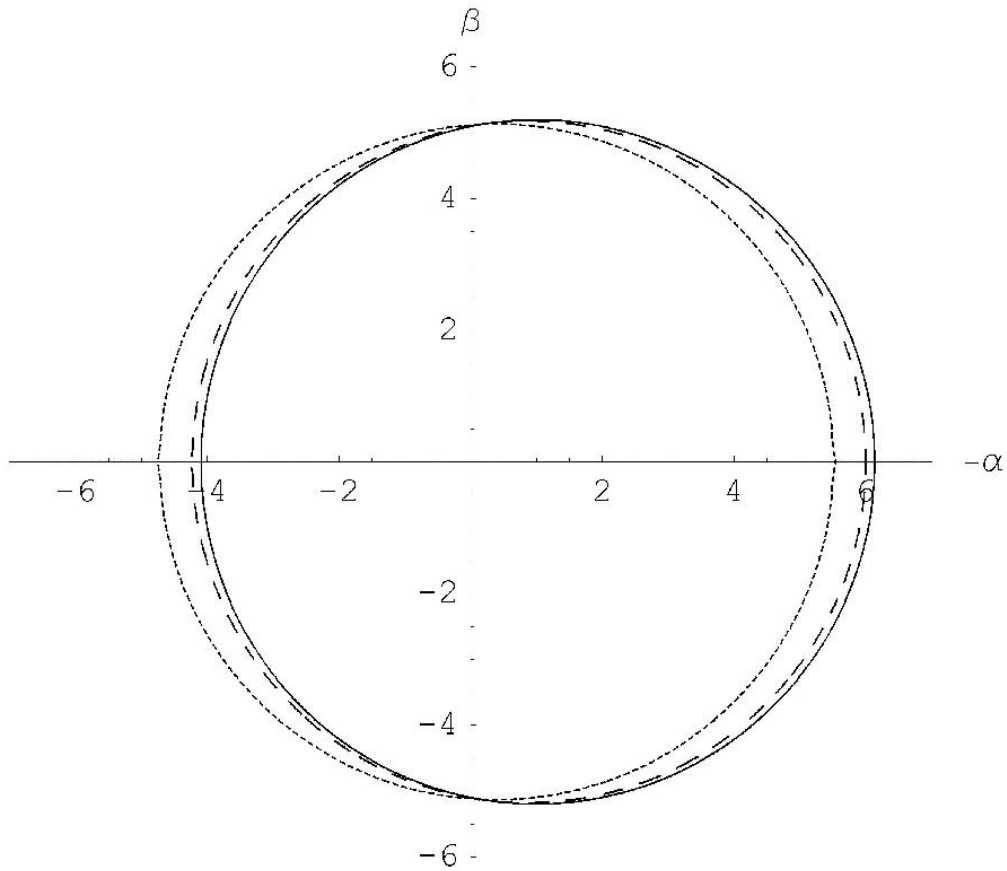


Fig. 4. Mirages around black hole for different angular positions of a distant observer and the spin $a = 0.5$. Solid, dashed and dotted lines correspond to $\theta_0 = \pi/2, \pi/3$ and $\pi/8$, respectively.

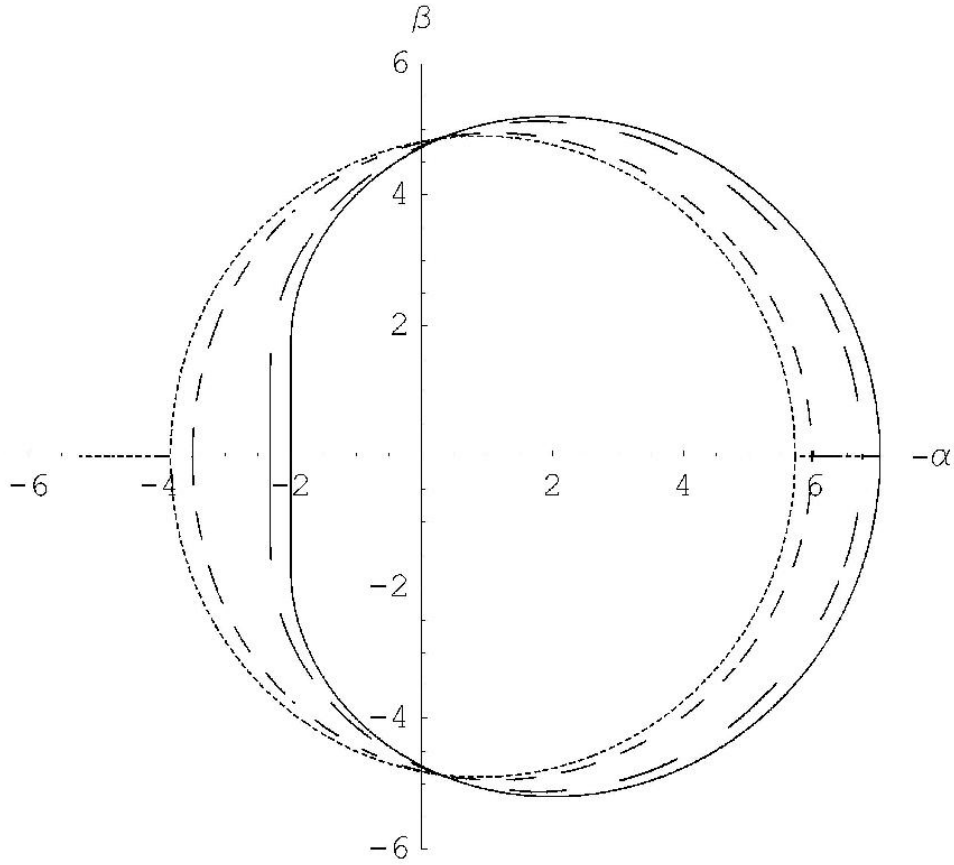


Fig. 5. Mirages around black hole for different angular positions of a distant observer and the spin $a = 1$. Solid, long dashed, short dashed and dotted lines correspond to $\theta_0 = \pi/2, \pi/3, \pi/6$ and $\pi/8$, respectively.

Direct Measurements of Black Hole Charge with Future Astrometrical Missions

A.F. Zakharov^{1,2,3}, F. De Paolis⁴, G. Ingrosso⁴, A.A. Nucita⁴

¹ Institute of Theoretical and Experimental Physics, 25, B.Cheremushkinskaya st., Moscow, 117259, Russia,

² Astro Space Centre of Lebedev Physics Institute, 84/32, Profsoyuznaya st., Moscow, 117810, Russia,

³ Joint Institute for Nuclear Research, Dubna, Russia

⁴ Department of Physics, University of Lecce and INFN, Section of Lecce, Via Arnesano, I-73100 Lecce, Italy

Received / accepted

Abstract. Recently, Zakharov et al. (2005a) considered the possibility of evaluating the spin parameter and the inclination angle for Kerr black holes in nearby galactic centers by using future advanced astrometrical instruments. A similar approach which uses the characteristic properties of gravitational retro-lensing images can be followed to measure the charge of Reissner-Nordström black hole. Indeed, in spite of the fact that their formation might be problematic, charged black holes are objects of intensive investigations. From the theoretical point of view it is well-known that a black hole is described by only three parameters, namely, its mass M , angular momentum J and charge Q . Therefore, it would be important to have a method for measuring all these parameters, preferably by model independent way. In this paper, we propose a procedure to measure the black hole charge by using the size of the retro-lensing images that can be revealed by future astrometrical missions. A discussion of the Kerr-Newmann black hole case is also offered.

$$R(r_{max}) = 0, \quad \frac{\partial R}{\partial r}(r_{max}) = 0, \quad (6)$$

as it was done, for example, by Chandrasekhar (1983) to solve similar problems.

Introducing the notation $\xi^2 = l$, $Q^2 = q$, we obtain

$$R(r) = r^4 - lr^2 + 2lr - qr. \quad (7)$$

The discriminant Δ of the polynomial $R(r)$ has the form (as it was shown by Zakharov (1991a,b, 1994a)):

$$\Delta = 16l^3[l^2(1 - q) + l(-8q^2 + 36q - 27) - 16q^3]. \quad (8)$$

The polynomial $R(r)$ thus has a multiple root if and only if

$$l^3[l^2(1 - q) + l(-8q^2 + 36q - 27) - 16q^3] = 0. \quad (9)$$

Excluding the case $l = 0$, which corresponds to a multiple root at $r = 0$, we find that the polynomial $R(r)$ has a multiple root for $r \geq r_+$ if and only if

$$l^2(1 - q) + l(-8q^2 + 36q - 27) - 16q^3 = 0. \quad (10)$$

If $q = 0$, we obtain the well-known result for a Schwarzschild black hole (Misner, Thorne and Wheeler 1973; Wald 1984; Lightman et al. 1975), $l = 27$, or $L_{cr} = 3\sqrt{3}$. If $q = 1$, then $l = 16$, or $L_{cr} = 4$, which also corresponds to numerical results given by Young (1976).

The photon capture cross section for an extreme charged black hole turns out to be considerably smaller than the capture cross section of a Schwarzschild black hole. The critical value of the impact parameter, characterizing the capture cross section for a Reissner - Nordström black hole, is determined by the equation (Zakharov 1991a,b, 1994a)

$$l = \frac{(8q^2 - 36q + 27) + \sqrt{(8q^2 - 36q + 27)^2 + 64q^3(1 - q)}}{2(1 - q)}. \quad (11)$$

A.F. Zakharov & F. De Paolis, A.A. Nucita, G.Ingrosso, **Astron. & Astrophys.**, 442, 795 (2005)

As it was explained by Zakharov et al. (2005a,b) this leads to the formation of shadows described by the critical value of L_{cr} or, in other words, in the spherically symmetric case, shadows are circles with radii L_{cr} . Therefore, measuring the shadow size, one could evaluate the black hole charge in black hole mass units M .

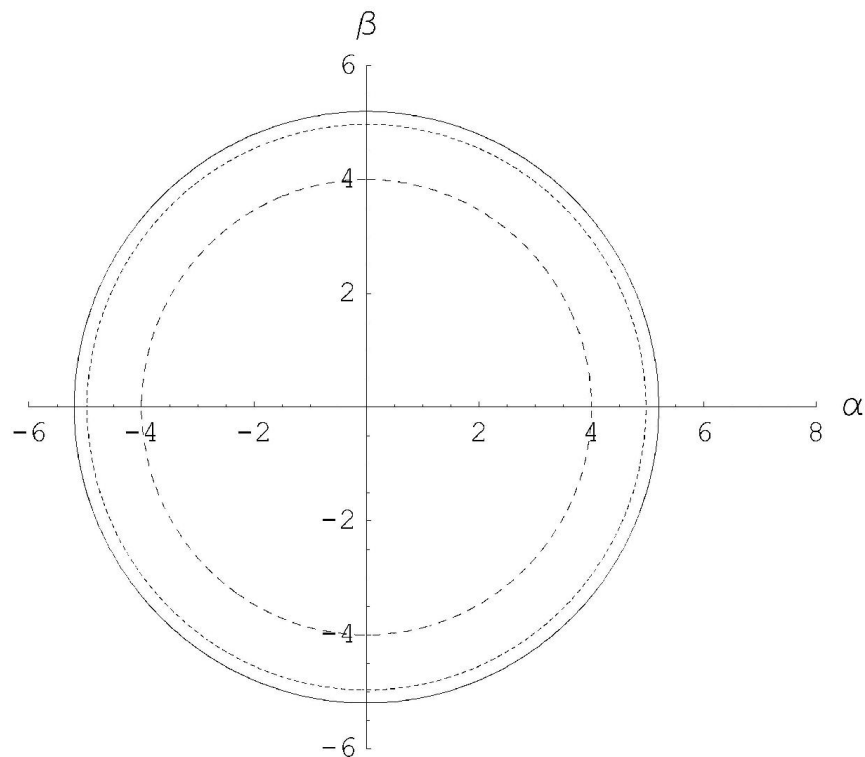


Fig. 1. Shadow (mirage) sizes are shown for selected charges of black holes $Q = 0$ (solid line), $Q = 0.5$ (short dashed line) and $Q = 1$ (long dashed line).

Constraints on a charge in the Reissner-Nordström metric for the black hole at the Galactic Center

Alexander F. Zakharov*

North Carolina Central University, Durham, North Carolina 27707, USA; Institute of Theoretical and Experimental Physics, Moscow 117218, Russia; Joint Institute for Nuclear Research, Dubna 141980, Russia; Institute for Computer Aided Design of RAS, 123056 Moscow, Russia; and National Research Nuclear University (NRNU MEPhI), 115409 Moscow, Russia
(Received 5 March 2013; published 9 September 2014)

Using an algebraic condition of vanishing discriminant for multiple roots of fourth-degree polynomials, we derive an analytical expression of a shadow size as a function of a charge in the Reissner-Nordström (RN) metric [1,2]. We consider shadows for negative tidal charges and charges corresponding to naked singularities $q = Q^2/M^2 > 1$, where Q and M are black hole charge and mass, respectively, with the derived expression. An introduction of a negative tidal charge q can describe black hole solutions in theories with extra dimensions, so following the approach we consider an opportunity to extend the RN metric to negative Q^2 , while for the standard RN metric Q^2 is always non-negative. We found that for $q > 9/8$, black hole shadows disappear. Significant tidal charges $q = -6.4$ (suggested by Bin-Nun [3–5]) are not consistent with observations of a minimal spot size at the Galactic Center observed in mm-band; moreover, these observations demonstrate that a Reissner-Nordström black hole with a significant charge $q \approx 1$ provides a better fit of recent observational data for the black hole at the Galactic Center in comparison with the Schwarzschild black hole.

DOI: 10.1103/PhysRevD.90.062007

PACS numbers: 04.80.Cc, 04.20.-q, 04.50.Gh, 04.70.Bw

I. INTRODUCTION

Soon after the discovery of general relativity (GR), the first solutions corresponding to spherical symmetric black holes were found [1,2,6]; however, initially people were rather sceptical about possible astronomical applications of the solutions corresponding to black holes [7] (see also, for instance, one of the first textbooks on GR [8]). Even after an introduction to the black hole concept by Wheeler [9] (he used the term in his public lecture in 1967 [10]), we did not know too many examples where we really need GR models with strong gravitational fields that arise near black hole horizons to explain observational data. The cases where we need strong field approximation are very important since they give an opportunity to check GR predictions in a strong field limit; therefore, one could significantly constrain alternative theories of gravity.

One of the most important options to test gravity in the strong field approximation is analysis of relativistic line shape as it was shown in [11], with assumptions that a line emission is originated at a circular ring area of a flat accretion disk. Later on, such signatures of the Fe $K\alpha$ line have been found in the active galaxy MCG-6-30-15 [12]. Analyzing the spectral line shape, the authors concluded the emission region is so close to the black hole horizon that one has to use Kerr metric approximation [13] to fit observational data [12]. Results of simulations of iron $K\alpha$ line formation are given in [14,15] (where we used our

approach [16]); see also [17] for a more recent review of the subject.

Now there are two basic observational techniques to investigate a gravitational potential at the Galactic Center, namely, (a) monitoring the orbits of bright stars near the Galactic Center to reconstruct a gravitational potential [18] (see also a discussion about an opportunity to evaluate black hole dark matter parameters in [19] and an opportunity to constrain some class of an alternative theory of gravity [20]) and (b) measuring in mm band, with VLBI technique, the size and shape of shadows around the black hole, giving an alternative possibility to evaluate black hole parameters. The formation of retro-lensing images (also known as mirages, shadows, or “faces” in the literature) due to the strong gravitational field effects nearby black holes has been investigated by several authors [21–24].

Theories with extra dimensions admit astrophysical objects (supermassive black holes in particular) which are rather different from standard ones. Tests have been proposed when it would be possible to discover signatures of extra dimensions in supermassive black holes since the gravitational field may be different from the standard one in the GR approach. So, gravitational lensing features are different for alternative gravity theories with extra dimensions and general relativity.

Recently, Bin-Nun [3–5] discussed the possibility that the black hole at the Galactic Center is described by the tidal Reissner-Nordström metric which may be admitted by the Randall-Sundrum II braneworld scenario [25]. Bin-Nun suggested an opportunity of evaluating the black hole

*zakharov@itep.ru

$$\text{Dis}(s_1, s_2, s_3, s_4) = \begin{vmatrix} 1 & 1 & 1 & 1 \\ X_1 & X_2 & X_3 & X_4 \\ X_1^2 & X_2^2 & X_3^2 & X_4^2 \\ X_1^3 & X_2^3 & X_3^3 & X_4^3 \end{vmatrix}^2 = \begin{vmatrix} 4 & p_1 & p_2 & p_3 \\ p_1 & p_2 & p_3 & p_4 \\ p_2 & p_3 & p_4 & p_5 \\ p_3 & p_4 & p_5 & p_6 \end{vmatrix}. \quad (20)$$

Expressing the polynomials p_k ($1 \leq k \leq 6$) in terms of the polynomials s_k ($1 \leq k \leq 4$) and using Newton's equations

$$\text{Dis}(s_1, s_2, s_3, s_4) = \begin{vmatrix} 4 & 0 & 2l & -6l \\ 0 & 2l & -6l & 2l(l+2q) \\ 2l & -6l & 2l(l+2q) & -10l^2 \\ -6l & 2l(l+2q) & -10l^2 & 2l^2(l+6+3q) \end{vmatrix} = 16l^3[l^2(1-q) + l(-8q^2 + 36q - 27) - 16q^3]. \quad (22)$$

The polynomial $R(r)$ thus has a multiple root if and only if

$$l^3[l^2(1-q) + l(-8q^2 + 36q - 27) - 16q^3] = 0. \quad (23)$$

Excluding the case $l = 0$, which corresponds to a multiple root at $r = 0$, we find that the polynomial $R(r)$ has a multiple root for $r \geq r_+$ if and only if

$$l^2(1-q) + l(-8q^2 + 36q - 27) - 16q^3 = 0. \quad (24)$$

If $q = 0$, we obtain the well-known result for a Schwarzschild black hole [38,39,49], $l_{\text{cr}} = 27$, or $\xi_{\text{cr}} = 3\sqrt{3}$ [where l_{cr} is the positive root of Eq. (24)]. If $q = 1$, then $l = 16$, or $\xi_{\text{cr}} = 4$, which also corresponds to numerical results given in paper [50]. The photon capture cross section for an extreme charged black hole turns out to be considerably smaller than the capture cross section of a Schwarzschild black hole. The critical value of the impact parameter, characterizing the capture cross section for a RN black hole, is determined by the equation

$$l_{\text{cr}} = \frac{(8q^2 - 36q + 27) + \sqrt{D_1}}{2(1-q)}, \quad (25)$$

where $D_1 = (8q^2 - 36q + 27)^2 + 64q^3(1-q) = -512(q - \frac{9}{8})^3$. It is clear from the last relation that there are circular unstable photon orbits only for $q \leq \frac{9}{8}$ (see also results in [37] about the same critical value). Substituting Eq. (25) into the expression for the coefficients of the polynomial $R(r)$ it is easy to calculate the radius of the unstable circular photon orbit (which is the same as the minimum periastron

distance). The orbit of a photon moving from infinity with the critical impact parameter, determined in accordance with Eq. (25) spirals into circular orbit. To find a radius of photon unstable orbit we will solve Eq. (7) substituting l_{cr} in the relation. From trigonometric formula for roots of cubic equation we have

$$\begin{aligned} p_1 &= s_1 = 0, & p_2 &= -2s_2, & p_3 &= 3s_3, \\ p_4 &= 2s_2^2 - 4s_4, & p_5 &= -5s_3s_2, \\ p_6 &= -2s_2^3 + 3s_3^2 + 6s_4s_2, \end{aligned} \quad (21)$$

where $s_1 = 0$, $s_2 = -l$, $s_3 = -2l$, $s_4 = -ql$, corresponding to the polynomial $R(r)$ in Eq. (8). The discriminant Dis of the polynomial $R(r)$ has the form

The orbit of a photon moving from infinity with the critical impact parameter, determined in accordance with Eq. (25) spirals into circular orbit. To find a radius of photon unstable orbit we will solve Eq. (7) substituting l_{cr} in the relation. From trigonometric formula for roots of cubic equation we have

$$r_{\text{crit}} = 2\sqrt{\frac{l_{\text{cr}}}{6}} \cos \frac{\alpha}{3}, \quad (26)$$

where

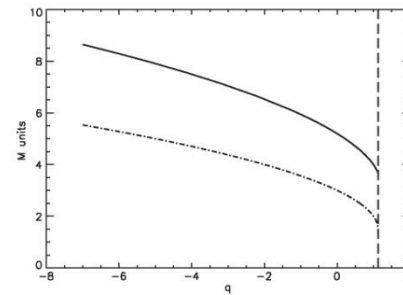


FIG. 1. Shadow (mirage) radius (solid line) and radius of the last circular unstable photon orbit (dot-dashed line) in M units as a function of q . The critical value $q = 9/8$ is shown with dashed vertical line.

Unstable photon orbits but not shadows could exist for naked singularities with $1 < Q^2 < 9/8$, while in paper arxiv:1802.08060[astro-ph.HE], the authors presented an example of naked singularities with a shadows.

Some time ago Bin-Nun (2010) discussed an opportunity that the black hole at the Galactic Center is described by the tidal Reissner--Nordstrom metric which may be admitted by the Randall--Sundrum II braneworld scenario. Bin-Nun suggested an opportunity of evaluating the black hole metric analyzing (retro-)lensing of bright stars around the black hole in the Galactic Center. Doeleman et al. (2008) evaluated a shadow size for the black hole at the Galactic Center. Measurements of the shadow size around the black hole may help to evaluate parameters of black hole metric Zakharov et al (2005). We derive an analytic expression for the black hole shadow size as a function of charge for the tidal Reissner--Nordstrom metric. We conclude that observational data concerning shadow size measurements are not consistent with significant negative charges, in particular, the significant negative charge $Q/(4M^2)=-1.6$ (discussed by Bin-Nun (2010) is practically ruled out with a very probability (the charge is roughly speaking is beyond 9σ confidence level, but a negative charge is beyond 3σ confidence level).

LETTERS

Event-horizon-scale structure in the supermassive black hole candidate at the Galactic Centre

Sheperd S. Doeleman¹, Jonathan Weintroub², Alan E. E. Rogers¹, Richard Plambeck³, Robert Freund⁴, Remo P. J. Tilanus^{5,6}, Per Friberg⁵, Lucy M. Ziurys⁴, James M. Moran², Brian Corey¹, Ken H. Young², Daniel L. Smythe¹, Michael Titus¹, Daniel P. Marrone^{7,8}, Roger J. Cappallo¹, Douglas C.-J. Bock⁹, Geoffrey C. Bower³, Richard Chamberlin¹⁰, Gary R. Davis⁵, Thomas P. Krichbaum¹¹, James Lamb¹², Holly Maness³, Arthur E. Niell¹, Alan Roy¹¹, Peter Strittmatter⁴, Daniel Werthimer¹³, Alan R. Whitney¹ & David Woody¹²

The cores of most galaxies are thought to harbour supermassive black holes, which power galactic nuclei by converting the gravitational energy of accreting matter into radiation¹. Sagittarius A* (Sgr A*), the compact source of radio, infrared and X-ray emission at the centre of the Milky Way, is the closest example of this phenomenon, with an estimated black hole mass that is 4,000,000 times that of the Sun^{2,3}. A long-standing astronomical goal is to resolve structures in the innermost accretion flow surrounding Sgr A*, where strong gravitational fields will distort the appearance of radiation emitted near the black hole. Radio observations at wavelengths of 3.5 mm and 7 mm have detected intrinsic structure in Sgr A*, but the spatial resolution of observations at these wavelengths is limited by interstellar scattering^{4–7}. Here we report observations at a wavelength of 1.3 mm that set a size of 37^{+16}_{-10} microarcseconds on the intrinsic diameter of Sgr A*. This is less than the expected apparent size of the event horizon of the presumed black hole, suggesting that the bulk of Sgr A* emission may not be centred on the black hole, but arises in the surrounding accretion flow.

The proximity of Sgr A* makes the characteristic angular size scale of the Schwarzschild radius ($R_{\text{Sch}} = 2GM/c^2$) larger than for any other black hole candidate. At a distance of ~ 8 kpc (ref. 8), the Sgr A* Schwarzschild radius is 10 μas , or 0.1 astronomical unit (AU). Multi-wavelength monitoring campaigns^{9–11} indicate that activity on scales of a few R_{Sch} in Sgr A* is responsible for observed short-term variability and flaring from radio to X-rays, but direct observations of structure on these scales by any astronomical technique has not been possible. Very-long-baseline interferometry (VLBI) at 7 mm and 3.5 mm wavelength shows the intrinsic size of Sgr A* to have a wavelength dependence, which yields an extrapolated size at 1.3 mm of 20–40 μas (refs 6, 7). VLBI images at wavelengths longer than 1.3 mm, however, are dominated by interstellar scattering effects that broaden images of Sgr A*. Our group has been working to extend VLBI arrays to 1.3 mm wavelength, to reduce the effects of interstellar scattering, and to utilize long baselines to increase angular resolution with a goal of studying the structure of Sgr A* on scales commensurate with the putative event horizon of the black hole. Previous pioneering VLBI work at 1.4 mm wavelength

uncertainties resulted in a range for the derived size of 50–170 μas (ref. 12).

On 10 and 11 April 2007, we observed Sgr A* at 1.3 mm wavelength with a three-station VLBI array consisting of the Arizona Radio Observatory 10-m Submillimetre Telescope (ARO/SMT) on Mount Graham in Arizona, one 10-m element of the Combined Array for Research in Millimeter-wave Astronomy (CARMA) in Eastern California, and the 15-m James Clerk Maxwell Telescope (JCMT) near the summit of Mauna Kea in Hawaii. A hydrogen maser time standard and high-speed VLBI recording system were installed at both the ARO/SMT and CARMA sites to support the observation. The JCMT partnered with the Submillimetre Array (SMA) on Mauna Kea, which housed the maser and the VLBI recording system and provided a maser-locked receiver reference to the JCMT. Two 480-MHz passbands sampled to two-bit precision were recorded at each site, an aggregate recording rate of 3.84×10^9 bits per second (Gbit s^{-1}). Standard VLBI practice is to search for detections over a range of interferometer delay and delay rate. Six bright quasars were detected with high signal to noise on all three baselines allowing array geometry, instrumental delays and frequency offsets to be accurately calibrated. This calibration greatly reduced the search space for detections of Sgr A*. All data were processed on the Mark4 correlator at the MIT Haystack Observatory in Massachusetts.

On both 10 and 11 April 2007, Sgr A* was robustly detected on the short ARO/SMT–CARMA baseline and the long ARO/SMT–JCMT baseline. On neither day was Sgr A* detected on the CARMA–JCMT baseline, which is attributable to the sensitivity of the CARMA station being about a third that of the ARO/SMT (owing to weather, receiver temperature and aperture efficiency). Table 1 lists the Sgr A* detections on the ARO/SMT–JCMT baseline. The high signal to noise ratio, coupled with the tight grouping of residual delays and delay rates, makes the detections robust and unambiguous.

There are too few visibility measurements to form an image by the usual Fourier transform techniques; hence, we fit models to the visibilities (shown in Fig. 1). We first modelled Sgr A* as a circular Gaussian brightness distribution, for which one expects a Gaussian relationship between correlated flux density and projected baseline length. The weighted least-squares best-fit model (Fig. 1) corre-

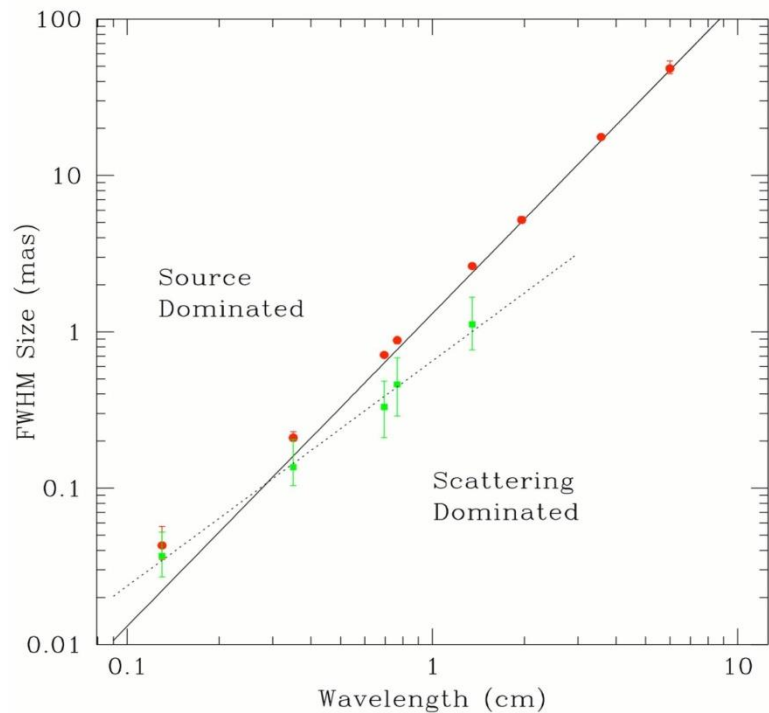


Fig 2

Figure 2 Observed and intrinsic size of Sgr A* as a function of wavelength. Red circles show major-axis observed sizes of Sgr A* from VLBI observations (all errors 3σ). Data from wavelengths of 6 cm to 7 mm are from ref. 13, data at 3.5 mm are from ref. 7, and data at 1.3 mm are from the observations reported here. The solid line is the best-fit λ^2 scattering law from ref. 13, and is derived from measurements made at $\lambda > 17$ cm. Below this line, measurements of the intrinsic size of Sgr A* are dominated by scattering effects, while measurements that fall above the line indicate intrinsic structures that are larger than the scattering size (a ‘source-dominated’ regime). Green points show derived major-axis intrinsic sizes from $2 \text{ cm} < \lambda < 1.3 \text{ mm}$ and are fitted with a λ^α power law ($\alpha = 1.44 \pm 0.07$, 1σ) shown as a dotted line. When the 1.3-mm point is removed from the fit, the power-law exponent becomes $\alpha = 1.56 \pm 0.11$ (1σ).

RADIO INTERFEROMETER MUCH LARGER THE EARTH

“SPECTR-R” (Mission “RadioAstron”)

Main scientific tasks of the mission –

syntheses of high-precision images of various Universe objects, its coordinates measurements and search their variability with the time. A fringe width of the system is up to 7 micro arc seconds.

Main characteristics of the space radio telescope

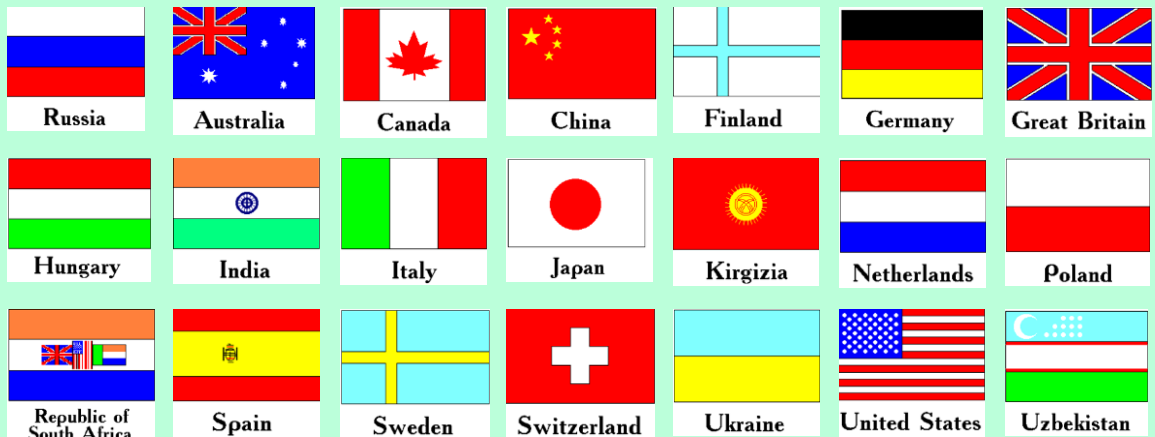
Spectral band:

- wavelength (cm) - 92; 18; 6.2; 1.19-1.63
- frequency (GHz) - 0.327; 1.66; 4.83; 18-26

Main organizations:

on scientific complex - Astro Space Center of Lebedev Physical Institute of Russian Academy of Science;

of spacecraft - Lavochkin Research Production Association of Russian Space Agency.

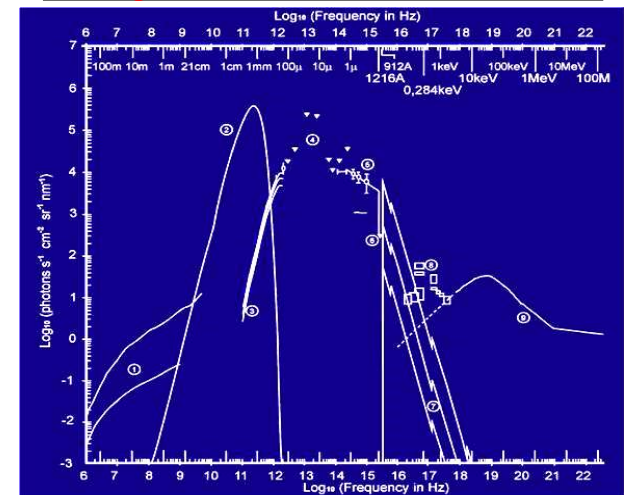


Planned launch date of the mission is **2007**.



The orbit of the mission :

apogee -	310 000 - 370 000 km
perigee -	10 000 - 70 000 km
declination -	51.6°
period variation -	7 - 10 days
Guaranteed time of activity -	5 years
Scientific payload mass -	2100 kg



- **ERC Synergy Grant to image event horizon of black hole**
- **Was Einstein right? The European Research Council (ERC) has awarded 14 Million Euros to a team of European astrophysicists to construct the first accurate image of a black hole. The team will test the predictions of current theories of gravity, including Einstein's theory of General Relativity. The funding is provided in the form of a 'Synergy Grant', the largest and most competitive type of grant of the ERC.**

Synergy grants are awarded by the ERC, on the basis of scientific excellence in an intricate and highly competitive selection procedure. The grants have a maximum limit of 15 Million Euros and require the collaboration of 2-4 principal investigators. In the current selection round the ERC honoured 13 out of 449 funding proposal, which corresponds to a success rate of less than 3%. Proposals were submitted from all areas of European science. This is the first time an astrophysics proposal has been awarded.

Black holes

Black holes are notoriously elusive with a gravitational field so large that even light cannot escape their grip. The team plans to make an image of the event horizon – the border around a black hole which light can enter, but not leave.

“While most astrophysicists believe black holes exists, nobody has actually ever seen one”, says Heino Falcke, Professor in radio astronomy at Radboud University in Nijmegen and ASTRON, The Netherlands. “The technology is now advanced enough that we can actually image black holes and check if they truly exist as predicted: If there is no event horizon, there are no black holes”.

Measure the tiniest shadow

So, if black holes are black and are hard to catch on camera, where should one look? The scientists want to peer into the heart of our own Galaxy, which hosts a mysterious radio source, called Sagittarius A*. The object is known to have a mass of around 4 million times the mass of the Sun and is considered to be the central supermassive black hole of the Milky Way.

As gaseous matter is attracted towards the event horizon by the black hole's gravitational attraction, strong radio emission is produced before the gas disappears. The event horizon should then cast a dark shadow on that bright emission. Given the huge distance to the centre of the Milky Way, the size of the shadow is equivalent to an apple on the moon seen from the earth.

However, by combining high-frequency radio telescopes around the world, in a technique called very long baseline interferometry, or VLBI, even such a tiny feature is in principle detectable. Falcke first proposed this experiment 15 years ago and now an international effort is forming to build a global “Event Horizon Telescope” to realize it. Falcke is convinced: “With this grant from the ERC and the excellent expertise in Europe, we will be able to make it happen together with our international partners”.

•

- *The BlackHoleCam network*

Find more radio pulsars

In addition, the group wants to use the same radio telescopes to find and measure pulsars around the very same black hole. Pulsars are rapidly spinning neutron stars, which can be used as highly accurate natural clocks in space. “A pulsar around a black hole would be extremely valuable”, explains Michael Kramer, managing director of the Max-Planck-Institut für Radioastronomie in Bonn. “They allow us to determine the deformation of space and time caused by black holes and measure their properties with unprecedented precision”. However, while radio pulsars are ubiquitous in our Milky Way, surprisingly none had been found in the centre of the Milky Way for decades. Only recently Kramer and his team found the very first radio pulsar around Sagittarius A*. “We suspect there are many more radio pulsars, and if they are there we will find them”, says Kramer.

Behaviour of light and matter

But how will scientists be really sure that there is a black hole in our Milky Way and not something else that behaves in a very similar way? To answer this question, the scientists will combine the information from the black hole shadow and from the motion of pulsars and stars around Sagittarius A* with detailed computer simulations of the behaviour of light and matter around black holes as predicted by theory.

We have made enormous progress in computational astrophysics in recent years”, states Luciano Rezzolla, Professor of theoretical astrophysics at the Goethe University in Frankfurt and leader of the gravitational-wave modelling group at the Max-Planck-Institut für Gravitationsphysik in Potsdam.

“We can now calculate very precisely how space and time are warped by the immense gravitational fields of a black hole, and determine how light and matter propagate around black holes”, he remarks. “Einstein’s theory of General Relativity is the best theory of gravity we know, but it is not the only one. We will use these observations to find out if black holes, one of the most cherished astrophysical objects, exist or not. Finally, we have the opportunity to test gravity in a regime that until recently belonged to the realm of science fiction; it will be a turning point in modern science”, says Rezzolla.

Partners in Europe

The principal investigators will closely collaborate with a number of groups throughout Europe. Team members in the ERC grant are:

- Robert Laing from the European Southern Observatory (ESO) in Garching, European project scientist of ALMA, a new high-frequency radio telescope, that the team seeks to use for their purpose,
- Frank Eisenhauer from the Max-Planck-Institut für extraterrestrische Physik in Garching, principal investigator of the upcoming GRAVITY instrument for the ESO Very Large Telescope Interferometer, to precisely measure the motion of stars and infrared flares around the Galactic Centre black hole.
- Huib van Langevelde, director of the Joint Institute for VLBI in Europe (JIVE) and Professor of Galactic radio astronomy at the University of Leiden.

The efforts of the Max-Planck-Institut für Radioastronomie will be conducted jointly with the VLBI group and the high-frequency radio astronomy groups at the institute and their directors Anton Zensus and Karl Menten.

The scientists also want to make use of the two major European millimeter radio observatories (NOEMA and the IRAM 30m telescope) operated by IRAM, a joint German/French/Spanish radio astronomy institute.

- The team led by three principal investigators (Heino Falcke, Radboud University Nijmegen and ASTRON, Michael Kramer, Max-Planck-Institut für Radioastronomie, and Luciano Rezzolla, Goethe University in Frankfurt and Max-Planck-Institut für Gravitationsphysik) will combine several telescopes around the globe to peer into the heart of our own Galaxy, which hosts a mysterious radio source, called Sagittarius A*. It is considered to be the central super massive black hole.

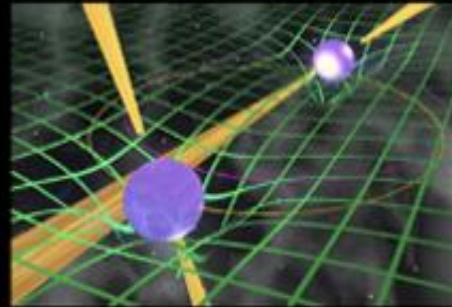
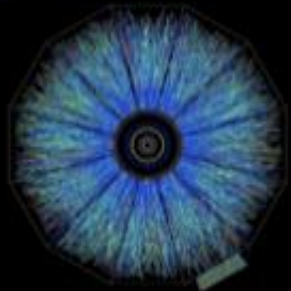
- H. Falcke, S. Markoff, Toward the event horizon—the supermassive black hole in the Galactic Center, *Classical and Quantum Gravity*, 30, Issue 24, 244003 (2013)
- The review has quoted two our papers

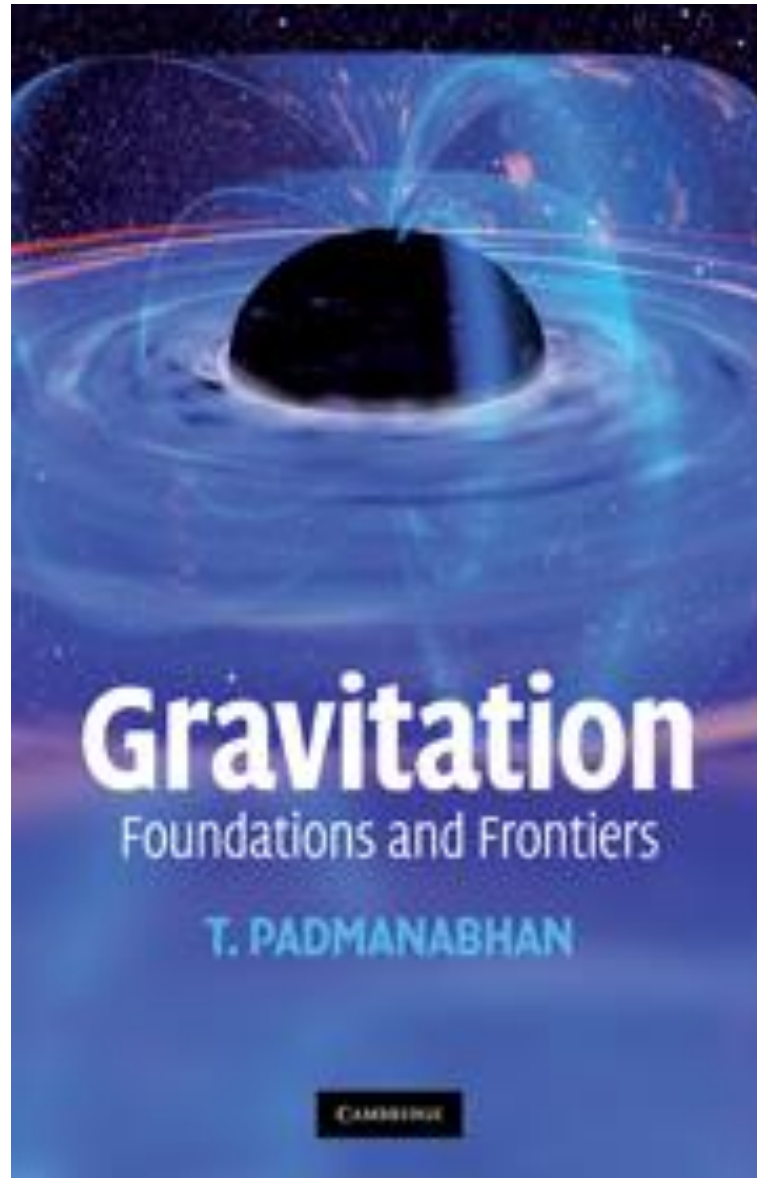




FIAS Frankfurt Institute
for Advanced Studies

Karl Schwarzschild Meeting 2015





Gravitation

Foundations and Frontiers

T. PADMANABHAN

CAMBRIDGE

An ultraluminous quasar with a twelve-billion-solar-mass black hole at redshift 6.30

Xue-Bing Wu^{1,2}, Feige Wang^{1,2}, Xiaohui Fan^{2,3}, Weimin Yi^{4,5,6}, Wenwen Zuo⁷, Fuyan Bian⁸, Linhua Jiang², Ian D. McGreer³, Ran Wang², Jinyi Yang^{1,2}, Qian Yang^{1,2}, David Thompson⁹ & Yuri Beletsky¹⁰

So far, roughly 40 quasars with redshifts greater than $z = 6$ have been discovered^{1–8}. Each quasar contains a black hole with a mass of about one billion solar masses ($10^9 M_{\odot}$)^{3,6,7,9–13}. The existence of such black holes when the Universe was less than one billion years old presents substantial challenges to theories of the formation and growth of black holes and the coevolution of black holes and galaxies¹⁴. Here we report the discovery of an ultraluminous quasar, SDSS J010013.02+280225.8, at redshift $z = 6.30$. It has an optical and near-infrared luminosity a few times greater than those of previously known $z > 6$ quasars. On the basis of the deep absorption trough¹⁵ on the blue side of the Lyman- α emission line in the spectrum, we estimate the proper size of the ionized proximity zone associated with the quasar to be about 26 million light years, larger than found with other $z > 6.1$ quasars with lower luminosities¹⁶. We estimate (on the basis of a near-infrared spectrum) that the black hole has a mass of $\sim 1.2 \times 10^{10} M_{\odot}$, which is consistent with the $1.3 \times 10^{10} M_{\odot}$ derived by assuming an Eddington-limited accretion rate.

High-redshift quasars have been efficiently selected using a combination of optical and near-infrared colours^{3,4}. We have carried out a systematic survey of quasars at $z > 5$ using photometry from the Sloan Digital Sky Survey (SDSS)¹⁷, the two Micron All Sky Survey (2MASS)¹⁸ and the Wide-field Infrared Survey Explorer (WISE)¹⁹, resulting in the discovery of a significant population of luminous high-redshift quasars. SDSS J010013.02+280225.8 (hereafter J0100+2802) was selected as a high-redshift quasar candidate owing to its red optical colour (with SDSS AB magnitudes $i_{AB} = 20.84 \pm 0.06$ and $z_{AB} = 18.33 \pm 0.03$) and a photometric redshift of $z \approx 6.3$. It has bright detections in the 2MASS J, H and K_s bands with Vega magnitudes of 17.00 ± 0.20 , 15.98 ± 0.19 and 15.20 ± 0.16 , respectively; it is also strongly detected in WISE, with Vega magnitudes in W1 to W4 bands of 14.45 ± 0.03 , 13.63 ± 0.03 , 11.71 ± 0.21 and 8.98 ± 0.44 , respectively (see Extended Data Figs 1 and 2 for images in different bands). Its colour in the two bluest WISE bands, W1 and W2, clearly differentiates it from the bulk of stars in our Galaxy²⁰. The object was within the SDSS-III imaging area. It is close to the colour selection boundary of SDSS $z \approx 6$ quasars¹, but was assigned to low priority earlier because of its relatively red $z_{AB} - J$ colour and its bright apparent magnitudes. It is undetected in both radio and X-ray bands by the wide-area, shallow survey instruments.

Initial optical spectroscopy on J0100+2802 was carried out on 29 December 2013 with the Lijiang 2.4-m telescope in China. The low-resolution spectrum clearly shows a sharp break at about $8,800 \text{ \AA}$, con-

We use the multiwavelength photometry to estimate the optical luminosity at rest-frame wavelength $3,000 \text{ \AA}$ ($L_{3,000}$), which is consistent with that obtained from K-band spectroscopy (see below). The latter gives a more reliable value of $(3.15 \pm 0.47) \times 10^{47} \text{ erg s}^{-1}$, adopting a Λ CDM cosmology with Hubble constant $H_0 = 70 \text{ km s}^{-1} \text{ Mpc}^{-1}$, matter density parameter $\Omega_M = 0.30$ and dark energy density parameter $\Omega_{\Lambda} = 0.7$. Assuming an empirical conversion factor from the luminosity at $3,000 \text{ \AA}$ to the bolometric luminosity²¹, this gives $L_{\text{bol}} = 5.15 \times L_{3,000} = 1.62 \times 10^{48} \text{ erg s}^{-1} = 4.29 \times 10^{14} L_{\odot}$ (where L_{\odot} is the solar luminosity). We obtain a similar result when estimating the bolometric luminosity from the Galactic extinction corrected absolute magnitude at rest-frame $1,450 \text{ \AA}$, which is $M_{1,450,AB} = -29.26 \pm 0.20$. The luminosity of this

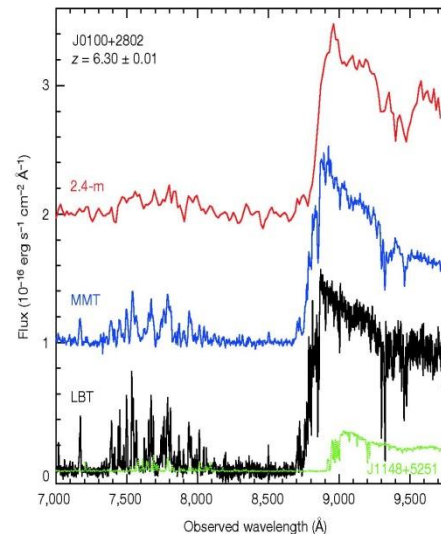


Figure 1 | The optical spectra of J0100+2802. From top to bottom, spectra taken with the Lijiang 2.4-m telescope, the MMT and the LBT (in red, blue and black colours), respectively. For clarity, two spectra are offset upward by

NATURE | NEWS

Young black hole had monstrous growth spurt

Super-massive object found in early Universe tests theories of cosmic evolution.

Davide Castelvecchi

25 February 2015

[Print](#)

Zhaoyu Li/SHAO

An artist's impression of a quasar with a supermassive black hole at its heart in the distant Universe.

A black hole that grew to gargantuan size in the Universe's first billion years is by far the largest yet spotted from such an early date, researchers have announced. The object, discovered by astronomers in 2013, is 12 billion times as massive as the Sun, and six times greater than its largest-known contemporaries. Its existence poses a challenge for theories of the evolution of black holes, stars and galaxies, astronomers say.

Light from the black hole took 12.9 billion years to reach Earth, so astronomers see the object as it was 900 million years after the Big Bang. That "is actually a very short time" for a black hole to have grown so large, says astronomer Xue-Bing Wu of Peking University in Beijing. He led an international collaboration that describes the discovery in *Nature*¹.

For its age, this black hole "is really much more massive than anything else we have seen so far", says Christian Veillet, director of the Large Binocular Telescope Observatory in Tucson, Arizona.

Interstellar





Figure 13. Inset: paint-swath accretion disk with inner and outer radii $r = 9.26M$ and $r = 18.70M$ before being placed around a black hole. Body: this paint-swath disk, now in the equatorial plane around a black hole with $a/M = 0.999$, as viewed by a camera at $r_c = 74.1M$ and $\theta_c = 1.511$ (86.56°), ignoring frequency shifts, associated colour and brightness changes, and lens flare. (Figure from *The Science of Interstellar* [40], used by permission of W. W. Norton & Company, Inc. and created by our Double Negative team, TM & © Warner Bros. Entertainment Inc. (s15)). This image may be used under the terms of the Creative Commons Attribution-NonCommercial-NoDerivs 3.0 (CC BY-NC-ND 3.0) license. Any further distribution of these images must maintain attribution to the author(s) and the title of the work, journal citation and DOI. You may not use the images for commercial purposes and if you remix, transform or build upon the images, you may not distribute the modified images.

itself. This entire image comes from light rays emitted by the disk's bottom face: the wide bottom portion of the image, from rays that originate behind the hole, and travel under the hole and back upward to the camera; the narrow top portion, from rays that originate on the disk's front underside and travel under the hole, upward on its back side, over its top, and down to the camera—making one full loop around the hole.

There is a third disk image whose bottom portion is barely visible near the shadow's edge. That third image consists of light emitted from the disk's top face, that travels around the hole once for the visible bottom part of the image, and one and a half times for the unresolved top part of the image.

In the remainder of this section 4 we deal with a moderately realistic accretion disk—but a disk created for *Interstellar* by Double Negative artists rather than created by solving astrophysical equations such as [32]. In appendix A.6 we give some details of how this and other Double Negative accretion disk images were created. This artists' *Interstellar* disk was chosen to be very anemic compared to the disks that astronomers see around black holes and that astrophysicists model—so the humans who travel near it will not get fried by x-rays and gamma-rays. It is physically thin and marginally optically thick and lies in the black hole's equatorial plane. It is not currently accreting onto the black hole, and it has cooled to a position-independent temperature $T = 4500$ K, at which it emits a black-body spectrum.

Figure 14 shows an image of this artists' disk, generated with a gravitational lensing geometry and computational procedure identical to those for our paint-swath disk, figure 13

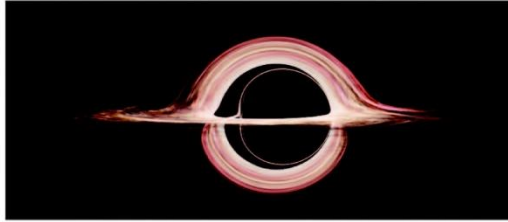


Figure 14. A moderately realistic accretion disk, created by Double Negative artists and gravitationally lensed by the same black hole with $a/M = 0.999$ as in figure 13 and with the same geometry.

(no frequency shifts or associated colour and brightness changes; no lens flare). Christopher Nolan and Paul Franklin decided that the flattened left edge of the black-hole shadow, and the multiple disk images alongside that left edge, and the off-centred disk would be too confusing for a mass audience. So—although *Interstellar*'s black hole had to spin very fast to produce the huge time dilations seen in the movie—for visual purposes Nolan and Franklin slowed the spin to $a/M = 0.6$, resulting in the disk of figure 15(a).

4.1.2. Colour and brightness changes due to frequency shifts. The influences of Doppler and gravitational frequency shifts on the appearance of this disk are shown in figures 15(b) and (c).

Since the left side of the disk is moving toward the camera and the right side away with speeds of roughly $0.55c$, their light frequencies get shifted blueward on the left and redward on the right—by multiplicative factors of order 1.5 and 0.4 respectively when one combines the Doppler shift with a $\sim 20\%$ gravitational redshift. These frequency changes induce changes in the disk's perceived *colours* (which we compute by convolving the frequency-shifted spectrum with the sensitivity curves of motion picture film) and also induce changes in the disk's perceived *brightness*; see appendix A.6 for some details.

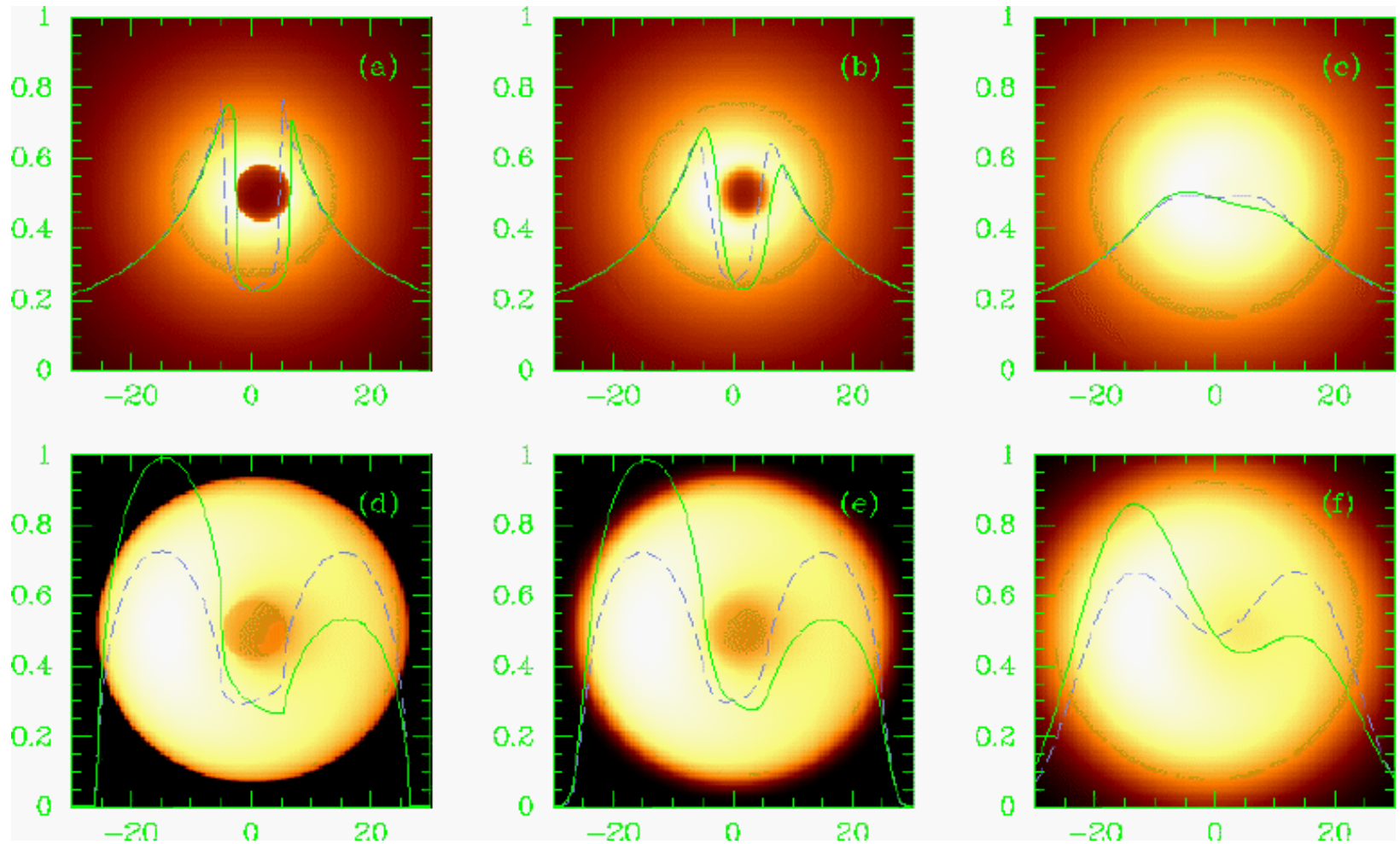
In figure 15(b), we have turned on the colour changes, but not the corresponding brightness changes. As expected, the disk has become blue on the left and red on the right.

In figure 15(c), we have turned on both the colour and the brightness changes. Notice that the disk's left side, moving toward the camera, has become very bright, while the right side, moving away, has become very dim. This is similar to astrophysically observed jets, emerging from distant galaxies and quasars; one jet, moving toward Earth is typically bright, while the other, moving away, is often too dim to be seen.

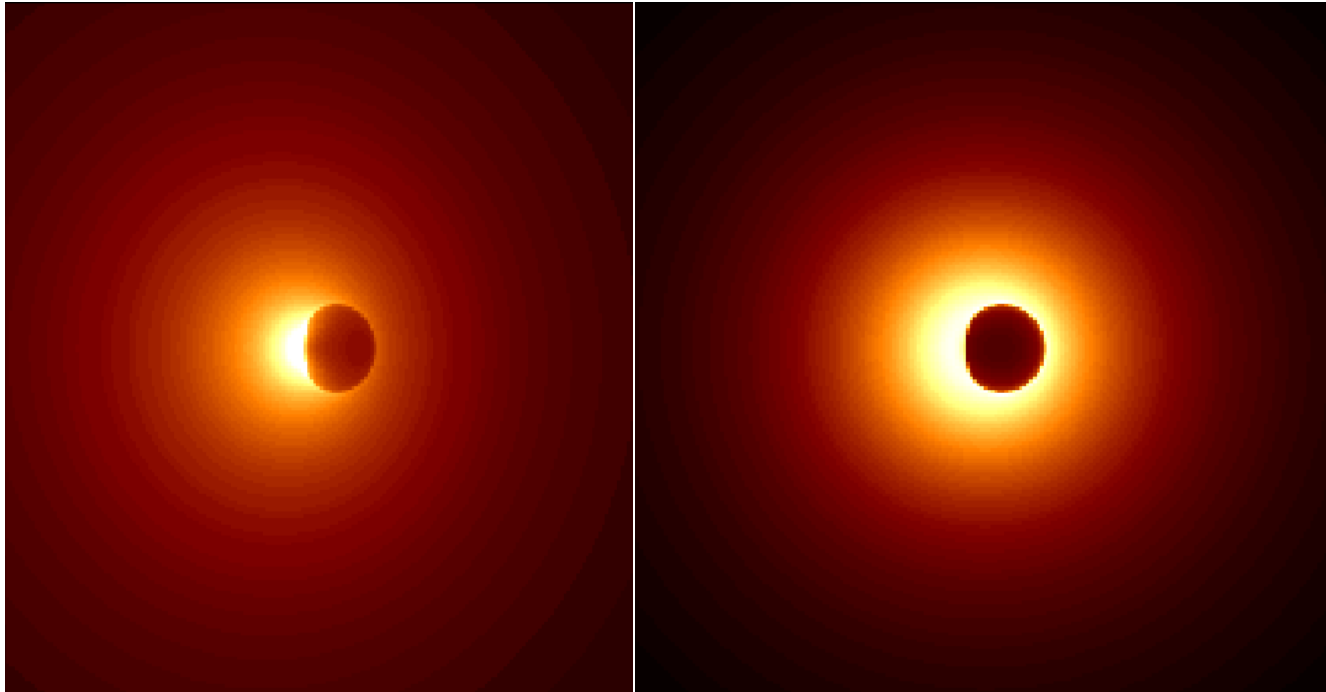
4.2. Lens flare and the accretion disk in the movie *Interstellar*

Christopher Nolan, the director and co-writer of *Interstellar*, and Paul Franklin, the visual effects supervisor, were committed to make the film as scientifically accurate as possible—within constraints of not confusing his mass audience unduly and using images that are exciting and fresh. A fully realistic accretion disk, figure 15(c), that is exceedingly lopsided, with the hole's shadow barely discernible, was obviously unacceptable.

Falcke, Melia, Agol



Shadows from Melia



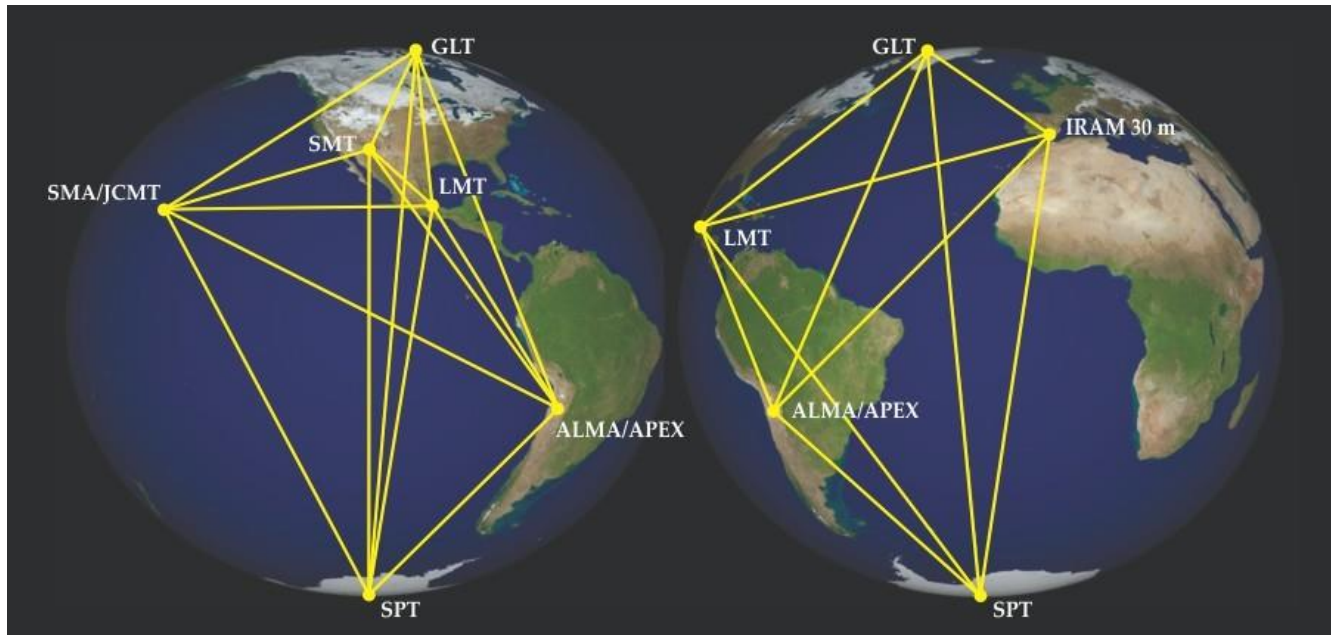


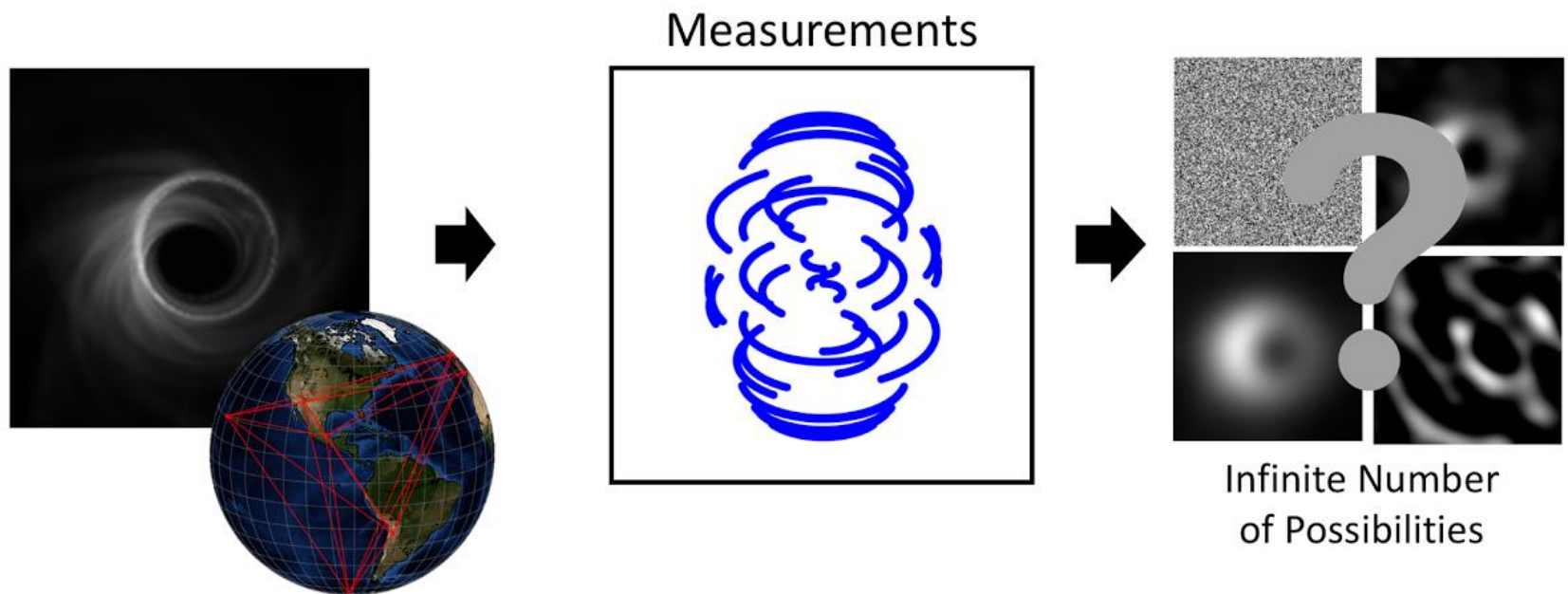
Figure 2. **The Event Horizon Telescope** is a global array of millimeter telescopes (see <http://eventhorizontelescope.org/array>) that aims to take the first pictures of black holes. (Courtesy of Dan Marrone/University of Arizona.)

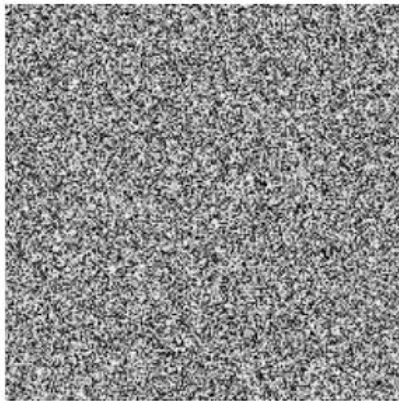
Published in: Dimitrios Psaltis; Feryal Özel; *Physics Today* **2018**, 71, 70-71.

DOI: 10.1063/PT.3.3906

Copyright © 2018 American Institute of Physics

EHT team: “Similarly, for the EHT, the data we take only tells us only a piece of the story, as there are an infinite number of possible images that are perfectly consistent with the data we measure. But not all images are created equal— some look more like what we think of as images than others. To chose the best image, we essentially take all of the infinite images that explain our telescope measurements, and rank them by how reasonable they look. We then choose the image (or set of images) that looks most reasonable. “

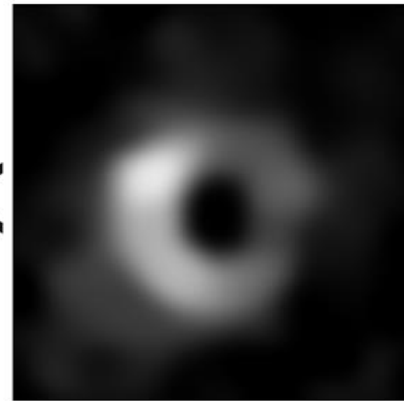




Unlikely



More Likely



Very Likely



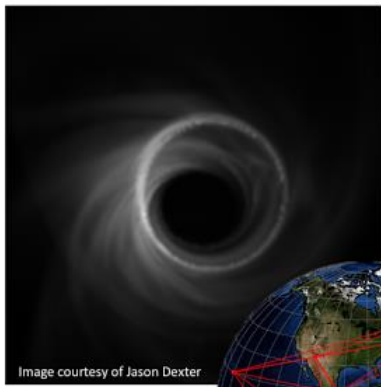
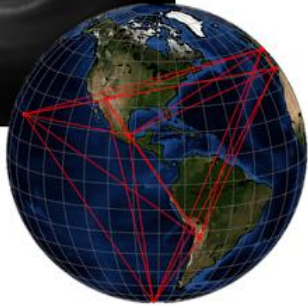
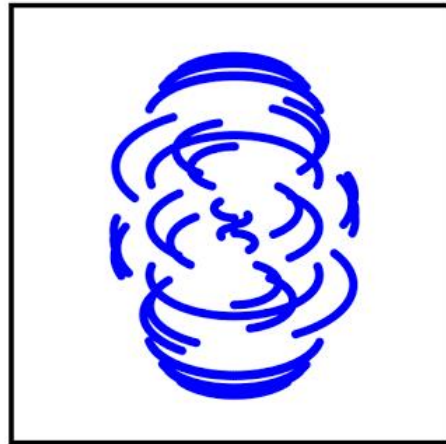


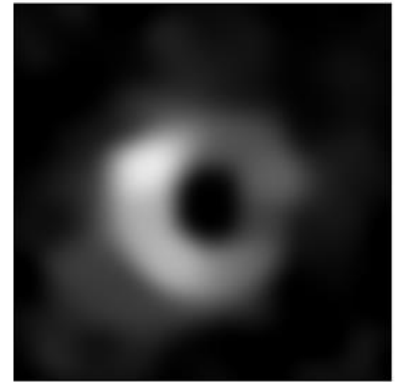
Image courtesy of Jason Dexter



Measurements



Reconstruction





The Size, Shape, and Scattering of Sagittarius A* at 86 GHz: First VLBI with ALMA

S. Issaoun^{1,2}, M. D. Johnson², L. Blackburn², C. D. Brinkerink¹, M. Mościbrodzka¹, A. Chael², C. Goddi^{1,3},
I. Martí-Vidal⁴, J. Wagner⁵, S. S. Doeleman², H. Falcke¹, T. P. Krichbaum⁵, K. Akiyama^{6,7}, U. Bach⁵, K. L. Bouman²,
G. C. Bower⁸, A. Broderick⁹, I. Cho^{10,11}, G. Crew⁶, J. Dexter¹², V. Fish⁶, R. Gold^{9,13}, J. L. Gómez¹⁴, K. Hada¹⁵,
A. Hernández-Gómez^{16,17}, M. Janßen¹, M. Kino¹⁵, M. Kramer⁵, L. Loinard^{16,18}, R.-S. Lu^{5,19}, S. Markoff²⁰,
D. P. Marrone²¹, L. D. Matthews⁶, J. M. Moran², C. Müller^{1,5}, F. Roelofs¹, E. Ros⁵, H. Rottmann⁵, S. Sanchez²²,

R. P. J. Tilanus^{1,3}, P. de Vicente²³, M. Wielgus², J. A. Zensus⁵, and G.-Y. Zhao¹⁰

¹ Department of Astrophysics/IMAPP, Radboud University, P.O. Box 9010, 6500 GL Nijmegen, The Netherlands

² Harvard-Smithsonian Center for Astrophysics, 60 Garden Street, Cambridge, MA 02138, USA

³ ALLEGRO/Leiden Observatory, Leiden University, P.O. Box 9513, 2300 RA, Leiden, The Netherlands

⁴ Department of Space, Earth and Environment, Chalmers University of Technology, Onsala Space Observatory, SE-439 92 Onsala, Sweden

⁵ Max-Planck-Institut für Radioastronomie, Auf dem Hügel 69, D-53121 Bonn, Germany

⁶ Massachusetts Institute of Technology, Haystack Observatory, 99 Millstone Road, Westford, MA 01886, USA

⁷ National Radio Astronomy Observatory, 520 Edgemont Road, Charlottesville, VA 22903, USA

⁸ Institute of Astronomy and Astrophysics, Academia Sinica, P.O. Box 23-141, Taipei 10617, Taiwan

⁹ Perimeter Institute for Theoretical Physics, 31 Caroline Street, North Waterloo, ON N2L 2Y5, Canada

¹⁰ Korea Astronomy and Space Science Institute, Daedeokdaero 776, Yuseonggu, Daejeon 34055, Republic of Korea

¹¹ University of Science and Technology, Gajeong-ro 217, Yuseong-gu, Daejeon 34113, Republic of Korea

¹² Max-Planck-Institut für Extraterrestrische Physik, Giessenbachstr. 1, D-85748 Garching, Germany

¹³ Institut für Theoretische Physik, Johann Wolfgang Goethe-Universität, Max-von-Laue-Straße 1, D-60438 Frankfurt, Germany

¹⁴ Instituto de Astrofísica de Andalucía-CSIC, Glorieta de la Astronomía s/n, E-18008 Granada, Spain

¹⁵ National Astronomical Observatory of Japan, 2-21-1 Osawa, Mitaka, Tokyo 181-8588, Japan

¹⁶ Instituto de Radioastronomía y Astrofísica, Universidad Nacional Autónoma de México, Morelia 58089, Mexico

¹⁷ IRAP, Université de Toulouse, CNRS, UPS, CNES, Toulouse, France

¹⁸ Instituto de Astronomía, Universidad Nacional Autónoma de México, Apartado Postal 70-264, 04510 Ciudad de México, Mexico

¹⁹ Shanghai Astronomical Observatory, Chinese Academy of Sciences, Shanghai 200030, People's Republic of China

²⁰ Anton Pannekoek Institute for Astronomy, University of Amsterdam, 1098 XH Amsterdam, The Netherlands

²¹ University of Arizona, 933 North Cherry Avenue, Tucson, AZ 85721, USA

²² Institut de RadioAstronomie Millimétrique (IRAM), Granada, Spain

²³ Observatorio de Yebes (IGN), Apartado 148, E-19180, Yebes, Spain

Received 2018 October 19; revised 2018 December 7; accepted 2018 December 7; published 2019 January 21

Abstract

The Galactic center supermassive black hole Sagittarius A* (Sgr A*) is one of the most promising targets to study the dynamics of black hole accretion and outflow via direct imaging with very long baseline interferometry (VLBI). At 3.5 mm (86 GHz), the emission from Sgr A* is resolvable with the Global Millimeter VLBI Array (GMVA). We present the first observations of Sgr A* with the phased Atacama Large Millimeter/submillimeter Array (ALMA) joining the GMVA. Our observations achieve an angular resolution of $\sim 87 \mu\text{as}$, improving upon previous experiments by a factor of two. We reconstruct a first image of the unscattered source structure of Sgr A* at 3.5 mm, mitigating the effects of interstellar scattering. The unscattered source has a major-axis size of $120 \pm 34 \mu\text{as}$ (12 ± 3.4 Schwarzschild radii) and a symmetrical morphology (axial ratio of $1.2^{+0.3}_{-0.2}$), which is further supported by closure phases consistent with zero within 3σ . We show that multiple disk-dominated models of Sgr A* match our observational constraints, while the two jet-dominated models considered are constrained to small viewing angles. Our long-baseline detections to ALMA also provide new constraints on the scattering of Sgr A*, and we show that refractive scattering effects are likely to be weak for images of Sgr A* at 1.3 mm with the Event Horizon Telescope. Our results provide the most stringent constraints to date for the intrinsic morphology and refractive scattering of Sgr A*, demonstrating the exceptional contribution of ALMA to millimeter VLBI.

Key words: accretion, accretion disks – galaxies: individual (Sgr A*) – Galaxy: center – techniques: interferometric

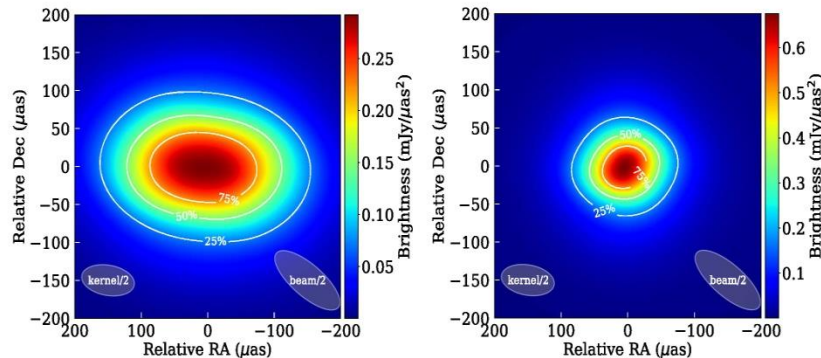


Figure 5. Left: scattered image of Sgr A*, reconstructed with the second-moment regularizer and stochastic optics ($\theta_{\text{maj}} = 228 \pm 46 \mu\text{as}$, $\theta_{\text{min}} = 143 \pm 20 \mu\text{as}$ from LSQ). Right: reconstructed image from stochastic optics (Johnson 2016) of the intrinsic source ($\theta_{\text{maj}} = 120 \pm 34 \mu\text{as}$, $\theta_{\text{min}} = 100 \pm 18 \mu\text{as}$ from LSQ). In each panel, the ellipses at the bottom indicate half the size of the scatter-broadening kernel ($\theta_{\text{maj}} = 159.9 \mu\text{as}$, $\theta_{\text{min}} = 79.5 \mu\text{as}$, PA = 81.9°) and the observing beam.

excellent accuracy in previous experiments, we do not expect either of these effects to significantly advantage the reconstructions of simulated data.

In Figure 6, we present the original 3D GRMHD model images, the model images scattered with the J18 scattering model (as observed in the simulated observations), and the reconstructed observed (scattered) and intrinsic images from the imaging method. In Table 2, we compare the true intrinsic source sizes from the models to the intrinsic source sizes derived from the imaging routine. We determined the source size parameters using two methods: (1) measuring the second central moment of the image (2nd mom.) and deriving Gaussian parameters and (2) doing a 2D Gaussian fit with a least-squares minimization (LSQ) onto the image.

Next, we evaluate the difference between true and reconstructed image parameters. We sought to define an approach that quantifies these differences in a way that is related to the reconstructed image properties and the observing beam. When expressed in this way, we can use parameter errors on these reconstructed simulated images to predict uncertainties on parameters derived from our reconstructed image with data.

To this end, Table 2 expresses the difference between the true and measured source major and minor axes as a fraction of the projected beam FWHM θ_{beam} along the corresponding axis. For the axial ratio, we express the difference between the true and measured ratios as a fraction of the cumulative error from both axes (the projected beam widths along the measured major and minor axes added quadratically).

However, while it is straightforward and well motivated to express uncertainties on axis lengths and their ratio in terms of the observing beam, uncertainty on the PA is more subtle. We opted to create an ensemble of beam-convolved reconstructed images and use the scatter in the PA of the ensemble as an estimate of the PA uncertainty. The ensemble of images is constructed by convolving the single reconstructed image with an ensemble of narrow beams, sampling all PAs. Each of these beams has a major-axis size given by the projected observing beam size along the same PA and a minor-axis size of zero. We thereby stretch the image along each direction, up to the extent of the observing beam, and examine the overall dependence of

the reconstructed image on this stretching. With this approach, images that are nearly isotropic will have large PA uncertainty, while highly elongated images (relative to the beam size) will have small PA uncertainty.

In general, we find that the LSQ method fares better than second moment for determining the source parameters, likely due to weak extended flux in the images skewing the second-moment parameters to larger values. As expected, both methods perform poorly when determining the PA of a fairly symmetrical source, for which it remains largely unconstrained. However, for more elongated source geometry, both methods are able to accurately recover the intrinsic PA. We adopt the LSQ method to quantify the size of Sgr A* via image-domain fitting. Although the Gaussian approximation does not fully describe our source morphology, it is suitable for comparisons to visibility-domain model fits from the previous observations of Sgr A* presented in Section 5.

5. Results

5.1. Intrinsic Source Constraints from Imaging

Figure 5 shows the unscattered and scattered images of Sgr A*, as imaged following the method described in Section 4. The (uniform-weighted) beam size of the Sgr A* observations is $(235 \times 87) \mu\text{as}$, with a PA (east of north) of 53.6° . While the shorter baselines of the array (intra-VLBA, VLBA-GBT, and intra-European) see primarily a Gaussian source elongated in the east–west direction, longer baselines are expected to pick up on non-Gaussian source structure or refractive noise from interstellar scattering. In this particular observation, our longest baselines are mainly north–south to ALMA (see Figure 1), where scattering has less of an effect on the source. As seen in Figure 5, left panel, the reconstructed scattered image looks very smooth and Gaussian-like, showing no obvious refractive noise in the image. We also see a similar outcome in our imaging tests, presented in Section 4.2.3. Although the scattered images (second column in Figure 6) have visible ripples of scattering substructure, the reconstructed scattered images (third column) appear very smooth. This is likely because our GMVA+ALMA observations sample low levels of refractive noise mainly along the north–south direction, whereas our east–west sensitivity and resolution do not

- On April 10th 2019, the [Event Horizon Telescope \(EHT\) Collaboration](#) presented its first results -- an image of the supermassive black hole in galaxy M87 -- in multiple simultaneous press conferences around the world. The official EHT press release appears on the [home page](#) of this website. This page contains links to recorded press conferences, press releases from our partner institutions, and supporting materials published along with press releases.
-
- **Press conference recordings:**
- [Brussels](#), hosted by the European Research Council (in English)
- [Santiago](#), hosted by the Joint ALMA Observatory (in Spanish and English)
- [Taipei](#), hosted by the Academia Sinica (in Chinese)
- [Tokyo](#), hosted by the National Astronomical Observatory of Japan (in Japanese)
- [Washington](#), hosted by the US National Science Foundation (in English)

EHT results in brief












- **First M87 Event Horizon Telescope Results. I. The Shadow of the Supermassive Black Hole, ApJL 875 L1.**
- To image and study this phenomenon, we have assembled the Event Horizon Telescope, a global very long baseline interferometry array observing at a wavelength of 1.3 mm. This allows us to reconstruct event-horizon-scale images of the supermassive black hole candidate in the center of the giant elliptical galaxy M87. We have resolved the central compact radio source as an asymmetric bright emission ring with a diameter of $42 \pm 3 \mu\text{as}$. derive a central mass of $M_{\text{BH}} = (6.5 \pm 0.7) \times 10^9 M_{\text{Sun}}$.
- In many AGNs, collimated relativistic plasma jets (Bridle & Perley 1984; Zensus 1997) launched by the central black hole contribute to the observed emission. These jets may be powered either by magnetic fields threading the event horizon,
- extracting the rotational energy from the black hole (Blandford & Znajek 1977), or from the accretion flow (Blandford & Payne 1982). The near-horizon emission from low-luminosity active galactic nuclei (LLAGNs; Ho 1999) is produced by
- synchrotron radiation that peaks from the radio through the far infrared. This emission may be produced either in the accretion flow (Narayan et al. 1995), the jet (Falcke et al. 1993), or both (Yuan et al. 2002).

Event Horizon Telescope (EHT)

A Global Network of Radio Telescopes

2018 Observatories



- ALMA**  Atacama Large Millimeter/submillimeter Array
CHAJNANTOR PLATEAU, CHILE
- APEX**  Atacama Pathfinder EXperiment
CHAJNANTOR PLATEAU, CHILE
- 30-M**  IRAM 30-M Telescope
PICO VELETA, SPAIN
- JCMT**  James Clerk Maxwell Telescope
MAUNAKEA, HAWAII
- LMT**  Large Millimeter Telescope
SIERRA NEGRA, MEXICO
- SMA**  Submillimeter Array
MAUNAKEA, HAWAII
- SMT**  Submillimeter Telescope
MOUNT GRAHAM, ARIZONA
- SPT**  South Pole Telescope
SOUTH POLE STATION
- GLT**  The Greenland Telescope
THULE AIR BASE, GREENLAND, DENMARK
- Kitt Peak**  Kitt Peak 12-meter Telescope
KITTE PEAK, ARIZONA, USA
- NOEMA**  NOEMA Observatory
PLATEAU DE BURE, FRANCE

Observing in 2020



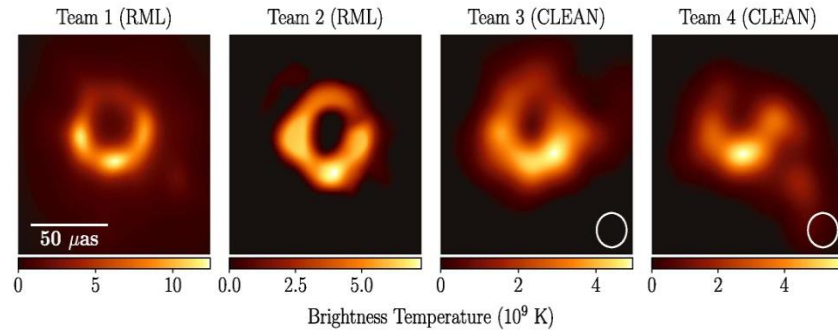


Figure 4. The first EHT images of M87, blindly reconstructed by four independent imaging teams using an early, engineering release of data from the April 11 observations. These images all used a single polarization (LCP) rather than Stokes I , which is used in the remainder of this Letter. Images from Teams 1 and 2 used RML methods (no restoring beam); images from Teams 3 and 4 used CLEAN (restored with a circular $20 \mu\text{as}$ beam, shown in the lower right). The images all show similar morphology, although the reconstructions show significant differences in brightness temperature because of different assumptions regarding the total compact flux density (see Table 2) and because restoring beams are applied only to CLEAN images.

Table 2.
Image Properties and Data Consistency Metrics
for the First M87 Images (See Figure 4)

	Team 1	Team 2	Team 3	Team 4
Image Properties				
Method	RML	RML	CLEAN	CLEAN
F_{peak} (Jy)	0.94	0.43	0.42	0.42
Engineering Data (10 s avg., LCP, 0% sys. error)				
χ^2_{CP}	2.06	2.48	2.44	2.33
$\chi^2_{\text{reg CA}}$	1.20	2.16	2.15	1.43
Science Release (scan-avg., Stokes I , 0% sys. error)				
χ^2_{CP}	1.13	5.40	2.28	1.89
$\chi^2_{\text{reg CA}}$	2.12	5.41	3.90	5.32
Science Release (scan-avg., Stokes I , 1% sys. error)				
χ^2_{CP}	1.00	3.85	2.04	1.55
$\chi^2_{\text{reg CA}}$	1.96	5.07	3.64	4.8
Science Release (scan-avg., Stokes I , 10% sys. error)				
χ^2_{CP}	0.49	0.95	1.11	0.48
$\chi^2_{\text{reg CA}}$	0.46	1.36	0.98	0.79

Note. Data metrics are shown as originally computed on April 11 data (using 10 s averaged engineering data with LCP) and using the data from the first EHT science release (scan-averaged, Stokes I) when 0%, 1% and 10% systematic error has been included. Teams 2–4 chose to exclude the intra-site baselines in their imaging. However, for consistency with our later χ^2 values computed from science release data, we include these baselines when computing χ^2 after adding an extended component to these images containing the missing flux density.

structures, including sources without the prominent ring observed in our images of M87.

We emphasize that the ensemble of results from these parameter surveys do not correspond to a posterior distribution of reconstructed images. Our surveys are coarse-grained and do not completely explore the choices in the imaging process. Nonetheless, they identify regions of imaging parameter space that consistently produce faithful image reconstructions on synthetic data, and they help us identify which features of our reconstructions are consistent and which features vary with specific parameter choices.

6.1. Synthetic Source Models and Data

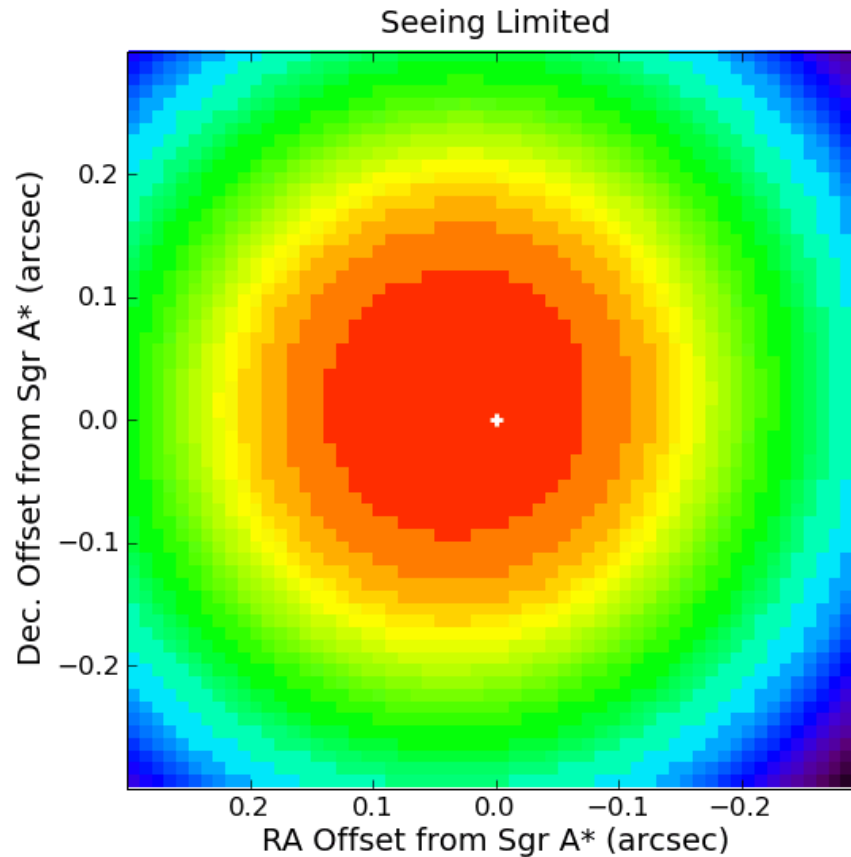
To create a testing suite of synthetic data, we selected simple geometric models that have corresponding visibility amplitudes that are similar to those observed in M87 (Figure 2). The primary data properties that we used to define similarity are (1) a large decrease in flux density on baselines between 0 and $1 \text{ G}\lambda$, indicating extended structure, (2) visibility nulls at ~ 3.4 and $\sim 8.3 \text{ G}\lambda$, and (3) a high secondary peak between the nulls at $\sim 6 \text{ G}\lambda$, which recovers $\sim 15\%$ of the total compact flux density.

We selected four models with distinct compact morphologies that each reproduce these features of the M87 data. The four models are (1) a tapered ring with $44 \mu\text{as}$ ring diameter, (2) a tapered crescent of the same diameter with its brightest point oriented directly south, (3) a tapered disk with $70 \mu\text{as}$ diameter, and (4) two different circular Gaussian components separated by $32.3 \mu\text{as}$ at a position angle of 292° . To ensure rough consistency and compatibility with the M87 parameters estimated in Section 4, we adopted a total compact flux density of 0.6 Jy for all these simple geometric models. Note that none of the synthetic EHT data sets generated from these simple models reproduces all features seen in the M87 data. For example, the ring and disk models both have point symmetry, so all their closure phases are either 0° or 180° .

To simulate the effects of a large-scale jet on our data (which only significantly affects intra-site visibilities), we added a three-component Gaussian model that approximates the inner M87 jet at 3 mm (e.g., Kim et al. 2018a). The jet also has 0.6 Jy of total flux density, giving a total image flux density in each case (compact+jet) of 1.2 Jy . To produce non-closing systematic errors from polarimetric leakage, we also included linear polarization in each model. For additional details on these simulated models and data, see Appendix C.1. Figure 5 shows these model images.

We generated synthetic data from each image using the `eht-imaging` software library. The synthetic data were produced with the baseline coverage and sensitivity of the EHT on all four days of the 2017 observations. Station-based errors were added in a Jones matrix formalism (Thompson et al. 2017; see Appendix C.2). To simulate a lack of absolute phase

Large telescopes, AO and bright stars in IR



http://www.astro.ucla.edu/~ghezgroup/gc/pictures/Future_GCorbits.shtml

1995.50

S0-8

0".1

S0-26

S0-16

S0-2

S0-3

S0-1

S0-19

*

S0-23

S0-4

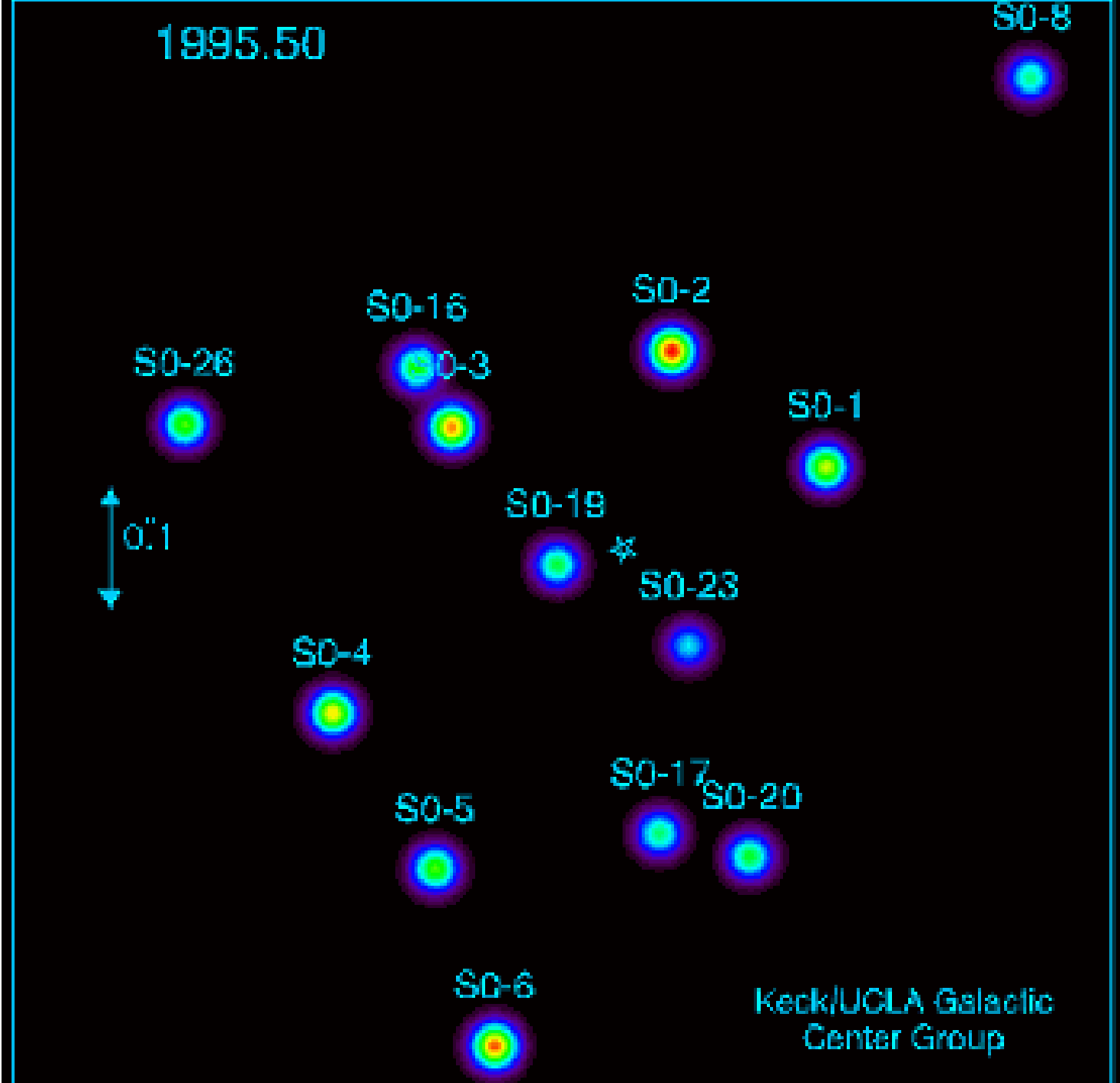
S0-5

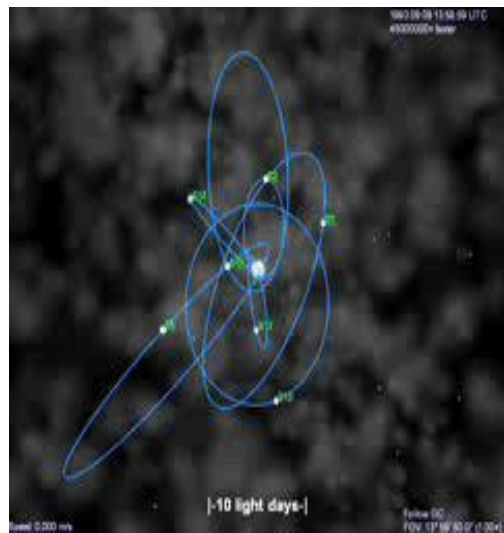
S0-17

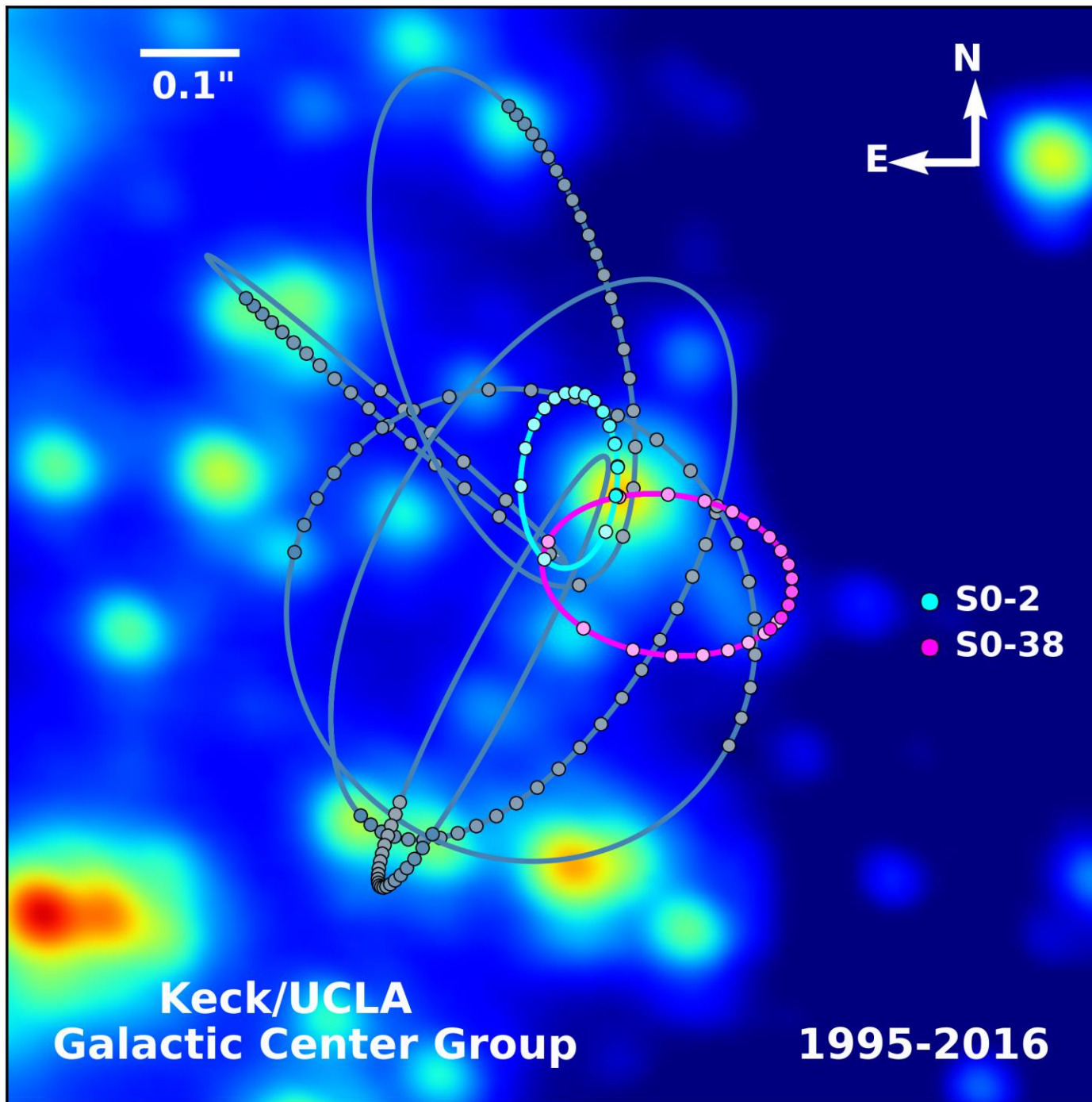
S0-20

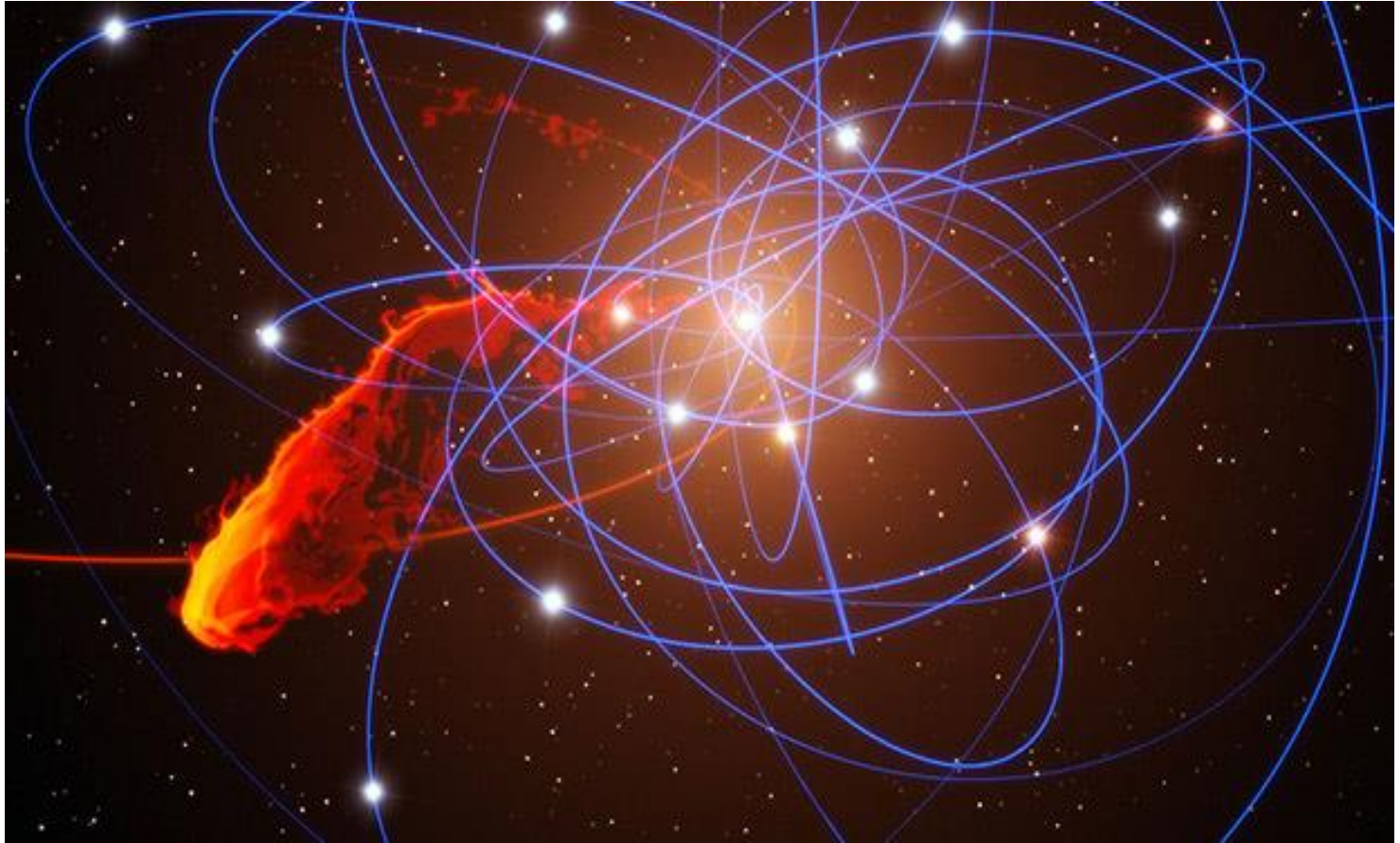
S0-6

Keck/UCLA Galactic
Center Group









2012 Crafoord Prize in Astronomy Goes to Genzel & Ghez

The Royal Swedish Academy of Sciences has decided to award the Crafoord Prize in Astronomy 2012 to Reinhard Genzel, Max Planck Institute for Extraterrestrial Physics, Garching, Germany and Andrea Ghez, University of California, Los Angeles, USA, "for their observations of the stars orbiting the galactic centre, indicating the presence of a supermassive black hole".

The Dark Heart of the Milky Way

This year's Crafoord Prize Laureates have found the most reliable evidence to date that supermassive black holes really exist. For decades Reinhard Genzel and Andrea Ghez, with their research teams, have tracked stars around the centre of the Milky Way galaxy. Separately, they both arrived at the same conclusion: in our home galaxy resides a giant black hole called Sagittarius A*.

The Anna-Greta and Holger Crafoord Fund



PHOTO: MARKUS MARCTIC

BACK ROW: LENNART NILSSON, WALTER FISCHER, GUNNAR ÖQUIST, GEORGIA DESTOUNI, SVANTE LINDQVIST. FRONT ROW: MARGARETA NILSSON, WALTER MUNK, H.M. KING CARL XVI GUSTAF, H.M. QUEEN SILVIA, EBBA FISCHER.

The Fund was established in 1980 by a donation to the Royal Swedish Academy of Sciences from Anna-Greta and Holger Crafoord. The Crafoord Prize was awarded for the first time in 1982. The purpose of the Fund is to promote basic scientific research worldwide in the following disciplines:



ASTRONOMY AND
MATHEMATICS



GEOSCIENCES



BIOSCIENCES
WITH EMPHASIS ON ECOLOGY



POLYARTHRITIS

Support to research takes the form of an international prize awarded annually to outstanding scientists, and of research grants to individuals or institutions in Sweden. Both awards and grants are made according to the following order:

- year 1: Astronomy and Mathematics
- year 2: Geosciences
- year 3: Biosciences
- year 4: Astronomy and Mathematics
- year 5: Geosciences
- year 6: Biosciences
- etc.



The Crafoord Prize in Astronomy 2016 to **Roy Kerr**, University of Canterbury, Christchurch, New Zealand, and **Roger Blandford**, Stanford University, CA, USA,
“for fundamental work concerning rotating black holes and their astrophysical consequences”.



Reinhard Genzel, Prof. Dr.

[Max Planck Institute for Extraterrestrial Physics](#), Garching

Curriculum Vitae

Born on March 24, 1952 in Bad Homburg v.d.H. Study of physics Bonn Univ., doctorate Max Planck Institute for Radioastronomy Bonn (1978), Postdoctoral Fellow, Harvard-Smithsonian Center for Astrophysics (1978-1980), Cambridge, MA, Associate Professor of Physics and Associate Research Astronomer, Space Sciences Laboratory, University of California, Berkeley (1981- 1985), Full Professor of Physics, University of California, Berkeley (1985-1986), Director and Scientific Member at the Max Planck Institute for Extraterrestrial Physics (since 1986), Honorary Professor Munich Univ. (since 1988), Full Professor of Physics University of California Berkeley (since 1999).



American citizen. Born 1965 in
New York City, NY, USA. Ph.D.
1992 at California Institute of
Technology, Pasadena, CA, USA.
Professor at University of
California, Los Angeles, CA, USA.

MEASURING DISTANCE AND PROPERTIES OF THE MILKY WAY'S CENTRAL SUPERMASSIVE BLACK HOLE WITH STELLAR ORBITS

A. M. GHEZ^{1,2}, S. SALIM^{1,4}, N. N. WEINBERG^{3,5}, J. R. LU¹, T. DO¹, J. K. DUNN¹, K. MATTHEWS³, M. MORRIS³, S. YELDA¹, E. E. BECKLIN¹, T. KREMENER¹, M. MILOSAVLJEVIC⁶, J. NAIMAN^{1,7}

Draft version August 21, 2008

ABSTRACT

We report new precision measurements of the properties of our Galaxy's supermassive black hole. Based on astrometric (1995-2007) and radial velocity (2000-2007) measurements from the W. M. Keck 10-meter telescopes, a fully unconstrained Keplerian orbit for the short period star S0-2 provides values for the distance (R_0) of 8.0 ± 0.6 kpc, the enclosed mass (M_{bh}) of $4.1 \pm 0.6 \times 10^6 M_\odot$, and the black hole's radial velocity, which is consistent with zero with 30 km/s uncertainty. If the black hole is assumed to be at rest with respect to the Galaxy (e.g., has no massive companion to induce motion), we can further constrain the fit and obtain $R_0 = 8.4 \pm 0.4$ kpc and $M_{bh} = 4.5 \pm 0.4 \times 10^6 M_\odot$. More complex models constrain the extended dark mass distribution to be less than $3.4 \times 10^5 M_\odot$ within 0.01 pc, $\sim 100\times$ higher than predictions from stellar and stellar remnant models. For all models, we identify transient astrometric shifts from source confusion (up to 5x the astrometric error) and the assumptions regarding the black hole's radial motion as previously unrecognized limitations on orbital accuracy and the usefulness of fainter stars. Future astrometric and RV observations will remedy these effects. Our estimates of R_0 and the Galaxy's local rotation speed, which it is derived from combining R_0 with the apparent proper motion of Sgr A* ($\theta_0 = 229 \pm 18$ km s⁻¹), are compatible with measurements made using other methods. The increased black hole mass found in this study, compared to that determined using projected mass estimators, implies a longer period for the innermost stable orbit, longer resonant relaxation timescales for stars in the vicinity of the black hole and a better agreement with the M_{bh} - σ relation.

Subject headings: black hole physics – Galaxy:center — Galaxy:kinematics and dynamics — infrared:stars – techniques:high angular resolution

1. INTRODUCTION

Ever since the discovery of fast moving ($v > 1000$ km s⁻¹) stars within 0."3 (0.01 pc) of our Galaxy's central supermassive black hole (Eckart & Genzel 1997; Ghez et al. 1998), the prospect of using stellar orbits to make precision measurements of the black hole's mass (M_{bh}) and kinematics, the distance to the Galactic center (R_0) and, more ambitiously, to measure post-Newtonian effects has been anticipated (Jaroszynski 1998, 1999; Salim & Gould 1999; Fragile & Mathews 2000; Rubilar & Eckart 2001; Weinberg, Milosavljevic & Ghez 2005; Zucker & Alexander 2007; Kraniotis 2007; Will 2008). An accurate measurement of the Galaxy's central black hole mass is useful for putting the Milky Way in context with other galaxies through the apparent relationship between the mass of the central black hole and the velocity dispersion, σ , of the host galaxy (e.g., Ferrarese & Merrit 2000; Gebhardt et al. 2000; Tremaine et al. 2002). It can also

be used as a test of this scaling, as the Milky Way has the most convincing case for a supermassive black hole of any galaxy used to define this relationship. Accurate estimates of R_0 impact a wide range of issues associated with the mass and structure of the Milky Way, including possible constraints on the shape of the dark matter halo and the possibility that the Milky Way is a lopsided spiral (e.g., Reid 1993; Olling & Merrifield 2000; Majewski et al. 2006). Furthermore, if measured with sufficient accuracy ($\sim 1\%$), the distance to the Galactic center could influence the calibration of standard candles, such as RR Lyrae stars, Cepheid variables and giants, used in establishing the extragalactic distance scale. In addition to estimates of M_{bh} and R_0 , precision measurements of stellar kinematics offer the exciting possibility of detecting deviations from a Keplerian orbit. This would allow an exploration of a possible cluster of stellar remnants surrounding the central black hole, suggested by Morris (1993), Miralda-Escudé & Gould(2000), and Freitag et al. (2006). Estimates for the mass of the remnant cluster range from 10^4 – $10^5 M_\odot$ within a few tenths of a parsec of the central black hole. Absence of such a remnant cluster would be interesting in view of the hypothesis that the inspiral of intermediate-mass black holes by dynamical friction could deplete any centrally concentrated cluster of remnants. Likewise, measurements of post-newtonian effects would provide a test of general relativity, and, ultimately, could probe the spin of the central black hole.

Tremendous observational progress has been made over the last decade towards obtaining accurate estimates of the orbital parameters of the fast moving stars at the

arXiv:0808.2870v1 [astro-ph] 21 Aug 2008

¹ UCLA Department of Physics and Astronomy, Los Angeles, CA 90095-1547; ghez, jlu, tdo, jkdunn, morris, syelda, becklin@astro.ucla.edu

² UCLA Institute of Geophysics and Planetary Physics, Los Angeles, CA 90095-1565

³ California Institute of Technology, Division of Mathematics, Physics and Astronomy, Pasadena, CA 91125; kym@caltech.edu

⁴ NOAO, 950 N Cherry Ave, Tucson, AZ 85719; samir@noao.edu

⁵ University of California Berkeley, Department of Astronomy Berkeley, CA 94720-3411; nmw@astron.berkeley.edu

⁶ University of Texas, Department of Astronomy, Austin, TX 78712; milos@astro.as.utexas.edu

⁷ UCSC, Department of Astronomy & Astrophysics, Santa Cruz, CA 95064; jnaiman@astro.ucsc.edu

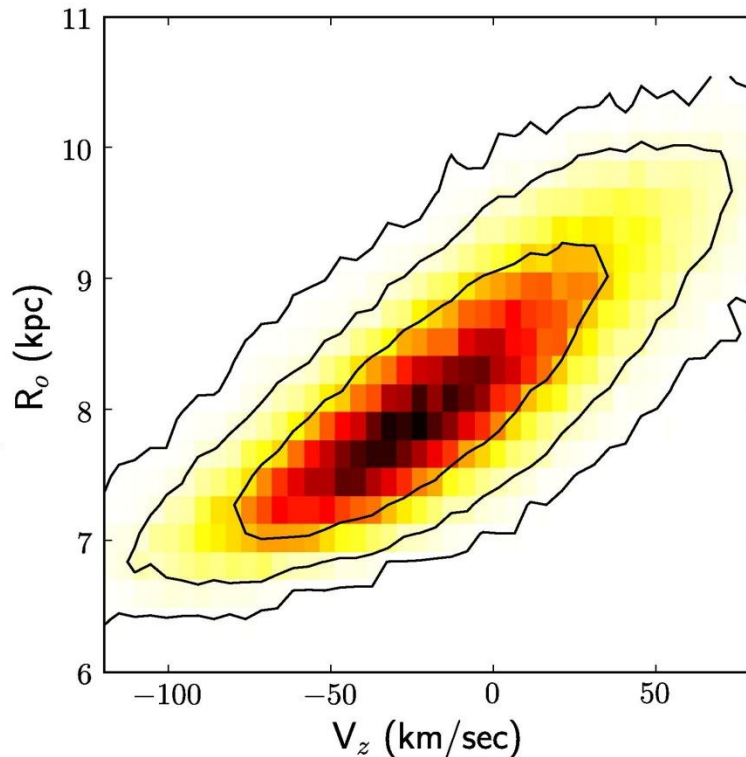


FIG. 12.— Correlation of the estimated black hole’s distance and line-of-sight velocity (V_z) from our 13 parameter model fit. V_z dominates the uncertainties in R_0 and consequently M_{bh} . Priors on V_z can reduce the uncertainties in R_0 by a factor of two. All previous studies have set V_z to zero, which implicitly assumes that there are no massive companions to our Galaxy’s central supermassive black hole and that the local standard of rest is perfectly known.

4.2. Point Mass Plus Extended Mass Distribution Analysis

Limits on an extended mass distribution within S0-2’s orbit are derived by assuming that the gravitational potential consists of a point mass and an extended mass distribution, and allowing for a Newtonian precession of the orbits (see, e.g., Rubilar & Eckart 2001). In order to do this, we use the orbit fitting procedure described in Weinberg et al. (2005), and adopt an extended mass distribution that has a power-law density profile $\rho(r) = \rho_0(r/r_0)^{-\gamma}$. This introduces two additional parameters to the model: the normalization of the profile and its slope γ . The total enclosed mass is then given by

$$M(< r) = M_{\text{BH}} + M_{\text{ext}}(< r_0) \left(\frac{r}{r_0} \right)^{3-\gamma}, \quad (1)$$

where we quote values for the normalization $M_{\text{ext}}(< r_0)$ at $r_0 = 0.01$ pc, corresponding to the characteristic scale of the orbit. Figure 13 shows the constraint on $M_{\text{ext}}(<$

0.01 pc) and γ from a fit to the astrometric and radial velocity measurements for S0-2. The 99.7% confidence upper-bound on the extended mass is $M_{\text{ext}}(< 0.01 \text{ pc}) \simeq 3 - 4 \times 10^5 M_\odot$ and has only a weak dependence on γ .

Mouawad et al. (2005) report a similar upper-bound on the extended mass in fits to the orbit of S0-2. Their analysis differs only slightly from that presented here in that it forces the focus to be at the inferred radio position of Sgr A*, assumes a Plummer model mass distribution, and is based on data presented in Eisenhauer et al. (2003). Similarly, Zakharov et al. (2007) use an order of magnitude analysis to show that if the total mass of the extended matter enclosed within the S0-2 orbit is $\gtrsim 10^5 M_\odot$, then it would produce a detectable apocenter shift $\Delta\phi \gtrsim 10$ mas (see also § 3.2 in Weinberg et al. 2005). Hall & Gondolo (2006) fit the total measured mass concentration $M(< r)$ given in Ghez et al. (2005) assuming a power-law density profile and obtain an upper bound of $\approx 10^5 M_\odot$ between 0.001 – 1 pc.

The Galactic Center massive black hole and nuclear star cluster

Reinhard Genzel,^{*} Frank Eisenhauer, and Stefan Gillessen

Max-Planck Institut für Extraterrestrische Physik, 85748 Garching, Germany

(Published 20 December 2010)

The Galactic Center is an excellent laboratory for studying phenomena and physical processes that may be occurring in many other galactic nuclei. The center of our Milky Way is by far the closest galactic nucleus, and observations with exquisite resolution and sensitivity cover 18 orders of magnitude in energy of electromagnetic radiation. Theoretical simulations have become increasingly more powerful in explaining these measurements. This review summarizes the recent progress in observational and theoretical work on the central parsec, with a strong emphasis on the current empirical evidence for a central massive black hole and on the processes in the surrounding dense nuclear star cluster. Current evidence is presented, from the analysis of the orbits of more than two dozen stars and from the measurements of the size and motion of the central compact radio source, Sgr A*, that this radio source must be a massive black hole of about $4.4 \times 10^6 M_\odot$, beyond any reasonable doubt. What is known about the structure and evolution of the dense nuclear star cluster surrounding this black hole is reported, including the astounding fact that stars have been forming in the vicinity of Sgr A* recently, apparently with a top-heavy stellar-mass function. A dense concentration of fainter stars centered in the immediate vicinity of the massive black hole are discussed, three of which have orbital peri-bothroi of less than one light day. This “S-star cluster” appears to consist mainly of young early-type stars, in contrast to the predicted properties of an equilibrium “stellar cusp” around a black hole. This constitutes a remarkable and presently not fully understood “paradox of youth.” What is known about the emission properties of the accreting gas onto Sgr A* is also summarized and how this emission is beginning to delineate the physical properties in the hot accretion zone around the event horizon.

DOI: 10.1103/RevModPhys.82.3121

PACS number(s): 98.35.Jk

CONTENTS

I. Introduction	3122	Massive Black Hole?	3144
A. Massive black holes	3122	A. Evidence for a central compact mass from gas motions	3144
B. The Galactic Center laboratory	3122	B. Evidence from stellar motions	3144
II. The Nuclear Star Cluster	3124	C. Constraints from stellar orbits	3145
A. The nuclear cluster of cool old stars	3125	D. Very long baseline interferometry of Sgr A*	3148
B. The disk(s) of young massive stars	3125	E. Does Sgr A* have an event horizon?	3150
1. The clockwise stellar disk	3125	F. Could Sgr A* be a binary?	3150
2. More than one disk?	3127	G. Alternatives to a black-hole configuration	3151
3. Massive binaries in the disk(s)	3128	V. Mass Distribution in the Nuclear Star Cluster	3152
C. The central S-star cluster and the distribution of B stars	3129	A. Outlier “high velocity” stars	3154
D. Is there an “equilibrium” stellar cusp?	3131	B. Dark matter in the central parsec?	3154
1. Radial distribution of different stellar components	3132	C. Comparison to earlier statistical mass estimates	3155
E. Stellar mass function	3135	D. Does IRS 13E contain an intermediate-mass black hole?	3156
F. Chemical abundances	3137	E. The distance to the Galactic Center	3157
III. Observed Properties of the Nuclear Interstellar Matter	3139	1. Direct estimates	3158
A. Ionized gas in Sgr A West	3139	2. Indirect estimates	3158
B. Neutral gas	3141	3. Model-based estimates	3159
C. Dust and interstellar extinction toward the Galactic Center	3142	4. Combined best estimate	3159
D. Hot gas and high-energy emission	3143	5. Discussion	3160
IV. Testing the Black-Hole Paradigm: Is Sgr A* a		VI. Paradox of Youth: How did the Young Stars Get into the Central Parsec?	3161
		A. Star-formation history in the central parsec	3161
		B. <i>In situ</i> star formation or in-spiral of a star cluster?	3163
		1. Star formation near the black hole	3163
		2. In-spiral of a massive star cluster	3166
		C. Origin of B stars in the central cusp: Scattering or migration?	3167
		1. The Hills capture mechanism	3168
		2. Hypervelocity stars	3169

^{*}Also at Department of Physics, University of California, Berkeley, CA 94720.

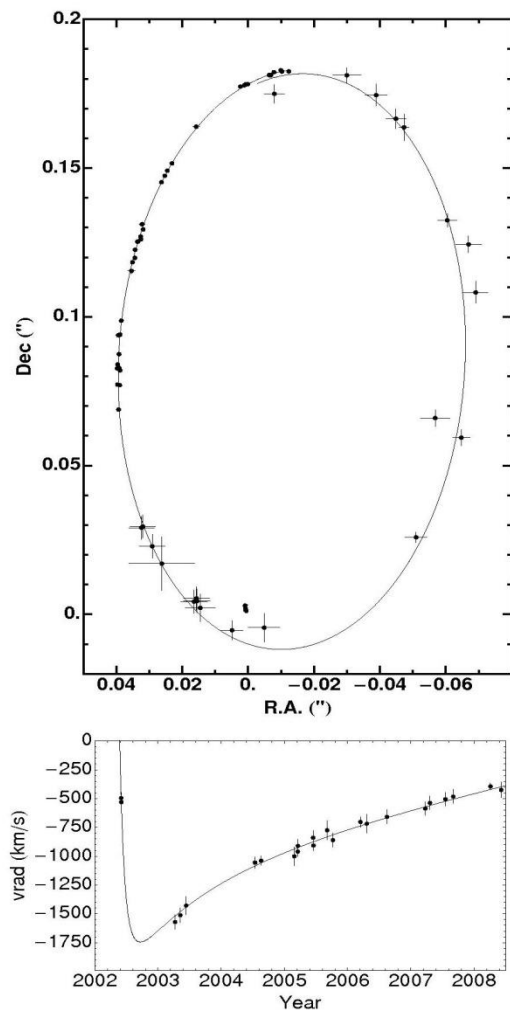


FIG. 13.— Top: The S2 orbital data plotted in the combined coordinate system and fitted with a Keplerian model in which the velocity of the central point mass and its position were free fit parameters. The non-zero velocity of the central point mass is the reason why the orbit figure does not close exactly in the overlap region 1992/2008 close to apocenter. The fitted position of the central point mass is indicated by the elongated dot inside the orbit near the origin; its shape is determined from the uncertainty in the position and the fitted velocity, which leads to the elongation. Bottom: The measured radial velocities of S2 and the radial velocity as calculated from the orbit fit.

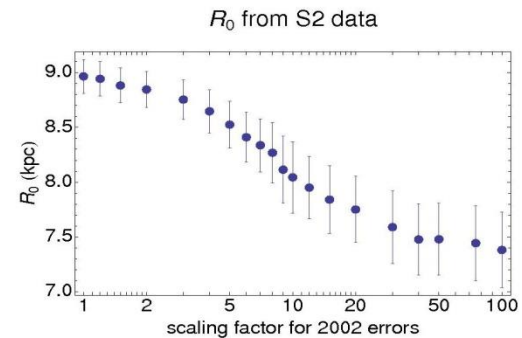


FIG. 14.— Fitted value of R_0 for various scaling factors of the S2 2002 data, using a fit with the coordinate system priors. The factor by which the 2002 astrometric errors of the S2 data is scaled up strongly influences the distance. The mean factor determined in Figure 9 is ≈ 7 , corresponding to $R_0 \approx 8.1$ kpc.

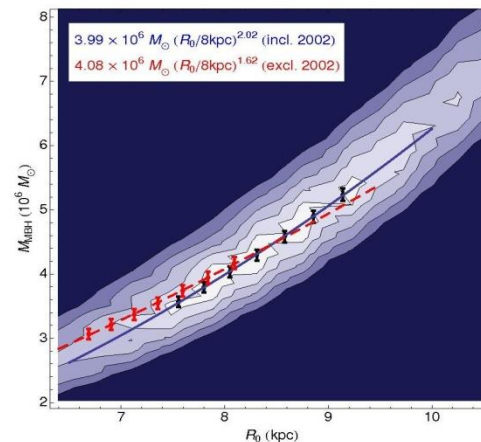


FIG. 15.— Contour plot of χ^2 as function of R_0 and central point mass. The two parameters are strongly correlated. The contours are generated from the S2 data including the 2002 data; fitting at each point all other parameters both of the potential and the orbital elements. The black dots indicate the position and errors of the best fit values of the mass for the respective distance; the blue line is a power law fit to these points; the corresponding function is given in the upper row of the text box. The central point is chosen at the best fitting distance. The red points and the red dashed line are the respective data and fit for the S2 data excluding the 2002 data; the fit is reported in the lower row of the text box. The contour levels are drawn at confidence levels corresponding to 1σ , 3σ , 5σ , 7σ , 9σ .

From the numbers it seems that the fit excluding the

An Expanded View of the Universe

Science with the
European Extremely Large Telescope



Black Holes

Black holes are some of the most bizarre objects in the Universe, challenging the imaginations of even the most creative scientists. They are places where gravity trumps all other forces in the Universe, pushing our understanding of physics to the limit. Even more strangely, supermassive black holes seem to play a key role in the formation of galaxies and structures in the Universe.

Galactic Centre

Over the last 15 years or so, an enormous amount of work has gone into improving our understanding of the closest supermassive black hole — Sagittarius A* at the centre of the Milky Way.

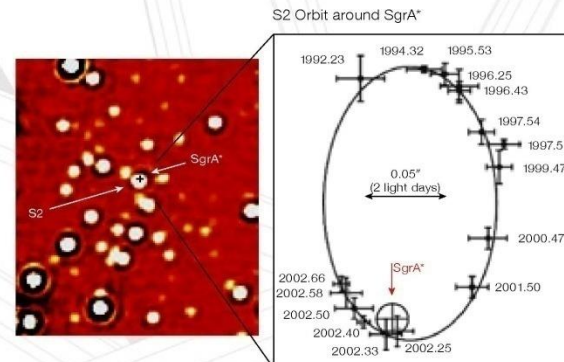
Technological progress, in particular in the areas of adaptive optics and high angular resolution with ground-based 8-metre-class telescopes, has allowed impressive progress in understanding supermassive black holes and their surroundings. Key progress was made in proving the very existence of a supermassive black hole at the centre of the Milky Way, in refining our knowledge of how matter falls into black holes, and in identifying gas discs and young stars in the immediate vicinity of the black hole. The Galactic Centre was thus established as the most important laboratory for the study of supermassive black holes and their surroundings.

But its potential for progress in fundamental physics and astrophysics is far from being fully exploited. The Galactic Centre remains the best place to test general relativity directly in a strong gravitational field. The E-ELT will enable extremely accurate measurements of the positions of stars (at the 50–100 microarcsecond

level over fields of tens of arcseconds), as well as radial velocity measurements with about 1 km/s precision, pushing our observations ever closer to the black hole event horizon. Stars can then be discovered at 100 Schwarzschild radii, where orbital velocities approach a tenth of the speed of light. This is more than ten times closer than can be achieved with the current generation of telescopes. Such stellar probes will allow us to test the predicted relativistic signals of black hole spin and the gravitational redshift caused by the black hole, and even to detect gravitational wave effects. Further out, the dark matter distribution around the black hole, predicted by cold dark matter cosmologies (Λ CDM), can be explored. The distance to the Galactic Centre can be measured to 0.1%, constraining in turn the size and shape of the galactic halo and the Galaxy's local rotation speed to unprecedented levels. Crucial progress in our understanding of the interaction of the black hole with its surroundings will be made. The puzzling stellar cusp around the Galactic Centre, as well as the observed star formation in the vicinity of the black hole will be studied in detail for the first time.

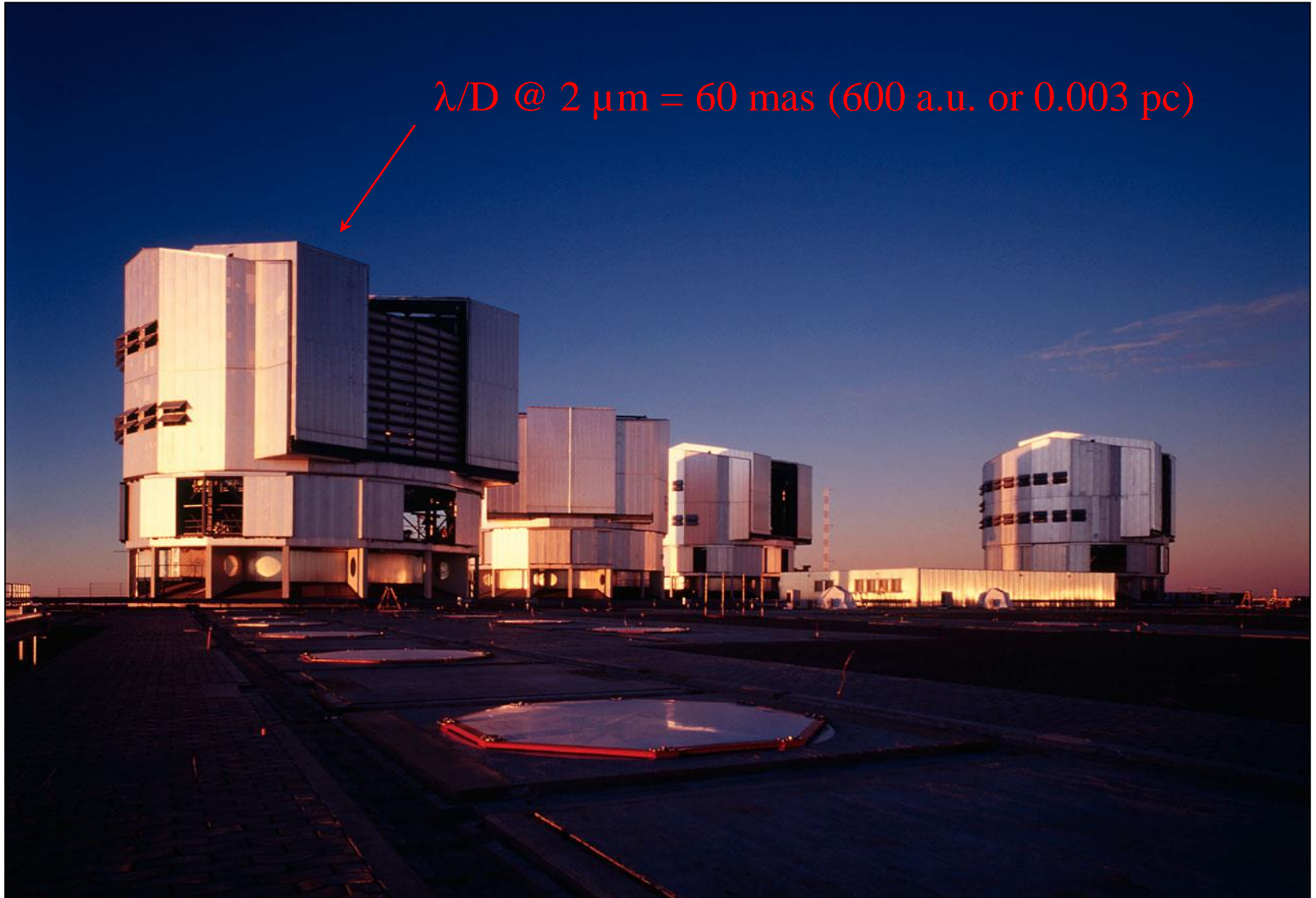
Left: Very Large Telescope (VLT) observations have revealed that the supermassive black hole closest to us is located in the centre of the Milky Way.

The Milky Way's central supermassive black hole has been weighed by measuring the proper motions of stars in its vicinity.



The VLT, *Very Large Telescope*
4 european 8 m telescopes at Cerro Paranal in Chili

$\lambda/D @ 2 \mu\text{m} = 60 \text{ mas (600 a.u. or 0.003 pc)}$



Going beyond boundaries thanks to accurate spatial information

- Bring the ultimate evidence that Sgr A* is a black hole: the mass is contained in the Schwarzschild radius.
- Understand the nature of flares.
- Use the black hole as a tool to study general relativity in the strong field regime

Scale $\sim 1 R_s$

10 μ as

- Study relativistic effects on nearby stars
- Understand the nature of S stars and their distribution

Scale $\sim 100 R_s$

1 mas

MG15 New talk in BH2 -

14 мая, 23:17

Eisenhauer, Frank

eisenhau@mpe.mpg.de

Max Planck Institute for Extraterrestrial Physics, , Giessenbachstr.

Garching, 85748

Bavaria, Germany

Parallel session: BH2 - Theoretical and observational studies of astrophysical black holes

type : Oral abstract

Title: The 2018 Peri-Passage of S2 - Testing General Relativity Near The Galactic Center Black Hole

Co-authors: GRAVITY

Abstract: The Galactic Center offers the unique possibility to quantitatively test general relativity in the so-far unexplored regime close to a super-massive black hole. Here we present the current status of measuring post-Newtonian effects in the orbit of the star S2 during its peri-passage in May 2018. As the star approaches the black hole as close as 17 light hours and a speed of almost 8000 km/s, we follow its orbit with infrared spectroscopy and interferometry at the ESO Very Large Telescope. The focus of the talk will be on the redshift measurements with SINFONI, and the deep interferometric imaging and astrometry with GRAVITY. This GRAVITY instrument, which we have developed specifically for the observations of the Galactic Center black hole and its orbiting stars, is now routinely achieving ~ 3 milli-arcsec imaging interferometry, with a sensitivity several hundred times better than previous instruments, and **an astrometric precision of few ten micro-arcseconds**, which corresponds to only few Schwarzschild radii of Galactic Center massive black hole.

AFZ, A.A. Nucita, F. De Paolis, G. Ingrosso, PRD 76, 062001 (2007)

The mass concentration at the Galactic Center

Recent advancements in infrared astronomy are allowing to test the scale of the mass profile at the center of our galaxy down to tens of AU. With the Keck 10 m telescope, the proper motion of several stars orbiting the Galactic Center black hole have been monitored and almost entire orbits, as for example that of the S2 star, have been measured allowing an unprecedented description of the Galactic Center region. Measurements of the amount of mass $M(< r)$ contained within a distance r from the Galactic Center are continuously improved as more precise data are collected. Recent observations (Ghez et al. (2003)) extend down to the periastron distance ($\simeq 3 \times 10^{-4}$ pc) of the S16 star and they correspond to a value of the enclosed mass within $\simeq 3 \times 10^{-4}$ pc of $\simeq 3.67 \times 10^6 M_{\odot}$. Several authors have used these observations to model the Galactic Center mass concentration. Here and in the following, we use the three component

For a test particle orbiting a Schwarzschild black hole of mass M_{BH} , the periastron shift is given by (see e.g. Weinberg, 1972)

$$\Delta\phi_S \simeq \frac{6\pi GM_{\text{BH}}}{d(1-e^2)c^2} + \frac{3(18+e^2)\pi G^2 M_{\text{BH}}^2}{2d^2(1-e^2)^2 c^4}, \quad (9)$$

d and e being the semi-major axis and eccentricity of the test particle orbit, respectively. For a rotating black hole with spin parameter $a = |\mathbf{a}| = J/GM_{\text{BH}}$, the space-time is described by the Kerr metric and, in the most favorable case of equatorial plane motion ($(\mathbf{a}, \mathbf{v}) = 0$), the shift is given by (Boyer and Price (1965))

$$\Delta\phi_K \simeq \Delta\phi_S + \frac{8a\pi M_{\text{BH}}^{1/2} G^{3/2}}{d^{3/2}(1-e^2)^{3/2} c^3} + \frac{3a^2\pi G^2}{d^2(1-e^2)^2 c^4}, \quad (10)$$

which reduces to eq. (9) for $a \rightarrow 0$. In the more general case, $\mathbf{a} \cdot \mathbf{v} \neq 0$, the

expected periastron shift has to be evaluated numerically.

The expected periastron shifts (mas/revolution), $\Delta\phi$ (as seen from the center) and $\Delta\phi_E$ (as seen from Earth at the distance $R_0 \simeq 8$ kpc from the GC), for the Schwarzschild and the extreme Kerr black holes, for the S2 and S16 stars turn out to be $\Delta\phi^{S2} = 6.3329 \times 10^5$ and 6.4410×10^5 and $\Delta\phi_E^{S2} = 0.661$ and 0.672 respectively, and $\Delta\phi^{S16} = 1.6428 \times 10^6$ and 1.6881×10^6 and $\Delta\phi_E^{S16} = 3.307$ and 3.399 respectively. Recall that

$$\Delta\phi_E = \frac{d(1+e)}{R_0} \Delta\phi_{S,K} . \quad (11)$$

Notice that the differences between the periastron shifts for the Schwarzschild and the maximally rotating Kerr black hole is at most 0.01 mas for the S2 star and 0.009 mas for the S16 star. In order to make these measurements with the required accuracy, one needs to know the S2 orbit with a precision of at least $10 \mu\text{as}$.

The star cluster surrounding the central black hole in the GC could be sizable. At least 17 members have been observed within 15 mpc up to now (Ghez et al. (2005)). However, the cluster mass and density distribution, that is to say its mass and core radius, is still unknown. The presence of this cluster affects the periastron shift of stars orbiting the central black hole. The periastron advance depends strongly on the mass density profile and especially on the central density and typical length scale.

We model the stellar cluster by a Plummer model density profile (Binney & Tremaine (1987))

$$\rho_{CL}(r) = \rho_0 f(r) , \quad \text{with} \quad f(r) = \left[1 + \left(\frac{r}{r_c} \right)^2 \right]^{-\alpha/2} , \quad (12)$$

and the mass contained within r is

$$M(r) = \lambda_{BH}M + \int_0^r 4\pi r'^2 \rho_0 f(r') dr' . \quad (15)$$

According to GR, the motion of a test particle can be fully described by solving the geodesic equations. Under the assumption that the matter distribution is static and pressureless, the equation of motion of the test particle becomes (see e.g. Weinberg 1972))

$$\frac{d\mathbf{v}}{dt} \simeq -\nabla(\Phi_N + 2\Phi_N^2) + 4\mathbf{v}(\mathbf{v} \cdot \nabla)\Phi_N - v^2\nabla\Phi_N . \quad (16)$$

For the S2 star, d and e given in the literature are 919 AU and 0.87 respectively. They yield the orbits of the S2 star for different values of the

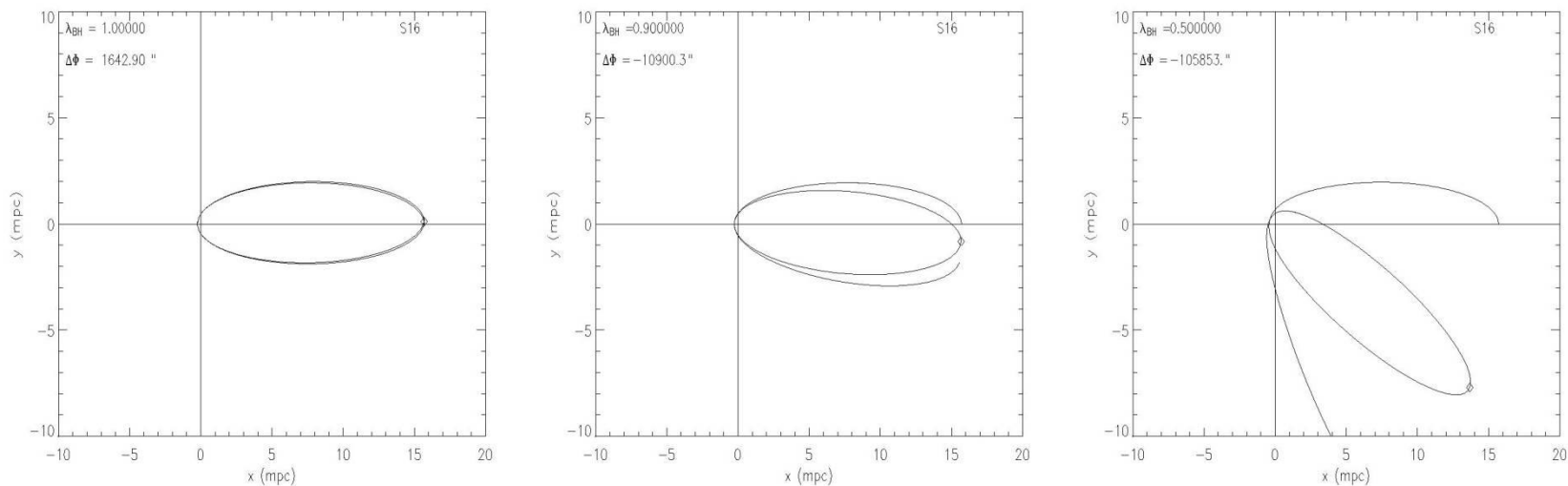


Figure 21: The same as in Figure 20 but for the S16–Sgr A* binary system. In this case, the binary system orbital parameters were taken from Ghez et al. (2005) assuming for the S16 mass a conservative value of $\simeq 10 M_{\odot}$.

model for the central region of our galaxy based on estimates of enclosed mass given by Ghez et al (2003, 2005) recently proposed by Hall and Gondolo (2006). This model is constituted by the central black hole, the central stellar cluster and the DM sphere (made of WIMPs), i.e.

$$M(< r) = M_{BH} + M_*(< r) + M_{DM}(< r) , \quad (17)$$

where M_{BH} is the mass of the central black hole Sagittarius A*. For the central stellar cluster, the empirical mass profile is

$$M_*(< r) = \begin{cases} M_* \left(\frac{r}{R_*} \right)^{1.6} , & r \leq R_* \\ M_* \left(\frac{r}{R_*} \right)^{1.0} , & r > R_* \end{cases} \quad (18)$$

with a total stellar mass $M_* = 0.88 \times 10^6 M_\odot$ and a size $R_* = 0.3878$ pc.

As far as the mass profile of the DM concentration is concerned, Hall & Gondolo (2006) have assumed a mass distribution of the form

$$M_{DM}(< r) = \begin{cases} M_{DM} \left(\frac{r}{R_{DM}} \right)^{3-\alpha}, & r \leq R_{DM} \\ M_{DM}, & r > R_{DM} \end{cases} \quad (19)$$

M_{DM} and R_{DM} being the total amount of DM in the form of WIMPs and the radius of the spherical mass distribution, respectively.

Hall and Gondolo (2006) discussed limits on DM mass around the black hole at the Galactic Center. It is clear that present observations of stars around the Galactic Center do not exclude the existence of a DM sphere with mass $\simeq 4 \times 10^6 M_{\odot}$, well contained within the orbits of the known stars, if its radius R_{DM} is $\lesssim 2 \times 10^{-4}$ pc (the periastron distance of the S16 star in the more recent analysis (Ghez et al. 2005)). However, if one

Apoastron Shift Constraints

According to GR, the motion of a test particle can be fully described by solving the geodesic equations. Under the assumption that the matter distribution is static and pressureless, the equations of motion at the first post-Newtonian (PN) approximation become (see e.g. (Fock 1961, Weinberg 1972, Rubilar & Eckart 2001))

$$\frac{d\mathbf{v}}{dt} \simeq -\nabla(\Phi_N + 2\Phi_N^2) + 4\mathbf{v}(\mathbf{v} \cdot \nabla)\Phi_N - v^2\nabla\Phi_N . \quad (21)$$

We note that the PN-approximation is the first relativistic correction from which the apoastron advance phenomenon arises. In the case of the S2 star, the apoastron shift as seen from Earth (from Eq. (23)) due to the presence of a central black hole is about 1 mas, therefore not directly

obtained by the black hole only, the black hole plus the stellar cluster and the contribution of two different DM mass density profiles. In each case the S2 orbit apoastron shift is given. As one can see, for selected parameters for DM and stellar cluster masses and radii the effect of the stellar cluster is almost negligible while the effect of the DM distribution is crucial since it enormously overcome the shift due to the relativistic precession. Moreover, as expected, its contribution is opposite in sign with respect to that of the black hole (Nucita et al. (2007)).

We note that the expected apoastron (or, equivalently, periastron) shifts (mas/revolution), $\Delta\Phi$ (as seen from the center) and the corresponding values $\Delta\phi_E^\pm$ as seen from Earth (at the distance $R_0 \simeq 8$ kpc from the GC) are related by

$$\Delta\phi_E^\pm = \frac{d(1 \pm e)}{R_0} \Delta\Phi, \quad (23)$$

where with the sign \pm are indicated the shift angles of the apoastron (+)

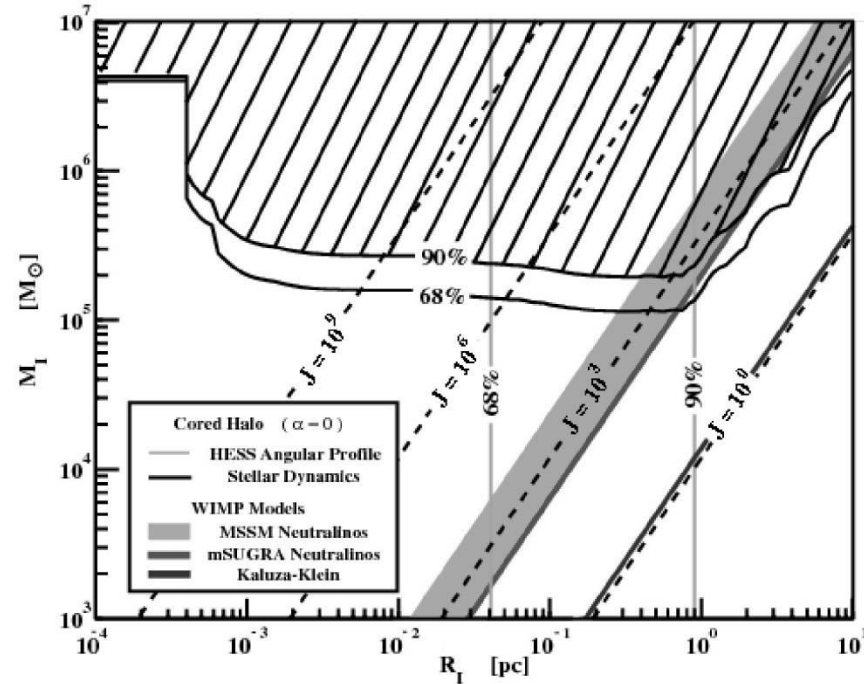
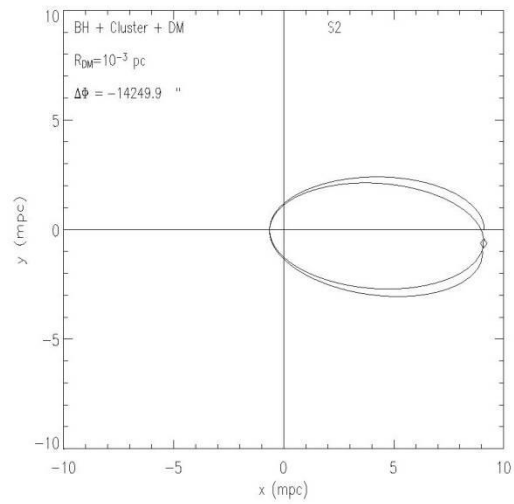
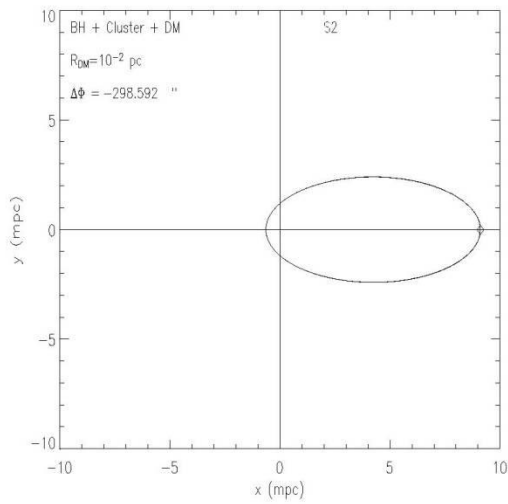
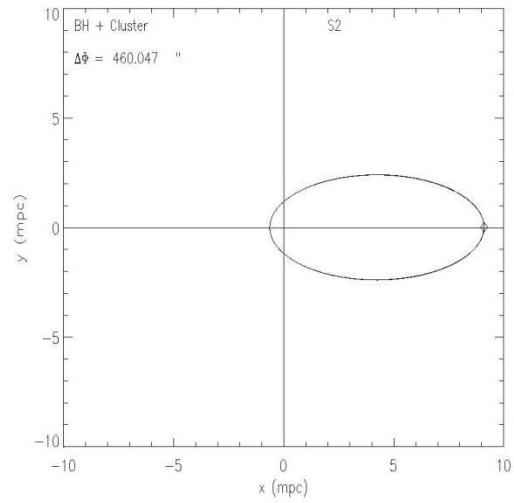
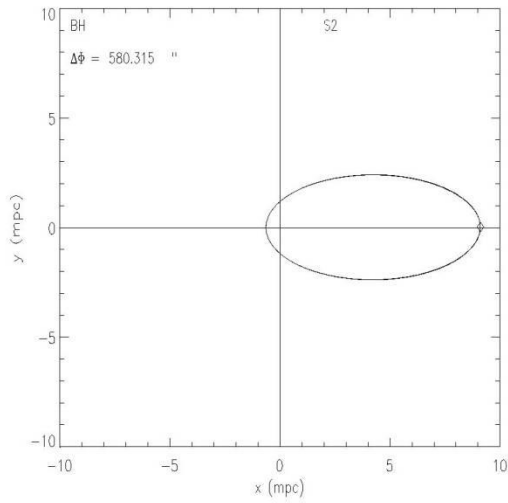


Figure 28: An allowed region for DM distribution from S2 like star trajectories near the Black Hole at the Galactic Center (Hall and Gondolo (2006)).



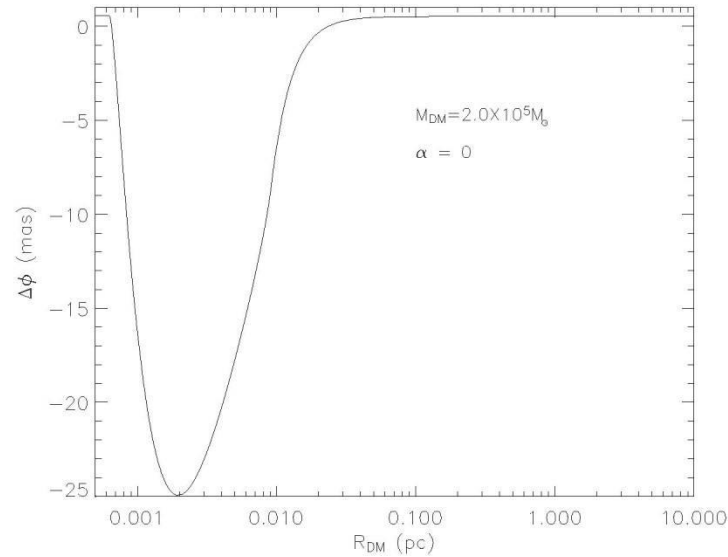
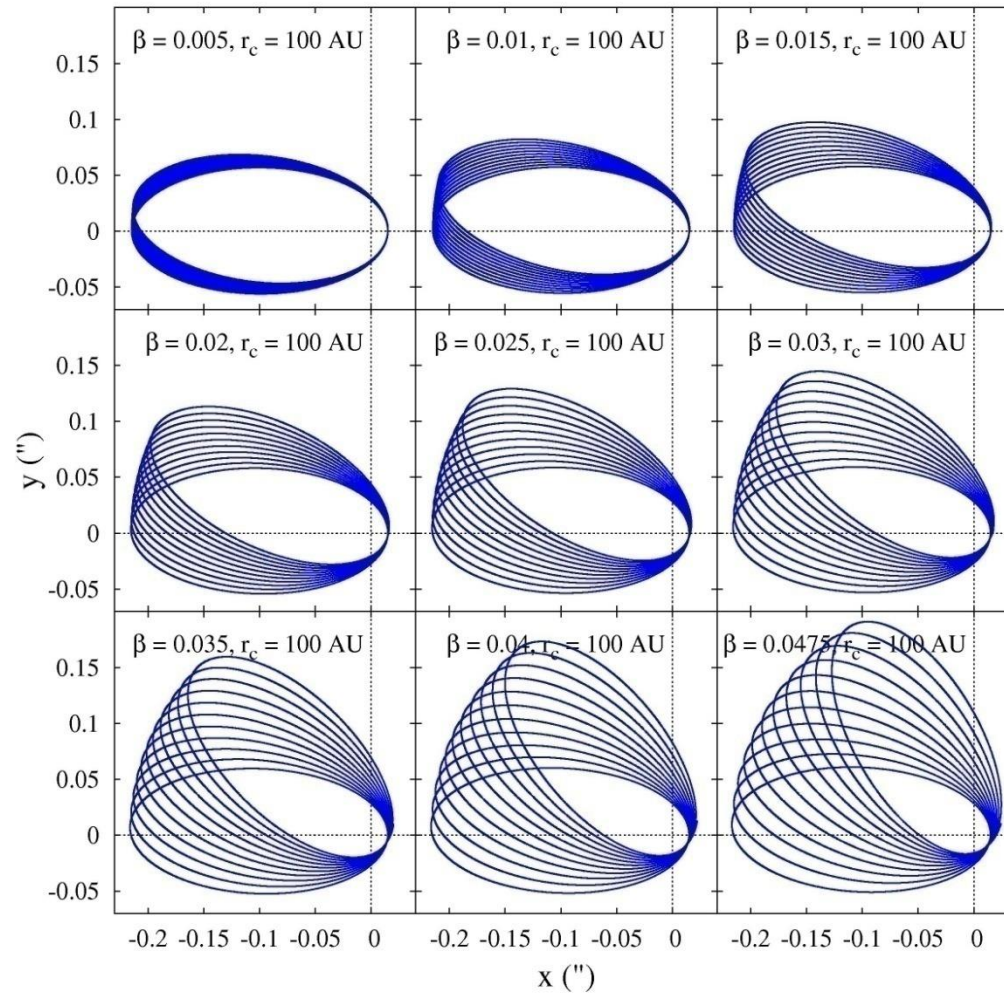


Figure 32: Apoastron shift as a function of the DM radius R_{DM} for $\alpha = 0$ and $M_{DM} \simeq 2 \times 10^5 M_{\odot}$. Taking into account present day precision for the apoastron shift measurements (about 10 mas) one can say that DM radii R_{DM} in the range $8 \times 10^{-4} - 10^{-2}$ pc are not acceptable.

D. Borka, P. Jovanovic, V. Borka Jovanovic and AFZ, PRD, **85**,
124004 (2012).



capabilities. They showed that the orbital precession can occur due to relativistic effects, resulting in a prograde shift and due to a possible extended mass distribution, producing a retrograde shift. Both prograde relativistic and retrograde Newtonian periastron shifts will result in rosette-shaped orbits. Weinberg *et al.* [12] discussed physical experiments achievable via the monitoring of stellar dynamics near the massive black hole at the Galactic center with a diffraction-limited, next-generation, extremely large telescope. They demonstrated that the lowest order relativistic effects, such as the prograde precession, will be detectable if the astrometric precision becomes less than 0.5 mas.

In this paper we continue to investigate constraints on the parameters of this class of gravity theories using S2-like star orbits under the uncertainty of 10 mas. In Sec. II the type of gravitational potential we use is given. In Sec. III we present the S2-like star orbits, gravity parameters, and angles of orbital precession, and also compare theoretical results with observations. The main conclusions are pointed out in Sec. IV.

II. THEORY

R^n gravity belongs to power-law fourth-order theories of gravity obtained by replacing the scalar curvature R with $f(R) = f_0 R^n$ in the gravity Lagrangian [1,2]. As a result, in the weak field limit [13], the gravitational potential is found to be [1,2]

$$\Phi(r) = -\frac{GM}{2r} \left[1 + \left(\frac{r}{r_c} \right)^\beta \right], \quad (1)$$

where r_c is an arbitrary parameter, depending on the typical scale of the considered system, and β is a universal parameter:

$$\beta = \frac{12n^2 - 7n - 1 - \sqrt{36n^4 + 12n^3 - 83n^2 + 50n + 1}}{6n^2 - 4n + 2}. \quad (2)$$

This formula corresponds to a modification of the gravity action in the form

$$A = \int d^4x \sqrt{-g} (f(R) + L_m), \quad (3)$$

where $f(R)$ is a generic function of the Ricci scalar curvature and L_m is the standard matter Lagrangian.

For $n = 1$ and $\beta = 0$ the R^n potential reduces to the Newtonian one, as expected. Parameter β controls the shape of the correction term and is related to n , which is part of the gravity Lagrangian. Since it is the same for all gravitating systems, as a consequence, β must be the same for all of them and therefore it is a universal parameter [2]. The parameter r_c is the scale length parameter, and it is related to the boundary conditions and the mass of the system [2].

III. RESULTS

A. Orbits of S2-like stars and parameters of R^n gravity

In order to study the effects of R^n gravity on the motion of S2, we performed two-body calculations of its orbit in the R^n potential [Eq. (1)] during two periods. We assumed the following input parameters taken from the paper of Zakharov *et al.* [10]: orbital eccentricity of the S2-like star, $e = 0.87$; major semiaxis $a = 919$ AU; mass of the S2-like star, $M_* = 1M_\odot$; mass of the central black hole, $M_{\text{BH}} = 3.4 \times 10^6 M_\odot$ (where M_\odot is the solar mass); and orbital period of the S2-like star is 15 years. We calculated the S2-like star orbit during two periods using Newtonian and R^n potentials. We also investigated the constraints on the parameters β and r_c for which the deviations between the S2-like star orbits in the R^n gravity potential [Eq. (1)] and its Keplerian orbit will stay within the maximum precision of the current instruments (about 10 mas), during one orbital period.

In Fig. 1 we present the trajectory of the S2-like star around a massive black hole in R^n gravity (blue solid line) and in Newtonian gravity (red dashed line) for $r_c = 100$ AU and for the following nine values of parameter β : 0.005, 0.01, 0.015, 0.02, 0.025, 0.03, 0.035, 0.04, 0.0475. The black hole is assumed to be located at the coordinate origin. We fix a value of parameter r_c at 100 AU, because this value corresponds to the maximal value of parameter β in the parameter space (see Fig. 3), and vary values of parameter β . All nine orbits presented fulfill the request that the R^n orbit and the corresponding Newtonian orbit differ by less than 10 mas (i.e. within the maximum precision of the current observations) during one orbital period. We can see that if parameter β increases, the R^n orbit differs more from the corresponding Newtonian orbit since the precession angle becomes larger. This indicates that the value of β should be small, as inferred from Solar System data [9] and in contrast to the value $\beta = 0.817$ (obtained by [2], which gives excellent agreement between theoretical and observed rotation curves). In the future, with improvements in observational facilities, the precision on constraints on values of parameters β and r_c will increase, as will the accuracy of the S2 orbit.

The corresponding distances between the S2-like star and the black hole as a function of time for the same values of parameters r_c and β as in Fig. 1 are presented in Fig. 2. There is an additional requirement on parameter space: the period of the S2-like star orbit has to remain $\approx 15 \pm 0.2$ yr. Like in the previous case, with increasing observational accuracy of the period, the precision on constraints on values of parameters β and r_c will also increase.

In Fig. 3 we present the parameter space for R^n gravity under the constraint that, during one orbital period, S2-like star orbits under R^n gravity differ by less than ε from their orbits under Newtonian gravity for ten values of parameter ε : 0.001, 0.002, 0.003, 0.004, 0.005, 0.006, 0.007, 0.008,

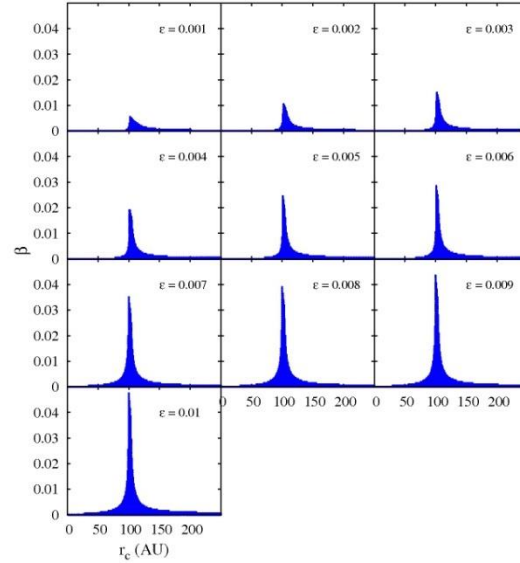


FIG. 3 (color online). The parameter space for R^n gravity under the constraint that, during one orbital period, the S2-like star orbits in R^n gravity differ by less than ϵ from the corresponding orbits in Newtonian gravity, for the following ten values of parameter ϵ : 0.001, 0.002, 0.003, 0.004, 0.005, 0.006, 0.007, 0.008, 0.009, and 0.01.

The exact expression (7) is inappropriate for practical applications. However, it can be easily approximated for $\beta \approx 0$ and $\beta \approx 1$. In the case of $\beta \approx 0$ expansion in Eq. (7) in Taylor's series over β , up to first order, leads to the following expression for the precession angle:

$$\Delta\theta = \frac{\pi^{\text{rad}}\beta(\sqrt{1-e^2}-1)}{e^2} = \frac{180^\circ\beta(\sqrt{1-e^2}-1)}{e^2}. \quad (8)$$

The above expression in the case of the S2-like star orbit is presented in Fig. 9 as a blue dash-dotted line. Similarly, the expansion of Eq. (7) in power series for $\beta \approx 1$ leads to the following expression for the precession angle (red dotted line in Fig. 9):

$$\begin{aligned} \Delta\theta &= \frac{\pi^{\text{rad}}a(\beta-1)(\sqrt{1-e^2}-1+e^2)}{r_c e^2} \\ &= \frac{180^\circ a(\beta-1)(\sqrt{1-e^2}-1+e^2)}{r_c e^2}. \end{aligned} \quad (9)$$

One can expect that, in general, the precession angle depends on the semimajor axis and eccentricity of the orbit (see e.g. Iorio and Ruggiero [17]), as well as on both

potential parameters β and r_c . This is indeed the case for $\beta \approx 1$ in Eq. (9). But as it can be seen from formula (8), the precession angle in the case when β is small ($\beta \approx 0$) depends only on the eccentricity and the universal constant β itself.

In order to test if the approximation from Eq. (8) is satisfactory in the case of the S2-like star, we derived its precession angle in two ways:

- (i) analytically from the approximative formula (8),
- (ii) numerically from the calculated orbits presented in Fig. 8.

Comparison of the obtained precession angles by these two methods is presented in Table I. As it can be seen from this table, the approximative formula (8) can be used for estimating the precession angle for all values of β from Fig. 8.

The above analysis indicates that R^n gravity results in the retrograde shift of the S2-like star orbit. Rubilar and Eckart [11] showed that the orbital precession can be due to relativistic effects, resulting in a prograde shift, or due to an extended mass distribution, producing a retrograde shift. We can conclude that the perturbing potential $V(r)$ has an

D. Borka, V. Borka Jovanovic, P. Jovanovic, AFZ

From an analysis of S2 orbit one can find signatures
of Yukawa gravity (JCAP, 2013)

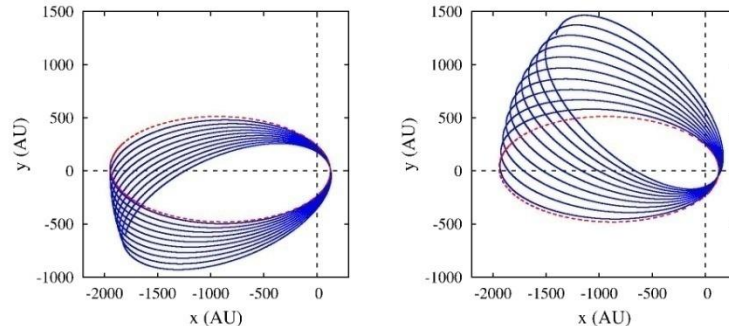


Figure 1. Comparisons between the orbit of S2 star in Newtonian gravity (red dashed line) and Yukawa gravity during 10 orbital periods (blue solid line) for $\Lambda = 2.59 \times 10^3$ AU. In the left panel $\delta = +1/3$, and in the right $\delta = -1/3$.

5. the reduced χ^2 is minimized and the final values of initial positions and velocities are obtained.

Finally, we kept the value of Λ which resulted with the smallest value of minimized reduced χ^2 .

In order to obtain some more general constraints on the parameters of Yukawa gravity, we also varied both δ and Λ and studied the simulated orbits of S2 star which give at least the same or better fits than the Keplerian orbit. For each pair of these parameters the reduced χ^2 of the best fit is obtained and used for generating the χ^2 maps over the $\Lambda - \delta$ parameter space. These maps are then used to study the confidence regions in $\Lambda - \delta$ parameter space.

3 Results and discussion

The simulated orbits of S2 star around the central object in Yukawa gravity (blue solid line) and in Newtonian gravity (red dashed line) for $\Lambda = 2.59 \times 10^3$ AU and $\delta = +1/3$ (left panel) and $\delta = -1/3$ (right panel) during 10 periods, are presented in Fig. 1. We can notice that for $\delta = -1/3$ the precession has negative direction and when $\delta = +1/3$ the precession has positive direction. Our analysis shows that the Yukawa gravity potential induces precession of S2 star orbit in the same direction as General Relativity for $\delta > 0$ and for $\delta < -1$, and in the opposite direction for $-1 < \delta < 0$ as in the case of extended mass distribution or in R^n gravity [22].

We used these simulated orbits to fit the observed orbits of S2 star. The best fit (according to NTT/VLT data) is obtained for the scale parameter: $\Lambda = 2.59 \times 10^3$ AU, for which even a significant strength of Yukawa interaction could be expected according to the planetary and Lunar Laser Ranging constraints [32].

In Fig. 2 we presented two comparisons between the fitted orbits in Yukawa gravity for $\delta = +1/3$ through the astrometric observations of S2 star by NTT/VLT alone (left) and NTT/VLT+Keck combination (right). In order to combine NTT/VLT and Keck data sets,

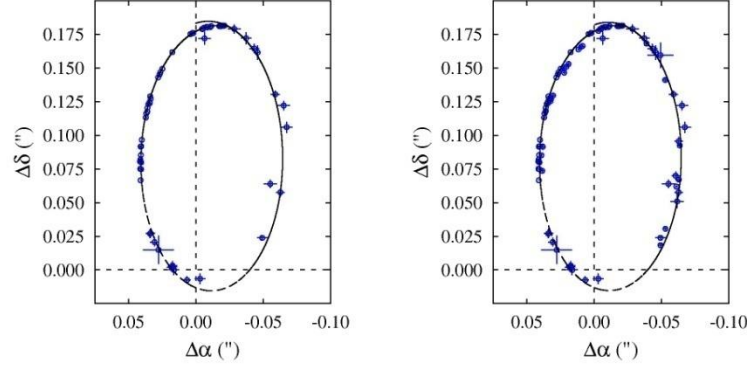


Figure 2. The fitted orbits in Yukawa gravity for $\delta = +1/3$ through the astrometric observations of S2 star (denoted by circles), obtained by NTT/VLT alone (left panel) and NTT/VLT+Keck (right panel). The best fits are obtained for $\Lambda = 2.59 \times 10^3$ AU and $\Lambda = 3.03 \times 10^3$ AU, respectively.

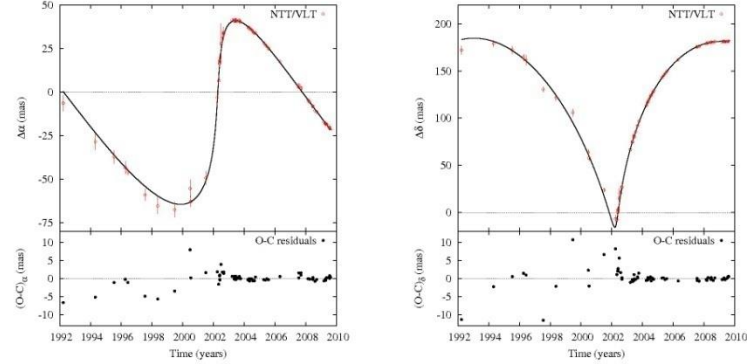


Figure 3. The comparisons between the observed (open circles with error bars) and fitted (solid lines) coordinates of S2 star (top), as well as the corresponding O-C residuals (bottom). The left panel shows the results for $\Delta\alpha$ and right panel for $\Delta\delta$ in the case of NTT/VLT observations and Yukawa gravity potential with $\delta = +1/3$ and $\Lambda = 2.59 \times 10^3$ AU.

the position of the origin of Keck observations is first shifted by $\Delta x = 3.7$ and $\Delta y = 4.1$ mas, following the suggestion given in [39]. In the first case the best fit is obtained for $\Lambda = 2.59 \times 10^3$ AU, resulting with reduced $\chi^2 = 1.54$, and in the second case for $\Lambda = 3.03 \times 10^3$ AU with reduced $\chi^2 = 3.24$. As one can see from these figures, in both cases there is a good agreement between the theoretical orbits and observations, although the higher value of reduced χ^2 in

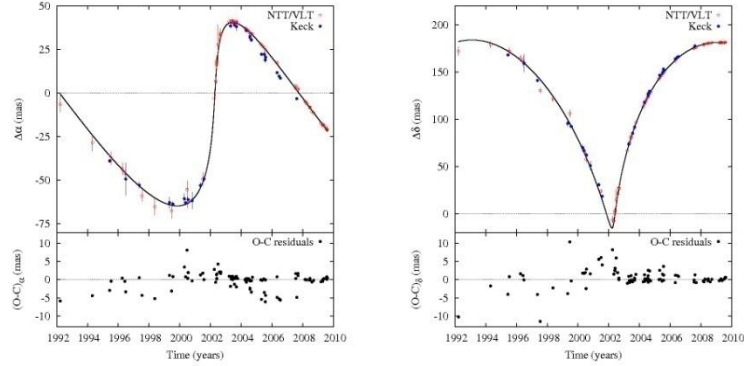


Figure 4. The same as in Fig. 3, but for NTT/VLT+Keck combined observations and for Yukawa gravity potential with $\Lambda = 3.03 \times 10^3$ AU.

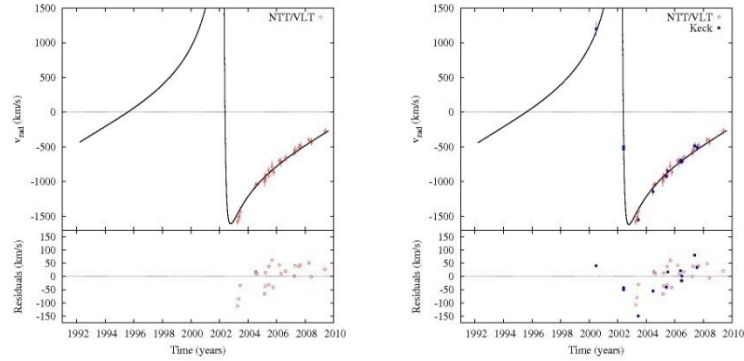


Figure 5. The comparisons between the observed (circles with error bars) and fitted (solid lines) radial velocities of S2 star (top), as well as the corresponding O-C residuals (bottom). The left panel shows the results in the case of NTT/VLT observations and Yukawa gravity potential with $\Lambda = 2.59 \times 10^3$ AU, while the right panel shows the results for NTT/VLT+Keck combined observations and for Yukawa gravity potential with $\Lambda = 3.03 \times 10^3$ AU. In both cases $\delta = +1/3$.

the second case indicates possibly larger positional difference between the two coordinate systems, as also noted in [39]. These figures also show that the simulated orbits of S2 are not closed in vicinity of apocenter, indicating a possible orbital precession.

In Figs. 3 and 4 we presented the comparisons between the observed and fitted coordinates of S2 star and their O-C residuals in the case of NTT/VLT observations, as well as NTT/VLT+Keck combined data set, respectively. One can notice that in both cases, O-C

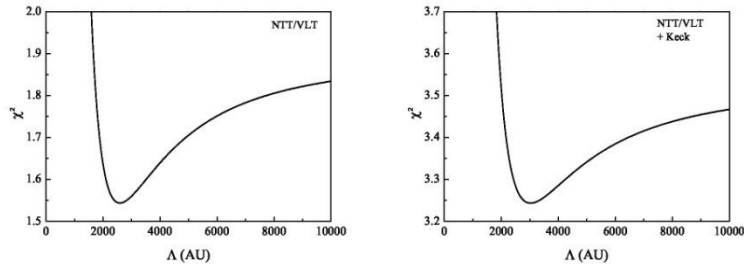


Figure 6. The reduced χ^2 for $\delta=1/3$ as a function of Λ in case of NTT/VLT alone (left) and combined NTT/VLT+Keck (right) observations.

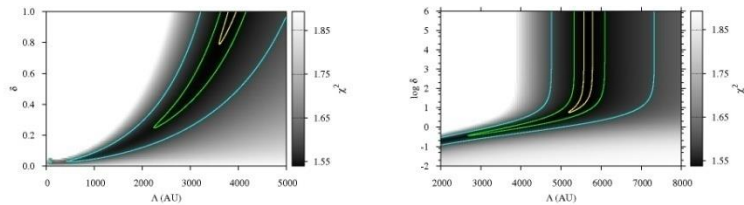


Figure 7. The maps of reduced χ^2 over the $\Lambda - \delta$ parameter space in case of NTT/VLT observations. The left panel corresponds to $\delta \in [0, 1]$, and the right panel to the extended range of $\delta \in [0.01, 10^6]$. The shades of gray color represent the values of the reduced χ^2 which are less than the corresponding value in the case of Keplerian orbit, and three contours (from inner to outer) enclose the confidence regions in which the difference between the current and minimum reduced χ^2 is less than 0.0005, 0.005 and 0.05, respectively.

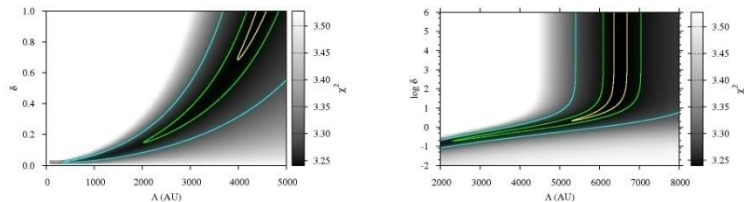


Figure 8. The same as in Fig. 7, but for the combined NTT/VLT+Keck observations.

residuals are higher in the first part of observing interval (up to the 12 mas) and much less in its second part (less than 2 mas). Due to adopted merit function given by expression (2.7), our fitting procedure assigned greater weight to these latter, more precise observations. Also, the O-C residuals are larger in the case of the combined NTT/VLT+Keck observations most likely due to the shift of the origin of the coordinate system, which was necessary in order to

Massive graviton theories

- M. Fierz and W. Pauli - 1939
- Zakharov; Veltman, van Dam – 1970
- Vainshtein - 1972
- Boulware, Deser -- 1972
- Logunov, Mestvirishvili, Gershtein et al.
- Visser – 1998 (review on such theories)
- Rubakov, Tinyakov – 2008
- DeRham -- 2016

Massive graviton theories (constraints)

- Sazhin (1978) GW's could be detected with pulsar timing
- Lee et al. (2010) array of pulsars and timing 60 pulsars – 5 years with accuracy 100 ns -- $\lambda_g > 4 \times 10^{12}$ km
-

**Observation of Gravitational Waves from a Binary Black Hole Merger**B. P. Abbott *et al.*^{*}

(LIGO Scientific Collaboration and Virgo Collaboration)

(Received 21 January 2016; published 11 February 2016)

On September 14, 2015 at 09:50:45 UTC the two detectors of the Laser Interferometer Gravitational-Wave Observatory simultaneously observed a transient gravitational-wave signal. The signal sweeps upwards in frequency from 35 to 250 Hz with a peak gravitational-wave strain of 1.0×10^{-21} . It matches the waveform predicted by general relativity for the inspiral and merger of a pair of black holes and the ringdown of the resulting single black hole. The signal was observed with a matched-filter signal-to-noise ratio of 24 and a false alarm rate estimated to be less than 1 event per 203 000 years, equivalent to a significance greater than 5.1σ . The source lies at a luminosity distance of 410_{-180}^{+140} Mpc corresponding to a redshift $z = 0.09_{-0.04}^{+0.03}$. In the source frame, the initial black hole masses are $36_{-4}^{+5} M_{\odot}$ and $29_{-4}^{+4} M_{\odot}$, and the final black hole mass is $62_{-4}^{+4} M_{\odot}$, with $3.0_{-0.5}^{+0.5} M_{\odot} c^2$ radiated in gravitational waves. All uncertainties define 90% credible intervals. These observations demonstrate the existence of binary stellar-mass black hole systems. This is the first direct detection of gravitational waves and the first observation of a binary black hole merger.

DOI: 10.1103/PhysRevLett.116.061102

I. INTRODUCTION

In 1916, the year after the final formulation of the field equations of general relativity, Albert Einstein predicted the existence of gravitational waves. He found that the linearized weak-field equations had wave solutions: transverse waves of spatial strain that travel at the speed of light, generated by time variations of the mass quadrupole moment of the source [1,2]. Einstein understood that gravitational-wave amplitudes would be remarkably small; moreover, until the Chapel Hill conference in 1957 there was significant debate about the physical reality of gravitational waves [3].

Also in 1916, Schwarzschild published a solution for the field equations [4] that was later understood to describe a black hole [5,6], and in 1963 Kerr generalized the solution to rotating black holes [7]. Starting in the 1970s theoretical work led to the understanding of black hole quasinormal modes [8–10], and in the 1990s higher-order post-Newtonian calculations [11] preceded extensive analytical studies of relativistic two-body dynamics [12,13]. These advances, together with numerical relativity breakthroughs in the past decade [14–16], have enabled modeling of binary black hole mergers and accurate predictions of their gravitational waveforms. While numerous black hole candidates have now been identified through electromagnetic observations [17–19], black hole mergers have not previously been observed.

^{*}Full author list given at the end of the article.

Published by the American Physical Society under the terms of the Creative Commons Attribution 3.0 License. Further distribution of this work must maintain attribution to the author(s) and the published article's title, journal citation, and DOI.

The discovery of the binary pulsar system PSR B1913+16 by Hulse and Taylor [20] and subsequent observations of its energy loss by Taylor and Weisberg [21] demonstrated the existence of gravitational waves. This discovery, along with emerging astrophysical understanding [22], led to the recognition that direct observations of the amplitude and phase of gravitational waves would enable studies of additional relativistic systems and provide new tests of general relativity, especially in the dynamic strong-field regime.

Experiments to detect gravitational waves began with Weber and his resonant mass detectors in the 1960s [23], followed by an international network of cryogenic resonant detectors [24]. Interferometric detectors were first suggested in the early 1960s [25] and the 1970s [26]. A study of the noise and performance of such detectors [27], and further concepts to improve them [28], led to proposals for long-baseline broadband laser interferometers with the potential for significantly increased sensitivity [29–32]. By the early 2000s, a set of initial detectors was completed, including TAMA 300 in Japan, GEO 600 in Germany, the Laser Interferometer Gravitational-Wave Observatory (LIGO) in the United States, and Virgo in Italy. Combinations of these detectors made joint observations from 2002 through 2011, setting upper limits on a variety of gravitational-wave sources while evolving into a global network. In 2015, Advanced LIGO became the first of a significantly more sensitive network of advanced detectors to begin observations [33–36].

A century after the fundamental predictions of Einstein and Schwarzschild, we report the first direct detection of gravitational waves and the first direct observation of a binary black hole system merging to form a single black hole. Our observations provide unique access to the

properties of space-time in the strong-field, high-velocity regime and confirm predictions of general relativity for the nonlinear dynamics of highly disturbed black holes.

II. OBSERVATION

On September 14, 2015 at 09:50:45 UTC, the LIGO Hanford, WA, and Livingston, LA, observatories detected

the coincident signal GW150914 shown in Fig. 1. The initial detection was made by low-latency searches for generic gravitational-wave transients [41] and was reported within three minutes of data acquisition [43]. Subsequently, matched-filter analyses that use relativistic models of compact binary waveforms [44] recovered GW150914 as the most significant event from each detector for the observations reported here. Occurring within the 10-ms intersite

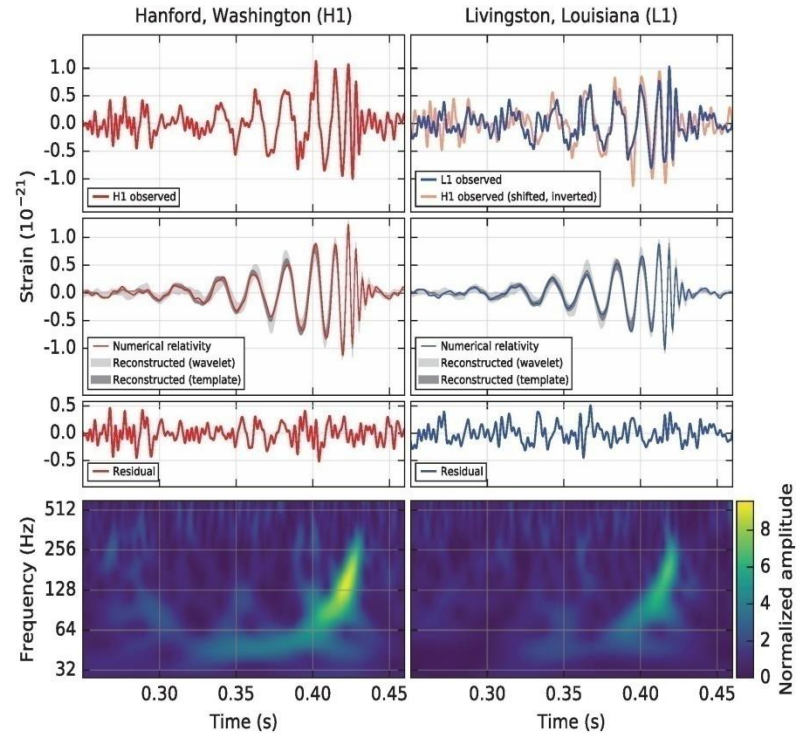


FIG. 1. The gravitational-wave event GW150914 observed by the LIGO Hanford (H1, left column panels) and Livingston (L1, right column panels) detectors. Times are shown relative to September 14, 2015 at 09:50:45 UTC. For visualization, all time series are filtered with a 35–350 Hz bandpass filter to suppress large fluctuations outside the detectors’ most sensitive frequency band, and band-reject filters to remove the strong instrumental spectral lines seen in the Fig. 3 spectra. *Top row, left:* H1 strain. *Top row, right:* L1 strain. GW150914 arrived first at L1 and $6.9^{+0.5}_{-0.4}$ ms later at H1; for a visual comparison, the H1 data are also shown, shifted in time by this amount and inverted (to account for the detectors’ relative orientations). *Second row:* Gravitational-wave strain projected onto each detector in the 35–350 Hz band. Solid lines show a numerical relativity waveform for a system with parameters consistent with those recovered from GW150914 [37,38] confirmed to 99.9% by an independent calculation based on [15]. Shaded areas show 90% credible regions for two independent waveform reconstructions. One (dark gray) models the signal using binary black hole template waveforms [39]. The other (light gray) does not use an astrophysical model, but instead calculates the strain signal as a linear combination of sine-Gaussian wavelets [40,41]. These reconstructions have a 94% overlap, as shown in [39]. *Third row:* Residuals after subtracting the filtered numerical relativity waveform from the filtered detector time series, as shown in [39]. *Bottom row:* A time-frequency representation [42] of the strain data, showing the signal frequency increasing over time.

propagation time, the events have a combined signal-to-noise ratio (SNR) of 24 [45].

Only the LIGO detectors were observing at the time of GW150914. The Virgo detector was being upgraded, and GEO 600, though not sufficiently sensitive to detect this event, was operating but not in observational mode. With only two detectors the source position is primarily determined by the relative arrival time and localized to an area of approximately 600 deg^2 (90% credible region) [39,46].

The basic features of GW150914 point to it being produced by the coalescence of two black holes—i.e., their orbital inspiral and merger, and subsequent final black hole ringdown. Over 0.2 s, the signal increases in frequency and amplitude in about 8 cycles from 35 to 150 Hz, where the amplitude reaches a maximum. The most plausible explanation for this evolution is the inspiral of two orbiting masses, m_1 and m_2 , due to gravitational-wave emission. At the lower frequencies, such evolution is characterized by the chirp mass [11]

$$\mathcal{M} = \frac{(m_1 m_2)^{3/5}}{(m_1 + m_2)^{1/5}} = \frac{c^3}{G} \left[\frac{5}{96} \pi^{-8/3} f^{-11/3} \dot{f} \right]^{3/5},$$

where f and \dot{f} are the observed frequency and its time derivative and G and c are the gravitational constant and speed of light. Estimating f and \dot{f} from the data in Fig. 1, we obtain a chirp mass of $\mathcal{M} = 30M_\odot$, implying that the total mass $M = m_1 + m_2$ is $\gtrsim 70M_\odot$ in the detector frame. This bounds the sum of the Schwarzschild radii of the binary components to $2GM/c^2 \gtrsim 210 \text{ km}$. To reach an orbital frequency of 75 Hz (half the gravitational-wave frequency) the objects must have been very close and very compact; equal Newtonian point masses orbiting at this frequency would be only $\approx 350 \text{ km}$ apart. A pair of neutron stars, while compact, would not have the required mass, while a black hole neutron star binary with the deduced chirp mass would have a very large total mass, and would thus merge at much lower frequency. This leaves black holes as the only known objects compact enough to reach an orbital frequency of 75 Hz without contact. Furthermore, the decay of the waveform after it peaks is consistent with the damped oscillations of a black hole relaxing to a final stationary Kerr configuration. Below, we present a general-relativistic analysis of GW150914; Fig. 2 shows the calculated waveform using the resulting source parameters.

III. DETECTORS

Gravitational-wave astronomy exploits multiple, widely separated detectors to distinguish gravitational waves from local instrumental and environmental noise, to provide source sky localization, and to measure wave polarizations. The LIGO sites each operate a single Advanced LIGO

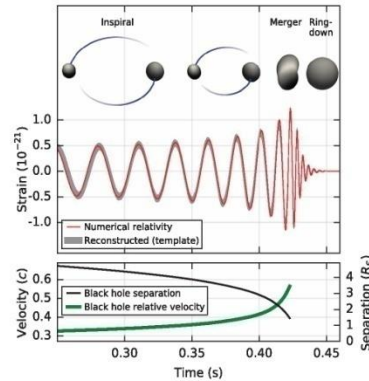


FIG. 2. *Top*: Estimated gravitational-wave strain amplitude from GW150914 projected onto H1. This shows the full bandwidth of the waveforms, without the filtering used for Fig. 1. The inset images show numerical relativity models of the black hole horizons as the black holes coalesce. *Bottom*: The Keplerian effective black hole separation in units of Schwarzschild radii ($R_S = 2GM/c^2$) and the effective relative velocity given by the post-Newtonian parameter $v/c = (GM\pi f/c^3)^{1/3}$, where f is the gravitational-wave frequency calculated with numerical relativity and M is the total mass (value from Table I).

detector [33], a modified Michelson interferometer (see Fig. 3) that measures gravitational-wave strain as a difference in length of its orthogonal arms. Each arm is formed by two mirrors, acting as test masses, separated by $L_x = L_y = L = 4 \text{ km}$. A passing gravitational wave effectively alters the arm lengths such that the measured difference is $\Delta L(t) = \delta L_x - \delta L_y = h(t)L$, where h is the gravitational-wave strain amplitude projected onto the detector. This differential length variation alters the phase difference between the two light fields returning to the beam splitter, transmitting an optical signal proportional to the gravitational-wave strain to the output photodetector.

To achieve sufficient sensitivity to measure gravitational waves, the detectors include several enhancements to the basic Michelson interferometer. First, each arm contains a resonant optical cavity, formed by its two test mass mirrors, that multiplies the effect of a gravitational wave on the light phase by a factor of 300 [48]. Second, a partially transmissive power-recycling mirror at the input provides additional resonant buildup of the laser light in the interferometer as a whole [49,50]: 20 W of laser input is increased to 700 W incident on the beam splitter, which is further increased to 100 kW circulating in each arm cavity. Third, a partially transmissive signal-recycling mirror at the output optimizes

Graviton Mass Estimate from Gravitational Wave Signal

Assuming that a graviton mass is small in comparison with energy of gravitational waves $hf \gg m_g c^2$, then

$$v_g/c \approx 1 - \frac{1}{2} \left(\frac{c}{\lambda_g f} \right)^2, \quad (1)$$

where $\lambda_g = h/(m_g c)$ is the graviton Compton wavelength and one could obtain (Will, 1998)

$$\lambda_g > 3 \times 10^{12} \text{km} \left(\frac{D}{200 \text{ Mpc}} \frac{100 \text{ Hz}}{f} \right)^{1/2} \left(\frac{1}{f \Delta t} \right)^{1/2}, \quad (2)$$

$$\Delta t = \Delta t_a - (1 + z)\Delta t_e, \quad (3)$$

where $\Delta t_a = t_a^{EM} - t_a^{GW}$, $\Delta t_e = t_e^{EM} - t_e^{GW}$, $t_a^{EM}(t_e^{EM})$ and $t_a^{GW}(t_e^{GW})$ are arrival (emission) instant of electromagnetic radiation and arrival (emission) instant for gravitational waves. As it was pointed out, one can use Eq. (2) if observers detected gravitational waves and electromagnetic radiations from one source and Δt_e is known or can be evaluated with a sufficient accuracy. Moreover, there is an opportunity to constrain a graviton mass in the case if there is only a gravitational wave signal. For numerical estimate, one can estimate $f\Delta t \sim \rho^{-1} \approx 10$ (where ρ is a signal-to-noise ratio) for LIGO-Virgo ground based interferometers, therefore, a graviton mass constraint can be at a level 2.5×10^{-22} eV for ground based LIGO-Virgo detectors.

The LIGO-Virgo collaboration reported about the first detection of gravitational waves from a merger of two black holes (it was detected on September 14, 2015. and it is called GW150914). According to estimates

from the shape of gravitational wave signal the source is located at a luminosity distance of around 410 Mpc (which corresponds to a redshift $z \approx 0.09$), the initial black hole masses were $36M_{\odot}$ and $29M_{\odot}$ and the final black hole mass is $62M_{\odot}$, therefore, around $3M_{\odot}$ was emitted in gravitational waves in 0.1 s. The collaboration not only discovered gravitational waves but also detected the first binary black hole system and one of the most powerful source of radiation in the Universe and the energy was released in gravitational waves. Moreover, the team constrained the graviton Compton wavelength $\lambda_g > 10^{13}$ km which could be interpreted as a constraint for a graviton mass $m_g < 1.2 \times 10^{-22}$ eV (Abbott et al. 2016) (the estimate roughly coincides with theoretical predictions).

In June 2017 the LIGO-Virgo collaboration published a paper where the authors described a detection of gravitational wave signal from a merger of binary black hole system with masses of components $31.2M_{\odot}$ and $19.4M_{\odot}$ at distance around 880 Mpc which corresponds to $z \approx 0.18$ (Abbott 2017). In

this case, around $2M_{\odot}$ was emitted in gravitational waves in around 0.4 s. The event is named GW170104. In this paper the authors significantly improved their previous graviton mass constraint, $m_g < 7.7 \times 10^{-23}$ eV.

On August 17, 2017 the LIGO-Virgo collaboration detected a merger of binary neutron stars with masses around $0.86M_{\odot}$ and $2.26M_{\odot}$ at a distance around 40 Mpc (GW170817) and after 1.7 s the Fermi-GBM detected γ -ray burst GRB 170817A associated with the GW170817. Since gravitational wave signal was observed before GRB 170817A one could conclude that the observational data are consistent with massless or very light graviton, otherwise, electromagnetic signal could be detected before gravitational one because in the case of relatively heavy gravitons gravitational waves could propagate slower than light.

In the consideration one assumes that photon is massless (but graviton may be massive). In the case of massive photon $m_{\gamma} > 0$ (see, (Jackson 1998) for introduction of Proca theory which describes a massive photon

case) to use the same logic at least we have to have $(c - v_\gamma) \ll (c - v_g)$ (c is a limiting speed of ultra high energy quanta, v_γ and v_g are velocities of quanta and gravitons respectively) or

$$m_g/f \gg m_\gamma/\nu, \quad (4)$$

as we see from Eq. (1), where m_g and m_γ are masses of graviton and photon, respectively; f and ν are their typical frequencies) and photon mass is constrained with another experimental (or observational) data. Different ways to evaluate photon mass are discussed in couple of reviews (Goldhaber and Nieto 2010, Tu et al. 2005, Okun 2006) and original papers. Laboratory experiments gave the upper limit as $m_\gamma < 7 \times 10^{-19}$ eV (Luo et al. 2003) or $m_\gamma < 5 \times 10^{-20}$ eV (Tu et al. 2006), while astrophysical constraint from analysis of plasma in Solar wind gave $m_\gamma < 10^{-18}$ eV (Ryutov 2007), analysis of Fast Radio Bursts gave weaker constraints on photon mass $m_\gamma < 10^{-14}$ eV .

One could roughly estimate frequency band for quanta where inequality (4) is hold. If we adopt the upper limit of graviton mass (around 10^{-22} eV) obtained by LIGO collaboration from the first GW events without electromagnetic counterpart and we assume $f \approx 100$, then the inequality (4) is hold for spectral band of quanta from radio up to higher frequencies if we use upper limit estimates from papers (Luo et al. 2003, Tu et al. 2006 and the inequality (4) is hold for spectral band of quanta from optical band up to higher frequencies if we use upper limit estimates from papers (Wu et al. 2016; Bonetti et al. 2016, 2017). Constraints on speed of gravitational waves have been found $-3 \times 10^{-15} < (v_g - c)/c < 7 \times 10^{-16}$ (Abbott et al., 2017). Graviton energy is $E = hf$, therefore, assuming a typical LIGO frequency range $f \in (10, 100)$, from the dispersion relation one could obtain a graviton mass estimate $m_g < 3 \times (10^{-21} - 10^{-20})$ eV which a slightly weaker estimate than previous ones obtained from binary black hole signals detected by the LIGO team.

GW170817

Binary neutron star merger

A LIGO / Virgo gravitational wave detection with associated electromagnetic events observed by over 70 observatories.



Distance
130 million light years

Discovered
17 August 2017

Type
Neutron star merger

12:41:04 UTC
A gravitational wave from a binary neutron star merger is detected.

gravitational wave signal
Two neutron stars, each the size of a city but with at least the mass of the sun, collided with each other.

gamma ray burst
A short gamma ray burst is an intense beam of gamma ray radiation which is produced just after the merger.

+ 2 seconds
A gamma ray burst is detected.

GW170817 allows us to measure the expansion rate of the universe directly using gravitational waves for the first time.

Detecting gravitational waves from a neutron star merger allows us to find out more about the structure of these unusual objects.

This multimessenger event provides confirmation that neutron star mergers can produce short gamma ray bursts.

The observation of a kilonova allowed us to show that neutron star mergers could be responsible for the production most of the heavy elements, like gold, in the universe.

Observing both electromagnetic and gravitational waves from the event provides compelling evidence that gravitational waves travel at the same speed as light.

kilonova
Decaying neutron-rich material creates a glowing kilonova, producing heavy metals like gold and platinum.

+10 hours 52 minutes
A new bright source of optical light is detected in a galaxy called NGC 4993, in the constellation of Hydra.

+11 hours 36 minutes
Infrared emission observed.

+15 hours
Bright ultraviolet emission detected.

+9 days
X-ray emission detected.

radio remnant
As material moves away from the merger it produces a shockwave in the interstellar medium - the tenuous material between stars. This produces emission which can last for years.

+16 days
Radio emission detected.

May 4, 2016 -- The Gruber Foundation has [announced](#) the award of the 2016 Gruber Cosmology Prize to LIGO's Ronald W.P. Drever (Caltech), Kip S. Thorne (Caltech), and Rainer Weiss (MIT) for the detection of gravitational waves.



- Yuri Milner, a Russian Internet entrepreneur and philanthropist, announced that he was giving \$3 million to the gravitational-wave discoverers. The award is a special addition to the \$3 million Breakthrough Prizes in Fundamental Physics he awards every fall. The three ringleaders of the gravitational-wave experiment, known as LIGO, Ronald P. Drever and Kip. S. Thorne of the California Institute of Technology, and Rainer Weiss of the Massachusetts Institute of Technology, will split \$1 million. The other \$2 million will be split among 1,012 scientists who were authors of the [article](#) in Physical Review Letters, or who made major contributions to the study of gravitational waves.



GW170104: Observation of a 50-Solar-Mass Binary Black Hole Coalescence at Redshift 0.2

B. P. Abbott *et al.**

(LIGO Scientific and Virgo Collaboration)

(Received 9 May 2017; published 1 June 2017)

We describe the observation of GW170104, a gravitational-wave signal produced by the coalescence of a pair of stellar-mass black holes. The signal was measured on January 4, 2017 at 10:11:58.6 UTC by the twin advanced detectors of the Laser Interferometer Gravitational-Wave Observatory during their second observing run, with a network signal-to-noise ratio of 13 and a false alarm rate less than 1 in 70 000 years. The inferred component black hole masses are $31.2^{+8.4}_{-6.0} M_{\odot}$ and $19.4^{+5.3}_{-3.9} M_{\odot}$ (at the 90% credible level). The black hole spins are best constrained through measurement of the effective inspiral spin parameter, a mass-weighted combination of the spin components perpendicular to the orbital plane, $\chi_{\text{eff}} = -0.12^{+0.21}_{-0.30}$. This result implies that spin configurations with both component spins positively aligned with the orbital angular momentum are disfavored. The source luminosity distance is 880^{+450}_{-390} Mpc corresponding to a redshift of $z = 0.18^{+0.08}_{-0.07}$. We constrain the magnitude of modifications to the gravitational-wave dispersion relation and perform null tests of general relativity. Assuming that gravitons are dispersed in vacuum like massive particles, we bound the graviton mass to $m_g \leq 7.7 \times 10^{-23}$ eV/c². In all cases, we find that GW170104 is consistent with general relativity.

DOI: 10.1103/PhysRevLett.118.221101

I. INTRODUCTION

The first observing run of the Advanced Laser Interferometer Gravitational-Wave Observatory (LIGO) [1] identified two binary black hole coalescence signals with high statistical significance, GW150914 [2] and GW151226 [3], as well as a less significant candidate LVT151012 [4,5]. These discoveries ushered in a new era of observational astronomy, allowing us to investigate the astrophysics of binary black holes and test general relativity (GR) in ways that were previously inaccessible [6,7]. We now know that there is a population of binary black holes with component masses $\gtrsim 25 M_{\odot}$ [5,6], and that merger rates are high enough for us to expect more detections [5,8].

Advanced LIGO's second observing run began on November 30, 2016. On January 4, 2017, a gravitational-wave signal was detected with high statistical significance. Figure 1 shows a time-frequency representation of the data from the LIGO Hanford and Livingston detectors, with the signal GW170104 visible as the characteristic chirp of a binary coalescence. Detailed analyses demonstrate that GW170104 arrived at Hanford ~ 3 ms before Livingston, and originated from the coalescence of two stellar-mass black holes at a luminosity distance of $\sim 3 \times 10^9$ light-years.

*Full author list given at the end of the Letter.

Published by the American Physical Society under the terms of the Creative Commons Attribution 4.0 International license. Further distribution of this work must maintain attribution to the author(s) and the published article's title, journal citation, and DOI.

GW170104's source is a heavy binary black hole system, with a total mass of $\sim 50 M_{\odot}$, suggesting formation in a subsolar metallicity environment [6]. Measurements of the black hole spins show a preference away from being (positively) aligned with the orbital angular momentum, but do not exclude zero spins. This is distinct from the case for GW151226, which had a strong preference for spins with positive projections along the orbital angular momentum [3]. The inferred merger rate agrees with previous calculations [5,8], and could potentially be explained by binary black holes forming through isolated binary evolution or dynamical interactions in dense stellar clusters [6].

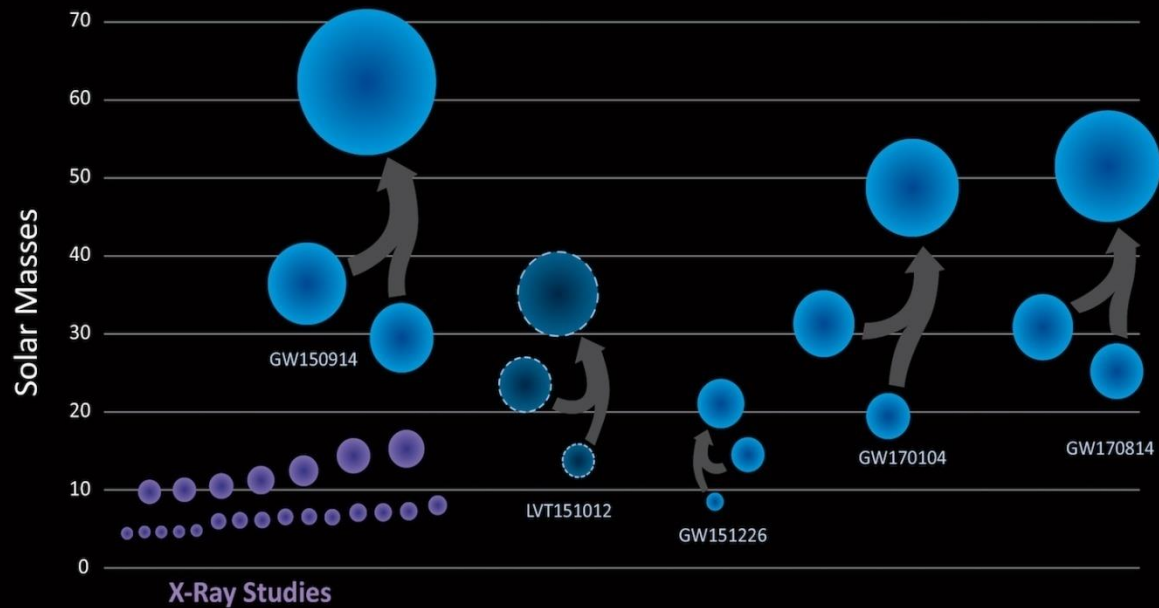
Gravitational-wave observations of binary black holes are the ideal means to test GR and its alternatives. They provide insight into regimes of strong-field gravity where velocities are relativistic and the spacetime is dynamic. The tests performed with the sources detected in the first observing run showed no evidence of departure from GR's predictions [5,7]; GW170104 provides an opportunity to tighten these constraints. In addition to repeating tests performed in the first observing run, we also test for modifications to the gravitational-wave dispersion relation. Combining measurements from GW170104 with our previous results, we obtain new gravitational-wave constraints on potential deviations from GR.

II. DETECTORS AND DATA QUALITY

The LIGO detectors measure gravitational-wave strain using two dual-recycled Fabry-Perot Michelson interferometers at the Hanford and Livingston observatories [1,10].

- On June 2, 2017 LIGO (Abbott et al. PRL 118, 21101 (2017)) reported about the discovery of the third GW event from merging the BHs with 31 and 19 solar masses at redshift $z=0.19$
- $m_g < 7.7 \times 10^{-23} \text{ eV}$

Black Holes of Known Mass



LIGO/VIRGO

Constraining the range of Yukawa gravity interaction from S2 star orbits II: bounds on graviton mass

A.F. Zakharov,^{a,b,c,d,e} P. Jovanović,^f D. Borka^g
and V. Borka Jovanović^g

^aNational Astronomical Observatories of Chinese Academy of Sciences,
Datun Road 20A, Beijing, 100012 China

^bInstitute of Theoretical and Experimental Physics,
117259 Moscow, Russia

^cNational Research Nuclear University MEPhI (Moscow Engineering Physics Institute),
115409, Moscow, Russia

^dBogoliubov Laboratory for Theoretical Physics, JINR,
141980 Dubna, Russia

^eNorth Carolina Central University,
Durham, NC 27707, U.S.A.

^fAstronomical Observatory,
Volgina 7, 11060 Belgrade, Serbia

^gAtomic Physics Laboratory (040), Vinča Institute of Nuclear Sciences,
University of Belgrade, P.O. Box 522, 11001 Belgrade, Serbia

E-mail: zakharov@itep.ru, pjovanovic@aob.rs, dusborka@vin.bg.ac.rs,
vborka@vin.bg.ac.rs

Received May 4, 2016

Accepted May 7, 2016

Published May 20, 2016

Abstract. Recently LIGO collaboration discovered gravitational waves [1] predicted 100 years ago by A. Einstein. Moreover, in the key paper reporting about the discovery, the joint LIGO & VIRGO team presented an upper limit on graviton mass such as $m_g < 1.2 \times 10^{-22} eV$ [1] (see also more details in another LIGO paper [2] dedicated to a data analysis to obtain such a small constraint on a graviton mass). Since the graviton mass limit is so small the authors concluded that their observational data do not show violations of classical general relativity. We consider another opportunity to evaluate a graviton mass from phenomenological consequences of massive gravity and show that an analysis of bright star

modification of the Newtonian potential [5, 14]:

$$V(r) = -\frac{GM}{(1+\delta)r} \left[1 + \delta e^{-\left(\frac{r}{\lambda}\right)} \right], \quad (1.1)$$

where δ is a universal constant. In our previous paper [35] we found constraints on parameters of Yukawa gravity.

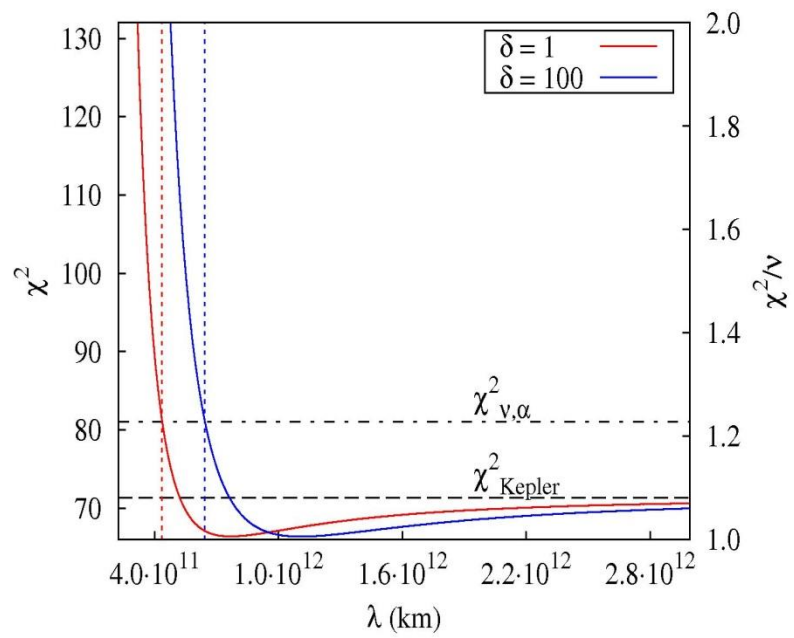
Will considered an opportunity to evaluate a graviton mass analyzing a time delay in electromagnetic waves such as supernova or gamma-ray burst [5], moreover earlier he demonstrated a possibility to constrain a graviton mass from from gravitational wave signal alone [4].

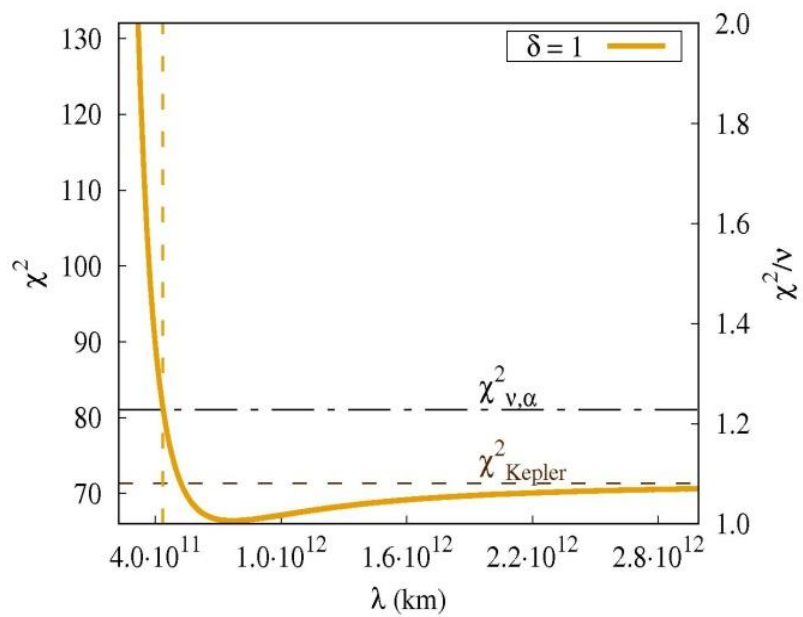
Pulsar timing may be used to evaluate a graviton mass [36]. In the paper it was concluded that, with 90% probability, massless gravitons can be distinguished from gravitons heavier than 3×10^{-22} eV (Compton wavelength $\lambda_g = 4.1 \times 10^{12}$ km), if bi-weekly observation of 60 pulsars is performed for 5 years with a pulsar rms timing accuracy of 100 ns and if 10 year observation of 300 pulsars with 100 ns timing accuracy would probe graviton masses down to 3×10^{-23} eV ($\lambda_g = 4.1 \times 10^{13}$ km). These conclusions are based on an analysis of cross-correlation functions of gravitational wave background. An idea to use pulsar timing for gravitational wave detection has been proposed many years ago [37]. An analysis of the cross-correlation function between pulsar timing residuals of pulsar pairs could give an opportunity to detect gravitational waves [38, 39]. If a graviton has a mass it gives an impact on cross-correlation functions [36]. However, as a first step people have to discover stochastic GW signal and only after a detailed analysis of cross-correlation it could help to put constraints on a graviton mass.

Here we show that our previous results concerning the constraints on parameters of Yukawa gravity, presented in the paper [35], can be extended in the way that one could also obtain a graviton mass bounds from the observations of trajectories of bright stars near the Galactic Center. As it is shown below our estimate of a graviton mass is slightly greater than the estimate obtained by the LIGO collaboration with the first detection of gravitational waves from the binary black hole system. However, we would like to note that: a) our estimate is consistent with the LIGO one; b) in principle, with analysis of trajectories of bright stars near the Galactic Center one could obtain such a graviton mass estimate before the LIGO report [1] about the discovery of gravitational waves and their estimate of a graviton mass; c) in the future our estimate may be improved with forthcoming observational facilities.

2 Graviton mass estimates from S2 star orbit

Two groups of observers are monitoring bright stars (including S2 one) to evaluate gravitational potential at the Galactic Center [40–48]. Recently, the astrometric observations of S2 star [49] were used to evaluate parameters of black hole and to test and constrain several models of modified gravity at mpc scales [50–54]. The simulations of the S2 star orbit around the supermassive black hole at the Galactic Centre (GC) in Yukawa gravity [35] and their comparisons with the NTT/VLT astrometric observations of S2 star [49] resulted with the constraints on the range of Yukawa interaction λ , which showed that λ is most likely on the order of several thousand astronomical units. However, it was not possible to obtain the reliable constrains on the universal constant δ because its values $0 < \delta < 1$ were highly correlated to λ while the values $\delta > 2$ corresponded to a practically fixed $\lambda \sim 5000\text{--}6000$ AU.





Constraints on graviton mass from S2 trajectory

- AFZ, D. Borka, P. Jovanovic, V. Borka Jovanovic gr-qc: 1605.00913v; JCAP (2016) :
- $\lambda_g > 2900 \text{ AU} = 4.3 \times 10^{11} \text{ km}$ with $P=0.9$ or
- $m_g < 2.9 \times 10^{-21} \text{ eV} = 5.17 \times 10^{-54} \text{ g}$
- Hees et al. PRL (2017) slightly improved our estimates with their new data $m_g < 1.6 \times 10^{-21} \text{ eV}$ (see discussion below)

Impact on our studies

Claudia de Rham, J. Tate Deskins, Andrew J. Tolley, Shuang-Yong Zhou, Graviton Mass Bounds, *Reviews in Modern Physics* 89, 0250004 (2017).

A. Hees, T. Do, A. M. Ghez, G. D. Martinez, S. Naoz, E. E. Becklin, A. Boehle, S. Chappell, D. Chu, A. Dehghanfar, K. Kosmo, J. R. Lu, K. Matthews, M. R. Morris, S. Sakai, R. Schodel, and G. Witze, Testing General Relativity with stellar orbits around the supermassive black hole in our Galactic center, [arXiv:1705.07902v1](https://arxiv.org/abs/1705.07902v1) [astro-ph.GA], *PRL* 118, 211101.

A couple of our papers have been quoted in the second paper.



Testing General Relativity with Stellar Orbits around the Supermassive Black Hole in Our Galactic Center

A. Hees,^{1*} T. Do,¹ A. M. Ghez,^{1†} G. D. Martinez,¹ S. Naoz,¹ E. E. Becklin,¹ A. Boehle,¹ S. Chappell,¹ D. Chu,¹
A. Dehghanfar,¹ K. Kosmo,¹ J. R. Lu,² K. Matthews,³ M. R. Morris,¹ S. Sakai,¹ R. Schödel,⁴ and G. Witzel¹

¹Department of Physics and Astronomy, University of California, Los Angeles, California 90095, USA

²Astronomy Department, University of California, Berkeley, California 94720, USA

³Division of Physics, Mathematics, and Astronomy, California Institute of Technology, MC 301-17, Pasadena, California 91125, USA

⁴Instituto de Astrofísica de Andalucía (CSIC), Glorieta de la Astronomía S/N, 18008 Granada, Spain

(Received 22 December 2016; revised manuscript received 14 March 2017; published 25 May 2017)

We demonstrate that short-period stars orbiting around the supermassive black hole in our Galactic center can successfully be used to probe the gravitational theory in a strong regime. We use 19 years of observations of the two best measured short-period stars orbiting our Galactic center to constrain a hypothetical fifth force that arises in various scenarios motivated by the development of a unification theory or in some models of dark matter and dark energy. No deviation from general relativity is reported and the fifth force strength is restricted to an upper 95% confidence limit of $|\alpha| < 0.016$ at a length scale of $\lambda = 150$ astronomical units. We also derive a 95% confidence upper limit on a linear drift of the argument of periastron of the short-period star S0-2 of $|\dot{\omega}_{S0-2}| < 1.6 \times 10^{-3}$ rad/yr, which can be used to constrain various gravitational and astrophysical theories. This analysis provides the first fully self-consistent test of the gravitational theory using orbital dynamic in a strong gravitational regime, that of a supermassive black hole. A sensitivity analysis for future measurements is also presented.

DOI: 10.1103/PhysRevLett.118.211101

The development of a quantum theory of gravitation or of a unification theory generically predicts deviations from general relativity (GR). In addition, observations requiring the introduction of dark matter and dark energy also challenge GR and the standard model of particle physics [1] and are sometimes interpreted as a modification of gravitational theory (see, e.g., Refs. [2,3]). It is thus important to test the gravitational interaction with different types of observations [4]. While GR is thoroughly tested in the Solar System (see, e.g., Refs. [5–8]) and with binary pulsars (see, e.g., Ref. [9]), observations of short-period stars orbiting the supermassive black hole (SMBH) at the center of our Galaxy allow one to probe gravity in a strong field regime unexplored so far, as shown in Fig. 1 (see also Refs. [10,11]). In this Letter, we report two results: (i) a search for a fifth force around our Galactic center and (ii) a constraint on the advance of the periastron of the short-period star S0-2 that can be used to constrain various gravitational and astrophysical theories in our Galactic center. This analysis provides the first fully self-consistent test of the gravitational theory using an orbital dynamic in a strong gravitational regime around a SMBH. The constraints presented in this Letter, resulting from 20 yr of observations, are therefore highly complementary with Solar System or binary pulsar tests of gravitation and open a new window to study gravitation.

One phenomenological framework widely used to search for deviations from GR is the fifth force formalism [13–18], which considers deviations from Newtonian gravity in

which the gravitational potential takes the form of a Yukawa potential

$$U = \frac{GM}{r} [1 + \alpha e^{-r/\lambda}], \quad (1)$$

with G the Newton's constant, M the mass of the central body, and r the distance to the central mass. This potential is characterized by two parameters: a length λ and a strength of interaction α . A Yukawa potential appears in several theoretical scenarios, such as unification theories that predict new fundamental interactions with a massive

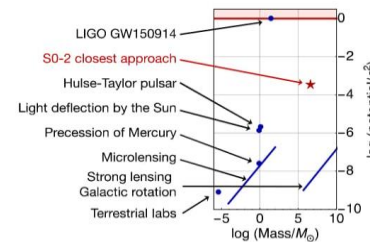


FIG. 1. The gravitational potential probed by different tests of gravitation against the mass of the central body that generates gravity in these tests. Short-period stars, such as S0-2, around our Galactic center explore a new region in this parameter space. The figure is inspired by Ref. [12].

stars are probing space-time in a higher potential and around a central body much more massive than in the other experiments. This is highlighted in the right panel of Fig. 2, where λ is expressed in terms of the gravitational radius of the central body. Furthermore, short-period stars probe the space-time around a SMBH, which is conceptually different from Solar System tests where the space-time curvature is generated by weakly gravitating bodies. Specifically, some nonperturbative effects may arise around strongly gravitating bodies (see, e.g., Ref. [76]). In addition, in models of gravity exhibiting screening mechanisms, deviations from GR may be screened in the Solar System (see, e.g., Ref. [77]). In this context, searches for alternative theories of gravitation in other environments are important.

A specific theoretical model covered by the fifth force framework is a massive graviton. In that context, we found a 90% confidence limit $\lambda > 5000$ A.U. for $\alpha = 1$, which can be interpreted as a lower limit on the graviton's Compton wavelength $\lambda_g > 7.5 \times 10^{11}$ km or, equivalently, as an upper bound on the graviton's mass $m_g < 1.6 \times 10^{-21}$ eV/ c^2 (see also Ref. [36]). This constraint is one order of magnitude less stringent than the recent bound obtained by LIGO [78], which, nevertheless, does not apply for all models predicting a fifth force.

From an empirical perspective, one of the effects produced by a fifth force is a secular drift of the argument of periastron ω [31,79]. Several theoretical scenarios predict such an effect, which can be constrained by observations. We produced a new orbital fit using a model that includes seven global parameters (the SMBH GM , R_0 , and the positions and velocities of the SMBH) and seven orbital parameters for each star, with the additional parameter being a linear drift of the argument of the periastron $\dot{\omega}$. As a result of our fit including the jackknife analysis, we obtained an upper confidence limit on a linear drift of the argument of periastron for S0-2 given by

$$|\dot{\omega}_{S0-2}| < 1.7 \times 10^{-3} \text{ rad/yr at 95\% C.L.} \quad (3)$$

This limit is currently one order of magnitude larger than the relativistic advance of the periastron $\dot{\omega}_{GR} = 6\pi GM/[Pc^2 a(1 - e^2)] = 1.6 \times 10^{-4}$ rad/yr for S0-2 (with a being the semimajor axis). Nevertheless, the limit from Eq. (3) can be used to derive a preliminary constraint on various theoretical scenarios (astrophysical or modified gravity) that predict an advance of the periastron for short-period stars in the Galactic center, like, for example,

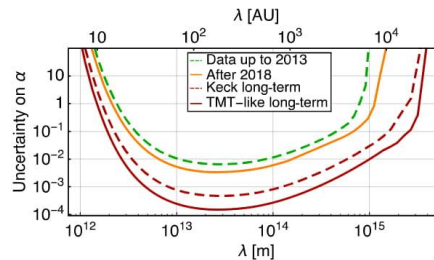


FIG. 3. Statistical uncertainty on the fifth force strength σ_α expected for various observational scenarios: the dashed green (light) line corresponds to the data used in this analysis, the continuous orange (light) line corresponds to data that will be available by the end of 2018. The two red (dark) lines include 16 additional years of observations with two astrometric observations and one spectroscopic observation per year with the following astrometric (spectroscopic) accuracy for an S0-2-like star: current Keck accuracy, 0.5 mas (30 km/s); TMT-like improved accuracy, 15 μ as (5 km/s).

improve the current results. Figure 3 shows a sensitivity analysis based on a Fisher matrix approach performed to assess the improvement expected by observations with a TMT-like telescope. We have simulated 16 additional years of data for two scenarios: (i) a scenario where Keck observations are used with an astrometric uncertainty of 0.16 mas, comparable to today's performance, and (ii) a scenario with an improved astrometric uncertainty of 0.015 mas, which corresponds to a TMT-like scenario. Extending the time baseline by one S0-2 period improves the result by a factor of 13, while an improved accuracy brings an additional improvement of a factor of 5. In addition, the discovery of new stars orbiting closer to the SMBH and unbiased measurements of the known faint short-period star S0-102 ($P = 11.5$ yr) [43] would improve this analysis.

In conclusion, we have used 19 yr of observations of S0-2 and S0-38 reported in Ref. [44] to constrain a hypothetical fifth interaction around the SMBH in our Galactic center. The constraints obtained in our analysis are summarized in Fig. 2. Our results complement the ones obtained in the Solar System since they are obtained in a completely different and unexplored strong field regime. We have shown that future observations—and especially the next generation of telescopes—will improve our results substantially. In addition, we have derived a limit on an hypothetical advance of the periastron of the short-period

- [35] A. Hees, W.M. Folkner, R.A. Jacobson, and R.S. Park, Constraints on MOND theory from radio tracking data of the Cassini spacecraft, *Phys. Rev. D* **89**, 102002 (2014); Z.-W. Li, S.-F. Yuan, C. Lu, and Y. Xie, New upper limits on deviation from the inverse-square law of gravity in the solar system: a Yukawa parameterization, *Res. Astron. Astrophys.* **14**, 139 (2014).
- [36] D. Borka, P. Jovanović, V.B. Jovanović, and A.F. Zakharov, Constraining the range of Yukawa gravity interaction from S2 star orbits I. *Cosmol. Astropart. Phys.* **11** (2013) 050; A. F. Zakharov, P. Jovanović, D. Borka, and V. B. Jovanović, Constraining the range of Yukawa gravity interaction from S2 star orbits II: Bounds on graviton mass, *J. Cosmol. Astropart. Phys.* **05** (2016) 045.
- [37] A. M. Ghez, B. L. Klein, M. Morris, and E. E. Becklin, High Proper-Motion Stars in the Vicinity of Sagittarius A*: Evidence for a Supermassive Black Hole at the Center of Our Galaxy, *Astrophys. J.* **509**, 678 (1998).
- [38] A. M. Ghez, M. Morris, E. E. Becklin, A. Tanner, and T. Kremernek, The accelerations of stars orbiting the Milky Way's central black hole, *Nature (London)* **407**, 349 (2000).
- [39] A. M. Ghez, G. Duchêne, K. Matthews, S. D. Hornstein, A. Tanner, J. Larkin, M. Morris, E. E. Becklin, S. Salim, T. Kremernek, D. Thompson, B. T. Soifer, G. Neugebauer, and I. McLean, The First Measurement of Spectral Lines in a Short-Period Star Bound to the Galaxy's Central Black Hole: A Paradox of Youth, *Astrophys. J. Lett.* **586**, L127 (2003).
- [40] A. M. Ghez, S. Salim, S. D. Hornstein, A. Tanner, J. R. Lu, M. Morris, E. E. Becklin, and G. Duchêne, Stellar Orbits around the Galactic Center Black Hole, *Astrophys. J.* **620**, 744 (2005).
- [41] A. M. Ghez, S. D. Hornstein, J. R. Lu, A. Bouchez, D. Le Mignant, M. A. van Dam, P. Wizinowich, K. Matthews, M. Morris, E. E. Becklin, R. D. Campbell, J. C. Y. Chin, S. K. Hartman, E. M. Johansson, R. E. Lafon, P. J. Stomski, and D. M. Summers, The First Laser Guide Star Adaptive Optics Observations of the Galactic Center: Sgr A*'s Infrared Color and the Extended Red Emission in its Vicinity, *Astrophys. J.* **635**, 1087 (2005).
- [42] A. M. Ghez, S. Salim, N. N. Weinberg, J. R. Lu, T. Do, J. K. Dunn, K. Matthews, M. R. Morris, S. Yelda, E. E. Becklin, T. Kremernek, M. Milosavljevic, and J. Naiman, Measuring distance and properties of the Milky Way's central supermassive black hole with stellar orbits, *Astrophys. J.* **689**, 1044 (2008).
- [43] L. Meyer, A. M. Ghez, R. Schödel, S. Yelda, A. Boehle, J. R. Lu, T. Do, M. R. Morris, E. E. Becklin, and K. Matthews, The Shortest-Known-Period Star Orbiting Our Galaxy's Supermassive Black Hole, *Science* **338**, 84 (2012).
- [44] A. Boehle, A. M. Ghez, R. Schödel, L. Meyer, S. Yelda, S. Albers, G. D. Martínez, E. E. Becklin, T. Do, J. R. Lu, K. Matthews, M. R. Morris, B. Sitarski, and G. Witzel, An improved distance and mass estimate for Sgr A* from a multistar orbit analysis, *Astrophys. J.* **830**, 17 (2016).
- [45] R. Genzel, A. Eckart, T. Ott, and F. Eisenhauer, On the nature of the dark mass in the centre of the Milky Way, *Mon. Not. R. Astron. Soc.* **291**, 219 (1997).
- [46] A. Eckart and R. Genzel, Stellar proper motions in the central 0.1 pc of the Galaxy, *Mon. Not. R. Astron. Soc.* **284**, 576 (1997).
- [47] R. Schödel *et al.*, A star in a 15.2-year orbit around the supermassive black hole at the centre of the Milky Way, *Nature (London)* **419**, 694 (2002).
- [48] A. Eckart, R. Genzel, T. Ott, and R. Schödel, Stellar orbits near Sagittarius A*, *Mon. Not. R. Astron. Soc.* **331**, 917 (2002).
- [49] F. Eisenhauer, R. Schödel, R. Genzel, T. Ott, M. Tecza, R. Abuter, A. Eckart, and T. Alexander, A Geometric Determination of the Distance to the Galactic Center, *Astrophys. J. Lett.* **597**, L121 (2003).
- [50] F. Eisenhauer *et al.*, SINFONI in the Galactic Center: Young Stars and Infrared Flares in the Central Light-Month, *Astrophys. J.* **628**, 246 (2005).
- [51] S. Gillessen, F. Eisenhauer, T. K. Fritz, H. Bartko, K. Dodds-Eden, O. Pfuhl, T. Ott, and R. Genzel, The orbit of the star S2 around SgrA* from VLT and Keck data, *Astrophys. J. Lett.* **707**, L114 (2009).
- [52] S. Gillessen, F. Eisenhauer, S. Trippe, T. Alexander, R. Genzel, F. Martins, and T. Ott, Monitoring stellar orbits around the massive black hole in the Galactic center, *Astrophys. J.* **692**, 1075 (2009).
- [53] S. Gillessen, P. M. Plewa, F. Eisenhauer, R. Sari, I. Waisberg, M. Habibi, O. Pfuhl, E. George, J. Dexter, S. von Fellenberg, T. Ott, and R. Genzel, An update on monitoring stellar orbits in the Galactic center, *Astrophys. J.* **837**, 30 (2017).
- [54] T. Alexander, Stellar processes near the massive black hole in the Galactic center, *Phys. Rep.* **419**, 65 (2005).
- [55] M. Jaroszynski, Relativistic effects in proper motions of stars surrounding the Galactic center, *Acta Astronaut.* **48**, 653 (1998); P. C. Fragile and G. J. Mathews, Reconstruction of Stellar Orbits Close to Sagittarius A*: Possibilities for Testing General Relativity, *Astrophys. J.* **542**, 328 (2000); G. F. Rubilar and A. Eckart, Periastron shifts of stellar orbits near the Galactic Center, *Astron. Astrophys.* **374**, 95 (2001); N. N. Weinberg, M. Milosavljevic, and A. M. Ghez, Stellar Dynamics at the Galactic Center with an Extremely Large Telescope, *Astrophys. J.* **622**, 878 (2005); S. Zucker, T. Alexander, S. Gillessen, F. Eisenhauer, and R. Genzel, Probing Post-Newtonian Physics near the Galactic Black Hole with Stellar Redshift Measurements, *Astrophys. J. Lett.* **639**, L21 (2006); G. V. Kraniotis, Periastron and gravitomagnetic precessions of stellar orbits in Kerr and Kerr–de Sitter black hole spacetimes, *Classical Quantum Gravity* **24**, 1775 (2007); C. M. Will, Testing the general relativistic “no-hair” theorems using the Galactic center black hole SgrA* *Astrophys. J. Lett.* **674**, L25 (2008); D. Merritt, T. Alexander, S. Mikkola, and C. M. Will, Testing properties of the Galactic center black hole using stellar orbits, *Phys. Rev. D* **81**, 062002 (2010); R. Angéilil and P. Saha, Relativistic redshift effects and the galactic-center stars, *Astrophys. J.* **711**, 157 (2010); R. Angéilil, P. Saha, and D. Merritt, Towards relativistic orbit fitting of Galactic center stars and pulsars, *Astrophys. J.* **720**, 1303 (2010); L. Iorio, Long-term classical and general relativistic effects on the radial velocities of the stars orbiting Sgr A*, *Mon. Not. R. Astron. Soc.* **411**, 453 (2011); R. Angéilil and P. Saha, Galactic-center S stars as a prospective test of the Einstein equivalence principle, *Astrophys. J. Lett.* **734**, L19 (2011);

Constraining the range of Yukawa gravity interaction from S2 star orbits III: improvement expectations for graviton mass bounds

A.F. Zakharov,^{a,b,c,d,e,1} P. Jovanović,^f D. Borka^g and V. Borka Jovanović^g

^aNational Astronomical Observatories of Chinese Academy of Sciences, Datun Road 20A, Beijing, 100012 China

^bInstitute of Theoretical and Experimental Physics, 117259 Moscow, Russia

^cNational Research Nuclear University MEPhI (Moscow Engineering Physics Institute), 115409, Moscow, Russia

^dBogoliubov Laboratory for Theoretical Physics, JINR, 141980 Dubna, Russia

^eNorth Carolina Central University, Durham, NC 27707, U.S.A.

^fAstronomical Observatory, Volgina 7, P.O. Box 74, 11060 Belgrade, Serbia

^gAtomic Physics Laboratory (040), Vinča Institute of Nuclear Sciences, University of Belgrade, P.O. Box 522, 11001 Belgrade, Serbia

E-mail: zakharov@itep.ru, pjovanovic@aob.rs, dusborka@vinca.rs, vborka@vinca.rs

Received January 17, 2018

Revised February 14, 2018

Accepted March 9, 2018

Published ???, 2018

¹Corresponding author.

Graviton mass estimate improvement forecast

Graviton Mass Estimates from Trajectories of Bright Stars near the Galactic Center

We use a modification of the Newtonian potential corresponding to a massive graviton case (Visser, 1998; Will, 1998, 2014):

$$V(r) = -\frac{GM}{(1+\delta)r} \left[1 + \delta e^{-\left(\frac{r}{\lambda}\right)} \right], \quad (5)$$

where δ is a universal constant (we put $\delta = 1$). In our previous studies we found constraints on parameters of Yukawa gravity. As it was described in we used observational data from NTT/VLT. If we wish to find a limiting value for λ_x , so that $\lambda > \lambda_x$ with a probability $P = 1 - \alpha$ (where we select $\alpha = 0.1$)

normalized χ^2 depending on λ_x has to be equal to the threshold depending on degree of freedom ν and parameter α or in other words, $\chi^2(\lambda_x) = \chi_{\nu, \alpha}^2$. Computing these quantities we obtain $\lambda_x = 2900 \text{ AU} \approx 4.3 \times 10^{11} \text{ km}$. Now we obtain the upper limit on a graviton mass and we could claim that with a probability $P = 0.9$, a graviton mass should be less than $m_g = 2.9 \times 10^{-21} \text{ eV}$ (since $m_g = h c / \lambda_x$) in the case of $\delta = 1$.

Orbital precession due to general central-force perturbations

A general expression for apocenter shifts for Newtonian potential and small perturbing potential is given as a solution of problem 3 in Section 15 in the classical Landau & Lifshitz (L & L) textbook [Mechanics].

Orbital precession $\Delta\varphi$ per orbital period, induced by small perturbations to the Newtonian gravitational potential $\Phi_N(r) = -\frac{GM}{r}$ could be evaluated as:

$$\Delta\varphi^{rad} = \frac{-2L}{GMe^2} \int_{-1}^1 \frac{z \cdot dz}{\sqrt{1-z^2}} \frac{dV(z)}{dz}, \quad (6)$$

while in the textbook it was given in the form

$$\Delta\varphi^{rad} = \frac{-2L}{GM_e} \int_0^\pi \cos\varphi r^2 \frac{dV(r)}{dr} d\varphi, \quad (7)$$

where $V(z)$ is the perturbing potential, r is related to z via: $r = \frac{L}{1+ez}$ in Eq. (6) (and $r = \frac{L}{1+e\cos\varphi}$ in Eq. (7)), and L being the semilatus rectum of the orbital ellipse with semi-major axis a and eccentricity e :

$$L = a(1 - e^2), \quad (8)$$

while $\Delta\varphi$ represents true precession in the orbital plane, and the corresponding apparent value Δs , as seen from Earth at distance R_0 ,

is (assuming that stellar orbit is perpendicular to line of sight and taking into account an inclination of orbit one has to write an additional factor which is slightly less than 1 in the following expression):

$$\Delta s \approx \frac{a(1+e)}{R_0} \Delta\varphi. \quad (9)$$

In order to compare the orbital precession of S-stars in both GR and Yukawa gravity, we applied the same procedure as described in to perform the two-body simulations of the stellar orbits in the framework of these two theories.

normalized χ^2 depending on λ_x has to be equal to the threshold depending on degree of freedom ν and parameter α or in other words, $\chi^2(\lambda_x) = \chi^2_{\nu, \alpha}$. Computing these quantities we obtain $\lambda_x = 2900 \text{ AU} \approx 4.3 \times 10^{11} \text{ km}$. Now we obtain the upper limit on a graviton mass and we could claim that with a probability $P = 0.9$, a graviton mass should be less than $m_g = 2.9 \times 10^{-21} \text{ eV}$ (since $m_g = h c / \lambda_x$) in the case of $\delta = 1$.

Orbital precession in Yukawa gravity

In order to simulate orbits of S-stars in Yukawa gravity we assumed the following gravitational potential (Borka et al. 2013):

$$\Phi_Y(r) = -\frac{GM}{(1+\delta)r} \left[1 + \delta e^{-\frac{r}{\Lambda}} \right], \quad (13)$$

where Λ is the range of Yukawa interaction and δ is a universal constant. Here we will assume that $\delta > 0$, as indicated by data analysis of astronomical observations. Yukawa gravity induces a perturbation to the Newtonian gravitational potential described by the following perturbing potential:

$$V_Y(r) = \Phi_Y(r) + \frac{GM}{r} = \frac{\delta}{1+\delta} \frac{GM}{r} \left[1 - e^{-\frac{r}{\Lambda}} \right] \quad (14)$$

The exact analytical expression for orbital precession in the case of the above perturbing potential could be presented in the integral form Eqs. (6) and (7), but we will calculate the approximate expression for $\Delta\varphi$ using power series expansion of $V_Y(r)$, assuming that $r \ll \Lambda$:

$$V_Y(r) \approx -\frac{\delta GM r}{2(1+\delta)\Lambda^2} \left[1 - \frac{r}{3\Lambda} + \frac{r^2}{12\Lambda^2} - \dots \right], \quad r \ll \Lambda, \quad (15)$$

where we neglected the constant term since it does not affect $\Delta\varphi$. By substituting the above expression into (6) we obtain the following approximation for the angle of orbital precession in Yukawa gravity:

$$\Delta\varphi_Y^{rad} \approx \frac{\pi\delta\sqrt{1-e^2}}{1+\delta} \left(\frac{a^2}{\Lambda^2} - \frac{a^3}{\Lambda^3} + \frac{4+e^2}{8} \frac{a^4}{\Lambda^4} - \dots \right). \quad (16)$$

The right-hand side in Eq. (16) could be presented as series of Gauss's hypergeometric function ${}_2F_1$ with different arguments.

Since $r \ll \Lambda$ also implies that $a \ll \Lambda$, we can neglect higher order terms in the above expansion. The first order term then yields the following approximate formula for orbital precession:

$$\Delta\varphi_Y^{rad} \approx \frac{\pi\delta\sqrt{1-e^2}}{1+\delta} \frac{a^2}{\Lambda^2}, \quad a \ll \Lambda. \quad (17)$$

Both, $\Delta\varphi_{GR}$ and $\Delta\varphi_Y$ represent the angles of orbital precession per orbital period in the orbital plane (i.e. true precession). The corresponding

apparent values in Yukawa case Δs_Y , as seen from Earth at distance R_0 is (for $\delta = 1$) according to (Weinberg et al. 2005) :

$$\Delta s_Y \approx \frac{a(1+e)}{R_0} \Delta \varphi_Y^{rad} \approx 0.5\pi \frac{a^3}{R_0 \Lambda^2} (1+e) \sqrt{1-e^2}. \quad (18)$$

If one believes that a gravitational field at the Galactic Center is described with a Yukawa potential, then the maximal Δs_Y value corresponds to $e = 1/2$ when function $(1+e)\sqrt{1-e^2}$ has its maximal value (assuming that all other parameters are fixed).

Expectations to constrain the range of Yukawa gravity with future observations

We assume that in future GR predictions about precession angles for bright star orbits around the Galactic Center will be successfully confirmed, therefore, for each star we have a constraint on Λ which can be obtained from the condition for Λ , so that Yukawa gravity induces the same orbital precession as GR. This constraint can be obtained directly from (11) and (17), assuming that $\Delta\varphi_Y = \Delta\varphi_{GR}$. In this way we obtain that:

$$\Lambda \approx \sqrt{\frac{\delta c^2 (a\sqrt{1-e^2})^3}{6(1+\delta)GM}}. \quad (19)$$

As it can be seen from the above expression, taking into account that δ is

universal constant, the corresponding values of Λ in the case of all S-stars depend only on the semi-major axes and eccentricities of their orbits. In order to stay in accordance with (Zakharov et al., 2016), here we will also assume that $\delta = 1$, in which case formula (19) reduces to:

$$\Lambda \approx \frac{c}{2} \sqrt{\frac{(a\sqrt{1-e^2})^3}{3GM}} \approx \sqrt{\frac{(a\sqrt{1-e^2})^3}{6R_S}}, \quad (20)$$

Using Kepler law we could write the previous equation in the following form

$$\Lambda \approx \frac{T}{T_0} \sqrt{\frac{(a_0\sqrt{1-e^2})^3}{6R_S}}. \quad (21)$$

Constraints on (tidal) charge of the supermassive black hole at the Galactic Center with trajectories of bright stars

In paper (Dadhich et al. 2001) it was shown that the Reissner – Nordström metric with a tidal charge could arise in Randall – Sundrum model with an extra dimension. Astrophysical of braneworld black holes are considered assuming that they could substitute conventional black holes in astronomy, in particular, geodesics and shadows in Kerr – Newman braneworld metric are analyzed in (Schee and Stuchlik, 2009a), while profiles of emission lines generated by rings orbiting braneworld Kerr black hole are considered in (Schee and Stuchlik, 2009a). Later it was proposed to consider signatures of gravitational lensing assuming a presence of the Reissner – Nordström black hole with a tidal charge at the Galactic Center (Bin-Nun

2010a, 2010b, 2011). In paper (Zakharov, 2014) analytical expressions for shadow radius of Reissner – Nordström black hole have been derived while shadow sizes for Schwarzschild – de Sitter (Köttler) metric have been found in papers (Stuchlik 1983, Zakharov 2014). In the paper we derive analytical expressions for Reissner – Nordström – de-Sitter metric in post-Newtonian approximation and discuss constraints on (tidal) charge from current and future observations of bright stars near the Galactic Center.

Basic notations

We use a system of units where $G = c = 1$. The line element of the spherically symmetric Reissner – Nordström – de-Sitter metric is

$$ds^2 = -f(r)dt^2 + f(r)^{-1}dr^2 + r^2d\theta^2 + r^2 \sin^2 \theta d\phi^2, \quad (1)$$

where function $f(r)$ is defined as

$$f(r) = 1 - \frac{2M}{r} + \frac{Q^2}{r^2} - \frac{1}{3}\Lambda r^2. \quad (2)$$

Here M is a black hole mass, Q is its charge and Λ is cosmological constant. In the case of a tidal charge (Dadnich et al. 2001), Q^2 could be negative.

Similarly to Carter (1973), geodesics could be obtained the Lagrangian

$$\mathcal{L} = -\frac{1}{2}g_{\mu\nu}\frac{dx^\mu}{d\lambda}\frac{dx^\nu}{d\lambda}, \quad (3)$$

where $g_{\mu\nu}$ are the components of metric (1). There are three constants of motion for geodesics which correspond metric (1), namely

$$g_{\mu\nu}\frac{dx^\mu}{d\lambda}\frac{dx^\nu}{d\lambda} = m, \quad (4)$$

which is a test particle mass and two constants connected with an independence of the metric on ϕ and t coordinates, respectively

$$g_{\phi\nu}\frac{dx^\nu}{d\lambda} = h, \quad (5)$$

and

$$g_{t\nu} \frac{dx^\nu}{d\lambda} = E. \quad (6)$$

For vanishing Λ -term these integrals of motion (h and E) could be interpreted as angular momentum and energy of a test particle, respectively. Geodesics for massive particles could be written in the following form

$$r^4 \frac{dr^2}{d\lambda} = E^2 r^4 - \Delta(m^2 r^2 + h^2), \quad (7)$$

where

$$\Delta = \left(1 - \frac{1}{3}\Lambda r^2\right) r^2 - 2Mr + Q^2. \quad (8)$$

or we could write Eq. (7) in the following form

$$r^4 \left(\frac{dr}{d\tau} \right)^2 = (\hat{E}^2 - 1)r^4 + 2Mr^3 - Q^2r^2 - \frac{1}{3}\Lambda r^6 - \hat{h}^2 \left(r^2 - \frac{\Lambda}{3}r^4 - 2Mr + Q^2 \right), \quad (9)$$

where $\hat{E} = \frac{E}{m}$ and $\hat{h} = \frac{h}{m}$. We will omit symbol \wedge below. Since

$$r^4 \left(\frac{d\phi}{d\tau} \right)^2 = h^2, \quad (10)$$

one could obtain

$$\left(\frac{dr}{d\phi} \right)^2 = \frac{1}{h^2} (E^2 - 1)r^4 + \frac{2Mr^3}{h^2} - \frac{Q^2r^2}{h^2} + \frac{1}{3}\Lambda r^6 - \left(r^2 - \frac{\Lambda}{3}r^4 - 2Mr + Q^2 \right), \quad (11)$$

It is convenient to introduce new variable $u = 1/r$. Since

$$\left(\frac{du}{d\tau}\right)^2 = \left(\frac{dr}{d\phi}\right)^2 u^4, \quad (12)$$

one obtains

$$\left(\frac{du}{d\tau}\right)^2 = \frac{1}{h^2}(E^2 - 1) + \frac{2Mu}{h^2} - \frac{Q^2u^2}{h^2} + \frac{\Lambda}{3h^2u^2} - \left(u^2 - \frac{\Lambda}{3} - 2Mu^3 + Q^2u^4\right), \quad (13)$$

therefore,

$$\frac{d^2u}{d\tau^2} + u = \frac{M}{h^2} + 3Mu^2 - \frac{Q^2u}{h^2} - 2Q^2u^3 - \frac{\Lambda}{3h^2u^3}, \quad (14)$$

and as it is known the first term in the right hand side of Eq. (14) corresponds to the Newtonian case, the second term corresponds to the

GR correction from the Schwarzschild metric, while third and fourth term correspond to a presence of Q parameter in metric (1), the fifth term corresponds to a Λ -term presence in the metric. Assuming that second, third, fourth and fifth terms in the right hand side of Eq. (14) are small in respect to the basic Newtonian solution, one could evaluate relativistic precession for each term and after that one has to calculate an algebraic sum of all shifts induced by different terms.

Relativistic precession evaluation

An expression for apocenter (pericenter) shifts for Newtonian potential plus small perturbing function is given as a solution in the classical (L & L) textbook (Landau and Lifshitz, 1976) (see also applications of the expressions for calculations of stellar orbit precessions in presence of the supermassive black hole and dark matter at the Galactic Center (Dokuchaev and Eroshenko 2015a, 2015b). In paper (Adkins and McDonnell 2007), the authors derived the expression which is equivalent to the (L & L) relation and which can be used for our needs. According to the procedure proposed in (Adkins and McDonnell 2007) one could re-write Eq. (14) in the following form

$$\frac{d^2u}{d\tau^2} + u = \frac{M}{h^2} - \frac{g(u)}{h^2}, \quad (15)$$

where $g(u)$ is a perturbing function which is supposed to be small and it

could be presented as a conservative force in the following form

$$g(u) = r^2 F(r)|_{r=1/u}, \quad F(r) = -\frac{dV}{dr}. \quad (16)$$

For potential $V(r) = \frac{\alpha_{-(n+1)}}{r^{-(n+1)}}$ (where n is a natural number) one obtains (Adkins and McDonnell 2007)

$$\Delta\theta(-(n+1)) = \frac{-\pi\alpha_{-(n+1)}\chi_n^2(e)}{ML^n}, \quad (17)$$

where

$$\chi_n^2(e) = n(n+1) {}_2F_1\left(\frac{1}{2} - \frac{n}{2}, \frac{1}{2} - \frac{n}{2}, 2, e^2\right), \quad (18)$$

${}_2F_1$ is the Gauss hypergeometrical function, L is the semilatus rectum ($L = h^2/M$) and we have $L = a(1 - e^2)$ (a is semi-major axis and e is eccentricity).

Adkins and McDonnell (2007) obtained orbital precessions for positive powers of perturbing function

$$\Delta\theta(n) = \frac{-\pi\alpha_n a^{n+1} \sqrt{1-e^2} \chi_n^2(e)}{M}. \quad (19)$$

For GR term in Eq. (14) the perturbing potential is $V_{GR}(r) = -\frac{Mh^2}{r^3}$ and one obtains the well-known result $n = 2$ (see, for instance (Adkins and McDonnell 2007) and textbooks on GR)

$$\Delta\theta(GR) := \Delta\theta(-3) = \frac{6\pi M}{L}. \quad (20)$$

For the third term in Eq. (14) one has potential $V_{RN1}(r) = \frac{Q^2}{2r^2}$ ($\alpha_{-2} = \frac{Q^2}{2}$)

Adkins and McDonnell (2007) obtained orbital precessions for positive powers of perturbing function

$$\Delta\theta(n) = \frac{-\pi\alpha_n a^{n+1} \sqrt{1-e^2} \chi_n^2(e)}{M}. \quad (19)$$

For GR term in Eq. (14) the perturbing potential is $V_{GR}(r) = -\frac{Mh^2}{r^3}$ and one obtains the well-known result $n = 2$ (see, for instance (Adkins and McDonnell 2007) and textbooks on GR)

$$\Delta\theta(GR) := \Delta\theta(-3) = \frac{6\pi M}{L}. \quad (20)$$

For the third term in Eq. (14) one has potential $V_{RN1}(r) = \frac{Q^2}{2r^2}$ ($\alpha_{-2} = \frac{Q^2}{2}$)

and $n = 1$), therefore, one obtains

$$\Delta\theta(RN1) := \Delta\theta(-(2))_{RN1} = -\frac{\pi Q^2}{ML}. \quad (21)$$

For the fourth term in Eq. (14) one has potential $V_{RN2}(r) = \frac{h^2 Q^2}{2r^4}$ ($\alpha_{-4} = \frac{h^2 Q^2}{2}$ and $n = 3$), therefore, one obtains

$$\Delta\theta(RN2) := \Delta\theta(-(4))_{RN2} = -\frac{3\pi Q^2(4 + e^2)}{2L^2}. \quad (22)$$

Since according to our assumptions $M \ll L$, one has $\frac{Q^2}{L^2} \ll \frac{Q^2}{ML}$ and we ignore the apocenter (pericenter) shift which is described with Eq. (22). For the fifth (de-Sitter or anti-de-Sitter) term in Eq. (14) one has potential

$V_{dS}(r) = -\frac{\Lambda r^2}{6}$ ($\alpha_2 = -\frac{\Lambda}{6}$) and one has the corresponding apocenter (pericenter) shift (Adkins and McDonnell 2007) (see also, (Kerr et al. 2003, Sereno and Jetzer 2006))

$$\Delta\theta(\Lambda) := \Delta\theta(2)_{dS} = \frac{\pi\Lambda a^3 \sqrt{1-e^2}}{M}. \quad (23)$$

Therefore, a total shift of a pericenter is

$$\Delta\theta(total) := \frac{6\pi M}{L} - \frac{\pi Q^2}{ML} + \frac{\pi\Lambda a^3 \sqrt{1-e^2}}{M}. \quad (24)$$

and one has a relativistic advance for a tidal charge with $Q^2 < 0$ and apocenter shift dependences on eccentricity and semi-major axis are the same for GR and Reissner – Nordström advance but corresponding factors

$(6\pi M$ and $-\frac{\pi Q^2}{M})$ are different, therefore, it is very hard to distinguish a presence of a tidal charge and black hole mass evaluation uncertainties. For $Q^2 > 0$, there is an apocenter shift in the opposite direction in respect to GR advance.

Estimates

As it was noted by the astronomers of the Keck group (Hees et al. 2017), pericenter shift has not been found yet for S2 star, however, an upper confidence limit on a linear drift is constrained

$$|\dot{\omega}| < 1.7 \times 10^{-3} \text{rad/yr.} \quad (25)$$

at 95% C.L., while GR advance for the pericenter is (Hees et al. 2017)

$$|\dot{\omega}_{GR}| = \frac{6\pi GM}{Pc^2(1 - e^2)} = 1.6 \times 10^{-4} \text{rad/yr,} \quad (26)$$

where P is the orbital period for S2 star (in this section we use dimensional constants G and c instead of geometrical units). Based on such estimates

one could constrain alternative theories of gravity following the approach used in (Hees et al. 2017).

Estimates of (tidal) charge constraints

Assuming $\Lambda = 0$ we consider constraints on Q^2 parameter from previous and future observations of S2 star. One could re-write orbital precession in dimensional form

$$\dot{\omega}_{RN} = \frac{\pi Q^2}{PGML}, \quad (27)$$

where P is an orbital period. Taking into account a sign of pericenter shift for a tidal charge with $Q^2 < 0$, one has

$$\dot{\omega}_{RN} < 1.54 \times 10^{-3} \text{rad/yr} \approx 9.625 \dot{\omega}_{GR}, \quad (28)$$

therefore,

$$-57.75M^2 < Q^2 < 0, \quad (29)$$

with 95% C. L. For $Q^2 > 0$, one has

$$|\dot{\omega}_{RN}| < 1.86 \times 10^{-3} \text{rad/yr} \approx 11.625 \dot{\omega}_{GR}, \quad (30)$$

therefore,

$$0 < |Q| < 8.3516M, \quad (31)$$

with 95% C. L. As it was noted in (Hees et al. 2017) in 2018 after the pericenter passage of S2 star the current uncertainties of $|\dot{\omega}|$ will be improved by a factor 2, so for a tidal charge with $Q^2 < 0$, one has

$$\dot{\omega}_{RN} < 6.9 \times 10^{-4} \text{rad/yr} \approx 4.31 \dot{\omega}_{GR}, \quad (32)$$

$$-25.875M^2 < Q^2 < 0, \quad (33)$$

For $Q^2 > 0$, one has

$$|\dot{\omega}_{RN}| < 9.1 \times 10^{-4} \text{rad/yr} \approx 5.69 \dot{\omega}_{GR}, \quad (34)$$

therefore,

$$0 < |Q| < 5.80M, \quad (35)$$

One could expect that subsequent observations with VLT, Keck, GRAVITY, E-ELT and TMT will significantly improve an observational constraint on $|\dot{\omega}|$, therefore, one could expect that a range of possible values of Q parameter would be essentially reduced.

As it was noted in paper (Hees et al. 2017), currently Keck astrometric uncertainty is around $\sigma = 0.16$ mas, therefore, an angle $\delta = 2\sigma$ (or two standard deviations) is measurable with around 95% C.L. In this case $\Delta\theta(GR)_{S2} = 2.59\delta$ for S2 star where we adopt $\Delta\theta(GR)_{S2} \approx 0.83$. Assuming that GR predictions about orbital precession will be confirmed in the next 16 years with δ accuracy (or $\left| \frac{\pi Q^2}{ML} \right| \lesssim \delta$), one could constrain Q parameter

$$|Q^2| \lesssim 2.32M^2, \quad (36)$$

where we wrote absolute value of Q^2 since for a tidal charge Q^2 could be negative.

If we adopt for TMT-like scenario uncertainty $\sigma_{TMT} = 0.015$ mas as it was used in (Hees et al. 2017) ($\delta_{TMT} = 2\sigma_{TMT}$) or in this case $\Delta\theta(GR)_{S2} = 27.67\delta_{TMT}$ for S2 star and assuming again that GR predictions about orbital precession of S2 star will be confirmed with δ_{TMT} accuracy (or $\left|\frac{\pi Q^2}{ML}\right| \lesssim \delta_{TMT}$), one could conclude that

$$|Q^2| \lesssim 0.216M^2, \quad (37)$$

or based on results of future observations one could expect to reduce significantly a possible range of Q^2 parameter in comparison with a possible hypothetical range of Q^2 parameter which was discussed in (Bin-Nun 2010a, 2010b).

Estimates of Λ -term constraints

In this subsection we assume that $Q = 0$. One could re-write orbital precession in dimensional form

$$\dot{\omega}_\Lambda = \frac{\pi \Lambda c^2 a^3 \sqrt{1 - e^2}}{PGM}, \quad (38)$$

Dependences of functions $\dot{\omega}_\Lambda$ and $\dot{\omega}_{GR}$ on eccentricity and semi-major axis are different and orbits with higher semi-major axis and smaller eccentricity could provide a better estimate of Λ -term (the S2 star orbit has a rather high eccentricity). However, we use observational constraints for S2 star. For positive Λ , one has relativistic advance and

$$\dot{\omega}_\Lambda < 1.54 \times 10^{-3} \text{rad/yr} \approx 9.625 \dot{\omega}_{GR}, \quad (39)$$

or

$$0 < \Lambda < 3.9 \times 10^{-39} \text{cm}^{-2}, \quad (40)$$

for $\Lambda < 0$ one has

$$0 < -\Lambda < 4.68 \times 10^{-39} \text{cm}^{-2}, \quad (41)$$

if we use current accuracy of Keck astrometric measurements $\sigma = 0.16$ mas and monitor S2 star for 16 years and assume that additional apocenter shift (2σ) could be caused by a presence of Λ -term, one obtains

$$|\Lambda| < 1.56 \times 10^{-40} \text{cm}^{-2}, \quad (42)$$

while for TMT-like accuracy $\delta_{TMT} = 0.015$ mas one has

$$|\Lambda| < 1.46 \times 10^{-41} \text{cm}^{-2}. \quad (43)$$

As one can see, constraints on cosmological constant from orbital precession of bright stars near the Galactic Center are much weaker than not only its cosmological estimates but also than its estimates from Solar system data.

LETTER TO THE EDITOR

Detection of the gravitational redshift in the orbit of the star S2 near the Galactic centre massive black hole[★]

GRAVITY Collaboration^{**}: R. Abuter⁸, A. Amorim^{6,14}, N. Anugu⁷, M. Bauböck¹, M. Benisty⁵, J. P. Berger^{5,8}, N. Blind¹⁰, H. Bonnet⁸, W. Brandner³, A. Buron¹, C. Collin², F. Chapron², Y. Clénet², V. Coudé du Foresto², P. T. de Zeeuw^{12,1}, C. Deen¹, F. Delplancke-Ströbele⁸, R. Dembet^{8,2}, J. Dexter¹, G. Duvert⁵, A. Eckart^{4,11}, F. Eisenhauer^{1,***}, G. Finger⁸, N. M. Förster Schreiber¹, P. Fédou², P. Garcia^{7,14}, R. Garcia Lopez^{15,3}, F. Gao¹, E. Gendron², R. Genzel^{1,13}, S. Gillessen¹, P. Gordo^{6,14}, M. Habibi¹, X. Haubois⁹, M. Haug⁸, F. Haußmann¹, Th. Henning³, S. Hippler³, M. Horrobin⁴, Z. Hubert^{2,3}, N. Hubin⁸, A. Jimenez Rosales¹, L. Jochum⁸, L. Jocou⁵, A. Kaufer⁹, S. Kellner¹¹, S. Kendrew^{16,3}, P. Kervella², Y. Kok¹, M. Kulas³, S. Lacour², V. Lapeyrère², B. Lazareff⁵, J.-B. Le Bouquin⁵, P. Léna², M. Lippa¹, R. Lenzen³, A. Mérand⁸, E. Müller^{8,3}, U. Neumann³, T. Ott¹, L. Palanca⁹, T. Paumard², L. Pasquini⁸, K. Perraut⁵, G. Perrin², O. Pfuhl¹, P. M. Plewa¹, S. Rabien¹, A. Ramírez⁹, J. Ramos³, C. Rau¹, G. Rodríguez-Coira², R.-R. Rohloff³, G. Rousset², J. Sanchez-Bermudez^{9,3}, S. Scheithauer³, M. Schöller⁸, N. Schuler⁹, J. Spyromilio⁸, O. Straub², C. Straubmeier⁴, E. Sturm¹, L. J. Tacconi¹, K. R. W. Tristram⁹, F. Vincent², S. von Fellenberg¹, I. Wank⁴, I. Waisberg¹, F. Widmann¹, E. Wieprecht¹, M. Wiest⁴, E. Wiezorrek¹, J. Woillez⁸, S. Yazici^{1,4}, D. Ziegler², and G. Zins⁹

(Affiliations can be found after the references)

Received 26 June 2018 / Accepted 29 June 2018

ABSTRACT

The highly elliptical, 16-year-period orbit of the star S2 around the massive black hole candidate Sgr A* is a sensitive probe of the gravitational field in the Galactic centre. Near pericentre at 120 AU \approx 1400 Schwarzschild radii, the star has an orbital speed of \approx 7650 km s⁻¹, such that the first-order effects of Special and General Relativity have now become detectable with current capabilities. Over the past 26 years, we have monitored the radial velocity and motion on the sky of S2, mainly with the SINFONI and NACO adaptive optics instruments on the ESO Very Large Telescope, and since 2016 and leading up to the pericentre approach in May 2018, with the four-telescope interferometric beam-combiner instrument GRAVITY. From data up to and including pericentre, we robustly detect the combined gravitational redshift and relativistic transverse Doppler effect for S2 of $z = \Delta\lambda/\lambda \approx 200$ km s⁻¹/c with different statistical analysis methods. When parameterising the post-Newtonian contribution from these effects by a factor f , with $f=0$ and $f=1$ corresponding to the Newtonian and general relativistic limits, respectively, we find from posterior fitting with different weighting schemes $f = 0.90 \pm 0.09_{\text{stat}} \pm 0.15_{\text{sys}}$. The S2 data are inconsistent with pure Newtonian dynamics.

Key words. Galaxy: center – gravitation – black hole physics

1. Introduction

General Relativity (GR) so far has passed all experimental tests with flying colours (Einstein 1916; Will 2014). The most stringent are tests that employ solar mass pulsars in binary systems (Kramer et al. 2006), and gravitational waves from 10 to 30 M_{\odot} black hole in-spiral events (Abbott et al. 2016a,b,c). These tests cover a wide range of field strengths and include the strong curvature limit (Fig. A.2). At much lower field strength, Earth

laboratories probe planetary masses that are about a factor 10⁶ lower than the stellar mass scale. For massive black hole (MBH) candidates with masses of 10^{6–10} M_{\odot} , only indirect evidence for GR effects has been reported, such as relativistically broadened, redshifted iron K α line emission in nearby active galaxies (Tanaka et al. 1995; Fabian et al. 2000). The closest MBH is at the centre of the Milky Way ($R_0 \approx 8$ kpc, $M_{\bullet} \approx 4 \times 10^6 M_{\odot}$), and its Schwarzschild radius subtends the largest angle on the sky of all known MBHs ($R_S \approx 10 \mu\text{as} \approx 0.08$ AU). It is coincident with a very compact, variable X-ray, infrared, and radio source, Sgr A*, which in turn is surrounded by a very dense cluster of orbiting young and old stars. Radio and infrared observations have provided detailed information on the distribution, kinematics, and physical properties of this nuclear star cluster and of the hot, warm, and cold interstellar gas interspersed in it (cf. Genzel et al. 2010; Morris et al. 2012; Falcke & Markoff 2013). High-resolution near-infrared (NIR) speckle and adaptive optics (AO) assisted imaging and spectroscopy of the nuclear star cluster over the past 26 years, mainly by two groups in Europe (the

[★] This paper is dedicated to Tal Alexander, who passed away about a week before the pericentre approach of S2.

^{**} GRAVITY is developed in a collaboration by the Max Planck Institute for extraterrestrial Physics, LESIA of Paris Observatory/CNRS/Sorbonne Université/Univ. Paris Diderot and IPAG of Université Grenoble Alpes/CNRS, the Max Planck Institute for Astronomy, the University of Cologne, the CENTRA – Centro de Astrofísica e Gravitação, and the European Southern Observatory.

^{***} Corresponding author: F. Eisenhauer
e-mail: eisenhau@mpe.mpg.de

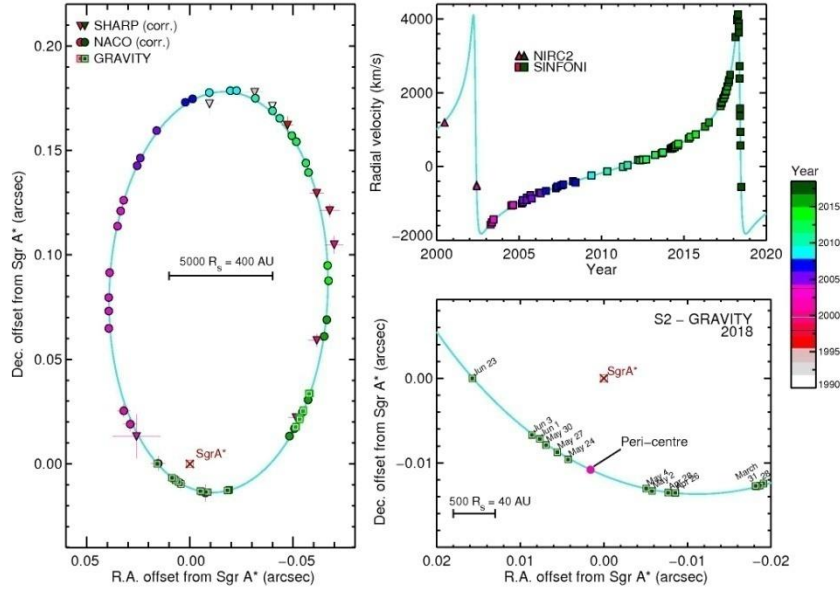


Fig. 2. Summary of the observational results of monitoring the S2 – Sgr A* orbit from 1992 to 2018. *Left:* projected orbit of the star S2 (J2000) relative to the position of the compact radio source Sgr A* (brown crossed square at the origin). Triangles and circles (and 1σ uncertainties) denote the position measurements with SHARP at the NTT and NACO at the VLT, colour-coded for time (colour bar on the right side). All data points are corrected for the best-fit zero-point (x_0, y_0) and drifts (\dot{x}_0, \dot{y}_0) of the coordinate system relative to Sgr A* (see Plewa et al. 2015). Green squares mark the GRAVITY measurements. The *bottom right panel* shows a zoom around pericentre in 2018. *Top right:* radial velocity of S2 as a function of time (squares: SINFONI/NACO at the VLT; triangles: NIRC2 at Keck). S2 reached pericentre of its orbit at the end of April 2002, and then again on May 19th, 2018 (MJD 58257.67). The data before 2017 are taken from Ghez et al. (2008), Boehle et al. (2016), Chu et al. (2018), and Gillessen et al. (2017, 2009b). The 2017/2018 NACO/SINFONI and GRAVITY data are presented here for the first time. The cyan curve shows the best-fitting S2 orbit to all these data, including the effects of General and Special Relativity.

and 26 additional spectroscopy epochs with SINFONI using the 25 mas pix^{-1} scale and the combined $H + K$ -band grating with a spectral resolution of $R \approx 1500$.

For more details on the data analysis of all three instruments, we refer to Appendix A.

3. Results

3.1. Relativistic corrections

The left panel of Fig. 2 shows the combined single-telescope and interferometric astrometry of the 1992–2018 sky-projected orbital motion of S2, where the zero point is the position of the central mass and of Sgr A*. All NACO points were corrected for a zero-point offset and drift in RA/Dec, which are obtained from the orbit fit. The bottom right panel zooms into the 2018 section of the orbit around pericentre measured with GRAVITY. The zoom demonstrates the hundred-fold improvement of astrometry between SHARP in the 1990s (≈ 4 mas precision) and NACO in the 2000s (≈ 0.5 mas) to GRAVITY in 2018 (as small as $\approx 30 \mu\text{as}$). While the motion on the sky of S2 could be detected with NACO over a month, the GRAVITY observations detect the

motion of the star from day to day. The upper right panel of Fig. 2 displays the radial velocity measurements with SINFONI at the VLT and NIRC2 at Keck in the 1992–2018 period.

At pericentre R_{peri} , S2 moves with a total space velocity of $\approx 7650 \text{ km s}^{-1}$, or $\beta = v/c = 2.55 \times 10^{-2}$. This means that the first-order parameterised post-Newtonian correction terms (PPN(1)), due to Special and General Relativity, beyond the orbital Doppler and Römer effects, are within reach of current measurement precision, $\text{PPN}(1) \sim \beta^2 \sim (R_S/R_{\text{peri}}) \sim 6.5 \times 10^{-4}$. These terms can be parameterised spectroscopically as (e.g. Misner et al. 1973; Alexander 2005; Zucker et al. 2006).

$$z = \frac{\Delta\lambda}{\lambda} = B_0 + B_{0.5}\beta + B_1\beta^2 + \mathcal{O}(\beta^3), \quad (1)$$

where the PPN(1)_z term $B_1 = B_{1,\text{TD}} + B_{1,\text{GR}}$, with $B_{1,\text{TD}} = B_{1,\text{gr}} = 0.5$, and $\beta^2 = [R_S(1+e)]/[2a(1-e)] = 6.51 \times 10^{-4}$ for S2. Here a is the semi-major axis and e is the eccentricity of the S2 orbit. $B_{0.5}\beta$ is the Newtonian Doppler shift.

Equation (1) indicates that PPN(1)_z consists in equal terms of the special relativistic transverse Doppler effect ($B_{1,\text{TD}}$) and the general relativistic gravitational redshift ($B_{1,\text{GR}}$), totalling $\approx 200 \text{ km s}^{-1}$ redshift at pericentre, while at apocentre, it amounts

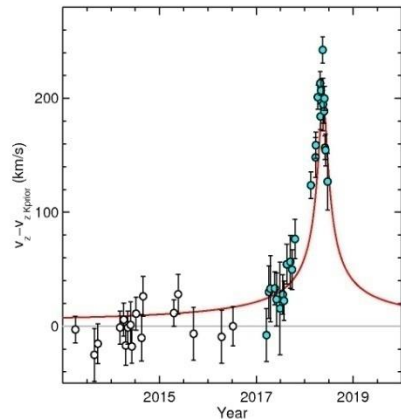


Fig. 3. Residual velocity $c\Delta z = c(z_{\text{GR}} - z_{\text{K}})$ for the best fitting prior Keplerian K_{prior} ($f=0$, grey) and the same orbit with $f=1$ (red GR_{prior}). K_{prior} was constructed from all 1992–2018 astrometric data with NACO & GRAVITY and the SINFONI data between 2004 and 2016 (open black circles). The 2017/2018 SINFONI data points (black circles with cyan shading) can then be added to test if the spectroscopic data around pericentre follow K_{prior} or the GR_{prior} predicted from K_{prior} . The new data points near and up to pericentre, where the β^2 effects in radial velocity are expected to be important, fall close to the predicted GR_{prior} curve, and exclude the Keplerian prior orbit.

to only 6 km s^{-1} . If the total orbital redshift z_{tot} is separated into a Newtonian/Kepler part z_{K} and a GR correction, one can write $z_{\text{tot}} = z_{\text{K}} + f(z_{\text{GR}} - z_{\text{K}})$, where f is zero for purely Newtonian physics and unity for GR. In the following we show the residuals $\Delta z = z_{\text{GR}} - z_{\text{K}}$. The Keplerian part of the orbit is at $\Delta z = 0$, and the $\text{PPN}(1)_z$ corrections appear as an excess.

3.2. Analysis with prior Kepler orbit

We define a prior orbit K_{prior} by excluding those data for which the $\text{PPN}(1)_z$ corrections matter. For K_{prior} we use the entire 1992–2018 SHARP/NACO and GRAVITY data and the SINFONI data from 2004 up to the end of 2016. We then obtained K_{prior} as described in Gillessen et al. (2017), which requires a simultaneous fit of 13 parameters. The Rømer delay is included in the calculation. The resulting orbit is a modest update of Gillessen et al. (2017). Using this as the prior orbit, we then added the radial velocities from 2017 and 2018 (Fig. 3). The 26 residual 2017/2018 spectroscopic data relative to K_{prior} clearly do not follow the best-fitting Keplerian orbit derived from all previous 51 spectroscopic and 196 positions in the past 26 years (grey line in Fig. 3), but instead follow the $f=1$ (i.e. $\text{GR}(K_{\text{prior}})$) version of K_{prior} (red line in Fig. 3). This test is fair: GR-corrections should only be detectable with our measurement errors within ± 1 year of pericentre.

This a priori test demonstrates that the spectroscopic data around the pericentre passage are inconsistent with Newtonian dynamics and consistent with GR. However, both K_{prior} ($\chi^2 = 21$) and $\text{GR}(K_{\text{prior}})$ ($\chi^2 = 8$) are poor fits to the data.

3.3. Posterior analysis

Because of the uncertainties in the parameters of K_{prior} , in particular, in the strongly correlated mass and distance, a more conservative approach is to determine the best-fit value of the parameter f a posteriori, including all data and fitting for the optimum values of all parameters. In carrying out the fitting, it is essential to realise that the inferred measurement uncertainties are dominated by systematic effects, especially when evidence from three or more very different measurement techniques is combined (see Appendix A.6 for a more detailed discussion). In particular the NACO measurements are subject to correlated systematic errors, for example from unrecognised confusion events (Plewa & Sari 2018), which typically last for one year and are comparable in size to the statistical errors. We therefore down-sampled the NACO data into 100 bins with equal path lengths along the projected orbit (Fig. 4, middle) and gave these data in addition a lower weight of 0.5. Depending on exactly which weighting or averaging scheme was chosen, the posterior analysis including all data between 1992 and 2018 yielded f values between 0.85 and 1.09. With a weighting of 0.5 of the NACO data, we find $f = 0.90 \pm 0.09$ (Fig. 4). GR ($f=1$) is favoured over pure Newtonian physics ($f=0$) at the $\approx 10 \sigma$ level.

The error on f is derived from the posterior probability distributions (Fig. 4, bottom) of a Markov chain Monte Carlo (MCMC) analysis. Fig. A.1 shows the full set of correlation plots and probability distributions for the fit parameters. The distributions are compact and all parameters are well determined. The best-fit values and uncertainties are given Table A.1.

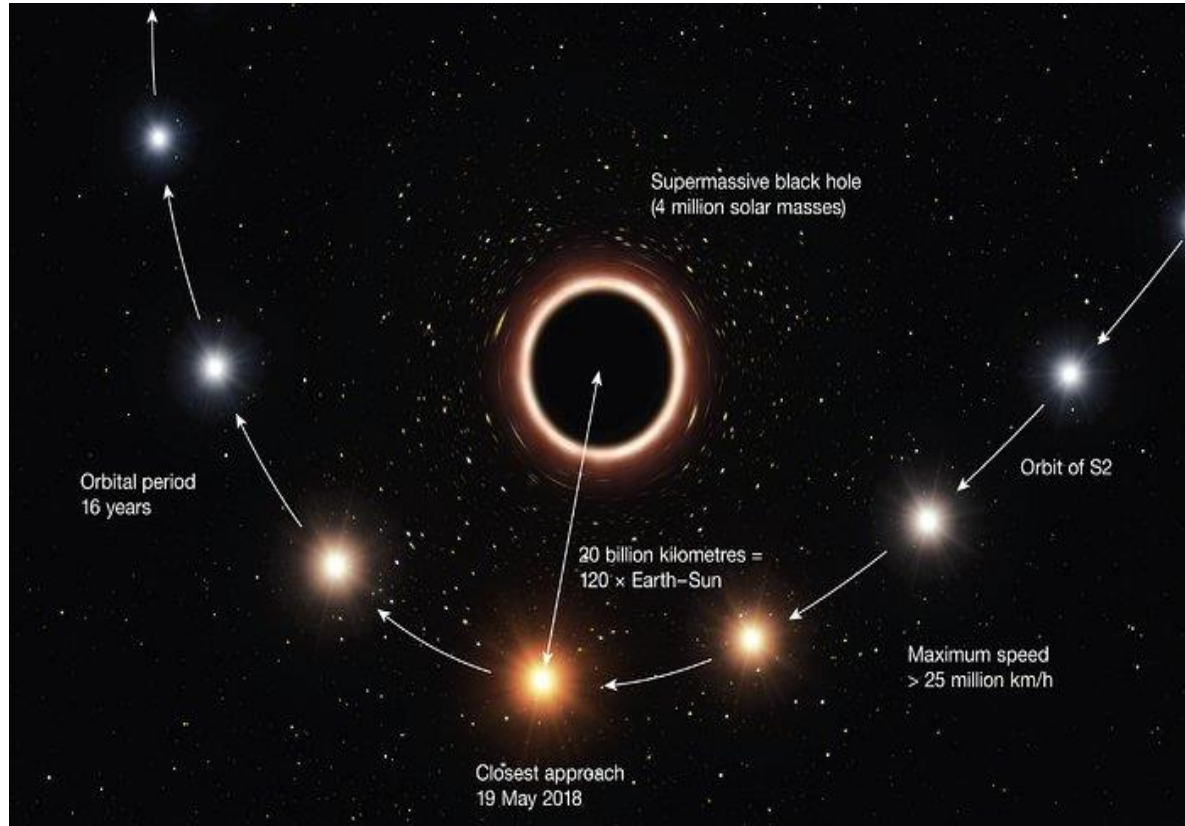
The superb GRAVITY astrometry demonstrably improves the quality of the fits and is crucial for overcoming the source confusion between Sgr A* and S2 near pericentre. A minimal detection of $\text{PPN}(1)_z$ (Eq. (1)) is provided by a combination using only NACO and SINFONI data ($f_{\text{NACO+SINFONI}} = 0.71 \pm 0.19$, 3.6σ), but the inclusion of the GRAVITY data very significantly improves the precision and significance of the fitted parameters: the improvement reaches a factor of 2–3.

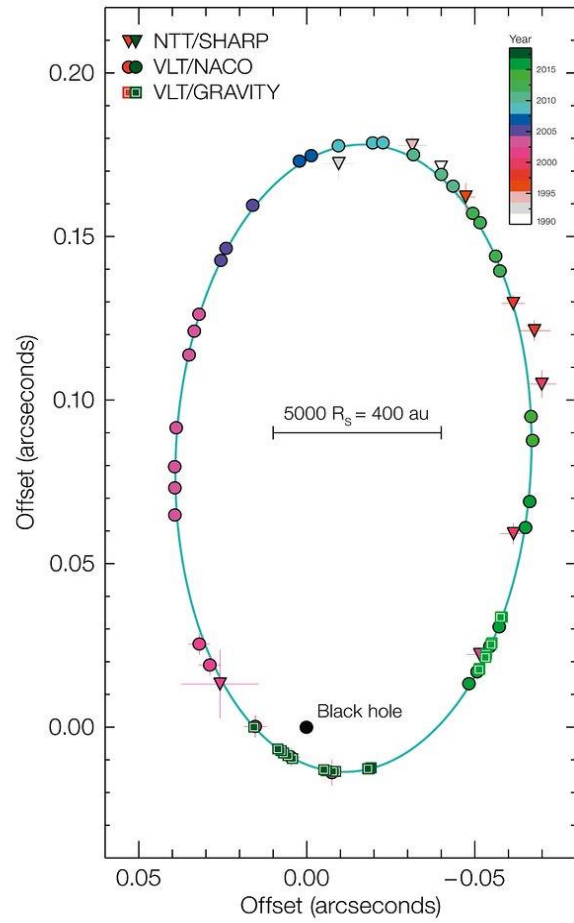
A still more demanding test is to search for any Keplerian fit to all data and determine whether its goodness of fit is significantly poorer than the goodness of fit of the best-fitting GR-orbit. For linear models the formula presented in Andrae et al. (2010) can be used to estimate the significance. However, the value for the degrees of freedom (d.o.f.) is not well defined for non-linear models (Andrae et al. 2010). In our case, we have two models that only differ significantly over a very critical short time-span given the uncertainties in the underlying data. We therefore used the number of those data points as d.o.f. for which the two models predict significant differences. The difference in χ^2 yields a formal significance of 5σ or greater in favour of the relativistic model.

For further comments on a Bayesian analysis of our data, see Appendix A.9.

4. Discussion

We have reported the first direct detection of the $\text{PPN}(1)$ gravitational redshift parameter around the MBH in the Galactic centre from a data set that extends up to and includes the pericentre approach in May 2018. Three different analysis methods of our data suggest that this detection favours the post-Newtonian model with robust significance. Further improvement of our results is expected as our monitoring continues post pericentre. Still, there are reasons to be cautious about the significance of these early results, mainly because of the systematic





GRAVITY result about PN(1) correction

- For orbital precession $f=0.94 \pm 0.09$
- For gravitational redshift $f=0.9 \pm 0.1$ (stat) ± 0.15 (sys)
- $\sigma = 3 * 10^{-5}$ as

[Send Feedback](#)
[Help](#)

PDG verification for: JCAP 1605 045 (ZAKHAROV 2016) Verifier: ZAKHAROV
checked by Alexander Zakharov (zakharov@itep.ru) on 2018-10-30, corrections marked in red

[Back to ZAKHAROV verifications](#)

Authors:

A.F. Zakharov, et al.

Collaboration:

<missing>

Assigned sections:

graviton

graviton MASS in graviton

Van Dam and Veltman (VANDAM 1970), Iwasaki (IWASAKI 1970), and Zakharov (ZAKHAROV 1970) almost simultaneously showed that "... there is a discrete difference between the theory with zero-mass and a theory with finite mass, no matter how small as compared to all external momenta." The resolution of this "vDVZ discontinuity" has to do with whether the linear approximation is valid. De Rham *et al.* (DE-RHAM 2011) have shown that nonlinear effects not captured in their linear treatment can give rise to a screening mechanism, allowing for massive gravity theories. See also GOLDHABER 2010 and DE-RHAM 2017 and references therein. Experimental limits have been set based on a Yukawa potential or signal dispersion. h_0 is the Hubble constant in units of 100 km s⁻¹ Mpc⁻¹.

The following conversions are useful: 1 eV = 1.783 × 10⁻³³ g = 1.957 × 10⁻⁶ m_e; $\lambda_C = (1.973 \times 10^{-7} \text{ m}) \times (1 \text{ eV}/m_g)$.

VALUE (eV)	DOCUMENT ID	TECN	COMMENT
< 6 × 10 ⁻³²	1 CHOUDHURY 2004	YUKA	Weak gravitational lensing
... We do not use the following data for averages, fits, limits, etc. ...			
< 1.4 × 10 ⁻²⁹	2 DESAI 2018	YUKA	Gal cluster Abell 1689
< 6 × 10 ⁻³⁰	3 RANA 2018	YUKA	Weak lensing in massive clusters
< 8 × 10 ⁻³⁰	4 RANA 2018	YUKA	SZ effect in massive clusters
< 7 × 10 ⁻²³	5 ABBOTT 2017	DISP	Combined dispersion limit from three BH mergers
< 1.2 × 10 ⁻²²	5 ABBOTT 2016	DISP	Combined dispersion limit from two BH mergers
< 2.9 × 10 ⁻²¹	6 ZAKHAROV 2016	YUKA	S2 star orbit
< 5 × 10 ⁻²³	7 BRITO 2013		Spinning black holes bounds
< 4 × 10 ⁻²⁵	8 BASKARAN 2008		Graviton phase velocity fluctuations
< 6 × 10 ⁻³²	9 GRUZINOV 2005	YUKA	Solar System observations
< 9.0 × 10 ⁻³⁴	10 GERSHTEIN 2004		From Ω_{tot} value assuming RTG
> 6 × 10 ⁻³⁴	11 DVALI 2003		Horizon scales
< 8 × 10 ⁻²⁰	12 ,FINN 2002	DISP	Binary pulsar orbital period decrease
	13		
	14 ,DAMOUR 1991		Binary pulsar PSR 1913+16
	13		
< 7 × 10 ⁻²³	TALMADGE 1988	YUKA	Solar system planetary astrometric data
< 2 × 10 ⁻²⁹ h ₀ ⁻¹	GOLDHABER 1974		Rich clusters
< 7 × 10 ⁻²⁸	HARE 1973		Galaxy
< 8 × 10 ⁴	HARE 1973		2γ decay

¹ CHOUDHURY 2004 concludes from a study of weak-lensing data that masses heavier than about the inverse of 100 Mpc seem to be ruled out if the gravitation field has the Yukawa form.

² DESAI 2018 limit based on dynamical mass models of galaxy cluster Abell 1689.

³ RANA 2018 limit, 68% CL, obtained using weak lensing mass profiles out to the radius at which the cluster density falls to 200 times the critical density of the Universe. Limit is based on the fractional change between Newtonian and Yukawa accelerations for the 50 most massive galaxy clusters in the Local Cluster Substructure Survey. Limits for other CL's and other density cuts are also given.

⁴ RANA 2018 limit, 68% CL, obtained using mass measurements via the SZ effect out to the radius at which the cluster density falls to 500 times the critical density of the Universe for 182 optically confirmed galaxy clusters in an Atacama Cosmology Telescope survey. Limits for other CL's and other density cuts are also given.

⁵ ABBOTT 2016 and ABBOTT 2017 assumed a dispersion relation for gravitational waves modified relative to GR.

⁶ ZAKHAROV 2016 constrains range of Yukawa gravity interaction from S2 star orbit about black hole at Galactic center. The limit is <

NODE=

OCCUR

OCCUR

NODE=

NODE=

NODE=

NODE=

NODE=

Main conclusions

- We found graviton mass constraints which are comparable with LIGO's ones
- Observers working with largest telescopes with AO (Keck, VLT, GRAVITY, TMT, E-ELT) follow our ideas to improve current graviton mass constraints with current and forthcoming facilities

• Conclusions

- VLBI systems in mm and sub-mm bands could detect mirages (“faces”) around black holes (for BH@ GC in particular) (see, EHT pictures for M87*)
- Shapes of images give an important information about BH parameters
- Trajectories of bright stars or bright spots around massive BHs are very important tool for an evaluation of BH parameters
- Trajectories of bright stars or bright spots around massive BHs can be used to obtain constraints on alternative theories of gravity ($f(R)$ theory, for instance)
- A significant tidal charge of the BH at GC is excluded by observations, but there signatures of extreme RN charge (perhaps non-electric one)
- Constraints on Yukawa potential has been found
- Constraints of graviton mass have been obtained (they are consistent with LIGO ones)
- Perspectives to improve the current graviton mass estimates with future observations (VLT, Keck, GRAVITY, E-ELT, TMT) are discussed
- Constraints of tidal charge have been obtained
- The EHT team will release a new image of the SMBH@GC shortly. Stay tuned!

- Thanks for your kind attention!
-